



VLAKNA TEXTIL

FIBRES AND TEXTILES

TECHNICAL
UNIVERSITY
OF LIBEREC

STU
FCHPT



2

Volume 30
May
2023

Indexed in:

SCOPUS
Chemical Abstract
World Textile Abstracts
EBSCO Essentials

ISSN 1335-0617
print version

ISSN 2585-8890
online version



VLÁKNA A TEXTIL

<http://www.vat.ft.tul.cz>

PUBLISHED BY

Technical University of Liberec, Faculty of Textile Engineering
Slovak University of Technology in Bratislava, Faculty of Chemical and Food Technology
Alexander Dubček University of Trenčín, Faculty of Industrial Technologies
Slovak Society of Industrial Chemistry, Bratislava
Research Institute of Man-Made Fibres, JSC, Svit
VÚTCH – CHEMITEX, Ltd., Žilina
Chemosvit Fibrochem, JSC, Svit

EDITOR IN CHIEF

Maroš TUNÁK, Technical University of Liberec, CZ

EXECUTIVE EDITOR

Veronika TUNÁKOVÁ, Technical University of Liberec, CZ

EDITORIAL BOARD

Ľudmila BALOGOVÁ, VÚTCH – CHEMITEX, Ltd., Žilina, SK
Marcela HRICOVÁ, Slovak University of Technology in Bratislava, SK
Vladimíra KRMELOVÁ, A. Dubček University of Trenčín, SK
Zita TOMČÍKOVÁ, Research Institute of Man-Made Fibres, JSC, Svit, SK
Maroš TUNÁK, Technical University of Liberec, CZ
Veronika TUNÁKOVÁ, Technical University of Liberec, CZ
Tomáš ZATROCH, Chemosvit Fibrochem, JSC, Svit, SK

HONOURABLE EDITORIAL BOARD

Vladimír BAJŽÍK, Technical University of Liberec, CZ
Martin BUDZÁK, Research Institute of Man-Made Fibres, JSC, Svit, SK
Anton GATIAL, Slovak University of Technology in Bratislava, SK
Ana Marija GRANCARIĆ, University of Zagreb, HR
Izabella KRUCIŇSKA, Technical University of Lodz, PL
Anton MARCINČIN, Slovak University of Technology in Bratislava, SK
Alenka M. LE MARECHAL, University of Maribor, SL
Jiří MILITKÝ, Technical University of Liberec, CZ
Darina ONDRUŠOVÁ, Alexander Dubček University in Trenčín, SK
Olga PARASKA, Khmelnytskyi National University, UA
Anna UJHELYIOVÁ, Slovak University of Technology in Bratislava, SK
Victoria VLASENKO, Kyiv National University of Technologies and Design, UA

PUBLISHER

Technical University of Liberec
Studentska 1402/2, 461 17 Liberec 1, CZ
Tel: +420 485 353615
e-mail: vat@tul.cz
IČO: 46747885

ORDER AND ADVERTISEMENT OF THE JOURNAL

Technical University of Liberec
Faculty of Textile Engineering
Studentska 1402/2, 461 17 Liberec 1, CZ
Tel: +420 485 353615
e-mail: vat@tul.cz

TYPESET AND PRINT

Vysokoškolský podnik, s.r.o., Voroněžská 1329/13, 460 01 Liberec 1, CZ

DATE OF ISSUE

May 2023

APPROVED BY

Rector's Office of Technical University of Liberec
Ref. no. RE 20/23, 9th May 2023

EDITION

First

PUBLICATION NUMBER

55-020-23

PUBLICATION

Quarterly

SUBSCRIPTION

60 EUR

VLÁKNA A TEXTIL

Volume 30, Issue 2, May 2023

CONTENT

- 3 **NAVARA, TOMÁŠ**
RESISTANCE OF ADDITIONAL ROOFING UNDERLAYS OF PITCHED ROOFS AGAINST ARTIFICIAL AND NATURAL AGEING
- 14 **HOSSAIN, MOHAMMAD MOBARAK; ALIMUZZAMAN, SHAH AND AHMED, DEWAN MURSHED**
TEAR AND TENSILE STRENGTH OF 100% COTTON WOVEN FABRICS' BASIC STRUCTURES: REGRESSION MODELLING
- 26 **THAO, PHAN THANH; MY, PHAM THI LE AND PHAN, DUY-NAM**
STATE PROBLEM OF BALANCING SEWING LINE OF INDUSTRIAL KNITTED PRODUCTS
- 34 **KŘÍŽ, VÍTĚZSLAV; KŘÍŽOVÁ, HANA; KOCICH, MARTIN AND DALÍKOVÁ, JOHANA**
A 2D CELLULAR AUTOMATON MODEL OF LIQUID ABSORPTION INTO PAPER FIBERS WITH HYDROPHOBIC TREATMENT
- 43 **ARABULI, ARSENI; ARABULI, SVITLANA; KYZYMCHUK, OLENA AND MELNYK, LIUDMYLA**
ELECTRIC HEATING CLOTHING FOR MOTORCYCLISTS
- 51 **TRI, YULIANA AND NOORYAN, BAHARI**
THE DEVELOPMENT AND ANALYSIS OF ECO-PRINT AND SCREEN PRINTING COMBINATION USING NATURAL DYES
- 56 **HUSSEN, MUKTAR SEID; KYOSEV, YORDAN; PIETSCH, KATHRIN; BOLL, JESSICA AND KABISH, ABERA KECHI**
MULTI-CRITERIA NUMERICAL OPTIMIZATION OF MECHANICAL PROPERTIES IN ULTRASONIC WELDING PROCESS PARAMETERS OF PVC-COATED HYBRID TEXTILES FOR WEATHER PROTECTION
- 74 **ALI, REHMAT; KARAMAT, UM E HABIBA; NAZIR, HAFIZA SABA; BAIG, MIRZA MUHAMMED MOHSIN; KHAN, BILAL ALAM; ULLAH, ASAD; USMAN, OSAMA; WASEEM, TANYA; TAHIR, AND MUHAMMAD FARRUKH**
ANTIMICROBIAL ACTIVITY OF COTTON FIBRES TREATED WITH PARTICLES EXTRACTED FROM CITRUS PLANTS: A REVIEW

RESISTANCE OF ADDITIONAL ROOFING UNDERLAYS OF PITCHED ROOFS AGAINST ARTIFICIAL AND NATURAL AGEING

NAVARA, TOMÁŠ*

Institute of Technology and Business in České Budějovice, Okružní 517/10, 370 01 České Budějovice, Czech Republic

ABSTRACT

In this paper, the author deals with the resistance of light polymer foils based on microporous functional film, used as additional waterproofing layers of pitched roofs. He exposes these foils to the effects of natural ageing and the effects of artificial ageing according to the methodology of the European test standard. Subsequently, it verifies the tensile properties of the exposed foils and compares the effects of natural and artificial ageing in order to determine the possible cause of premature degradation of these materials, which often occurs in practice. He concludes that the cause of this degradation is not excessive leniency of testing standards, but the insufficient quality of materials supplied to the European market.

KEYWORDS

Additional roofing underlay; Artificial ageing; Natural ageing; Roof membrane; Polymer degradation.

INTRODUCTION

Due to their versatile applicability, polymer materials are used in a wide range of industries, such as healthcare, the automotive industry, the textile industry and even the construction industry. It is in the construction industry that they are used, among other things, in the form of polymer waterproofing coatings [1], which protect buildings from underground water in the case of substructures, or against rainwater, as is the case with roofs. An example can be additional roofing underlays of pitched roofs.

Additional roofing underlays (ARU) are layers inserted under the folded covering of pitched roofs, in order to protect the interior from the action of water, snow, wind and dirt that penetrate through this covering. When designing ARU, you can choose from a whole range of different materials, depending on whether the so-called safe slope of the covering (BSK) required by the manufacturer of this covering is met or exceeded, and depending on the structural complexity of the roof or the way the attic spaces are used. ARU can be designed in the form of heavy polymer or asphalt waterproofing strips, sheet materials, or, most often, in the form of lightweight polymer foils.

Light-type polymer foils can be further divided according to the structural basis, into microperforated, microporous, microfibrinous (see for

example [2]), monolithic and other special types of films. Each of these foils has its advantages and disadvantages. The most used type are microporous foils.

These foils are a multi-layer material consisting of two layers of protective geotextile, which has the task of ensuring the mechanical properties of the final product, and one (middle) layer, in the form of a microporous polyethylene or polypropylene functional film (see Figure 1), produced by hot or cold drawing [3], which ensures waterproofness and vapor permeability of the material. Microporous foils stand out for their good workability, relatively low purchase price and excellent vapor permeability, which is key for the proper functioning of the roof covering [4]. Their biggest problem is a relatively high susceptibility to premature degradation and loss of key properties due to the influence of the external environment, which can lead to a loss of waterproofing and a limitation of the functionality of the roof covering as a whole.

The degree of degradation of ARU is mainly influenced by sunlight, temperature changes, rainwater, humidity, air, dirt and chemicals. According to available materials [7] [8], the key influences are mainly solar radiation and increased temperature. The part of the solar radiation spectrum referred to as ultra violet (UV) radiation, with a wavelength of 100 - 400 nm, representing up to 5% [9] of all solar radiation

* Corresponding author: Navara T., e-mail: navarat@mail.vstecb.cz

Received August 18, 2022; accepted February 3, 2023

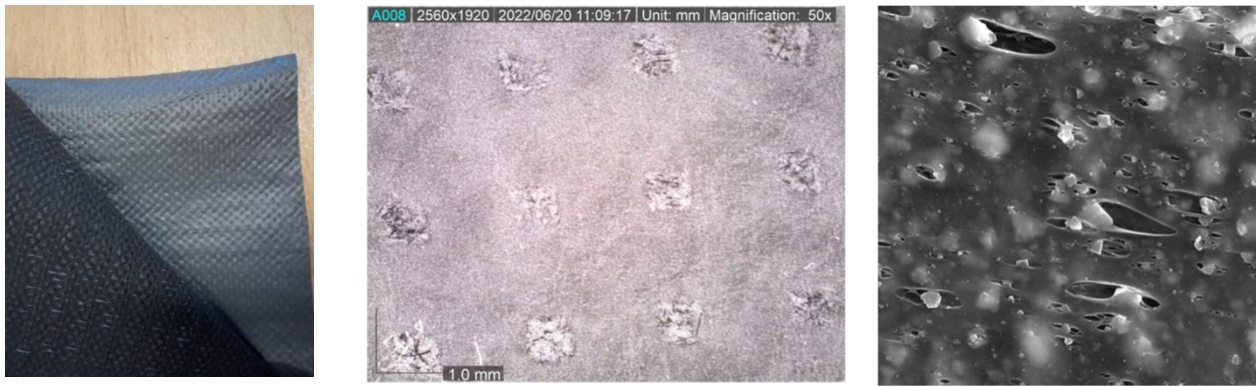


Figure 1. Detail of microporous functional film [5], [6].

(see Figure 2), causes photooxidation of polymers. It is a chemical reaction that results in changes in the chemical structure of the material, such as branching or cross-linking of polymer macromolecules, as a result of which the mechanical properties of these materials change. The combination of elevated temperatures and atmospheric oxygen further accelerates the degradation processes (see for example [10]).

Determination of the resistance of ARU against external influences in the territory of the European Union is governed by the European test standard 13859-1:2014 [11], which precisely defines the conditions of artificial ageing as tests simulating natural ageing. The qualitative requirements for ARU are then regulated at the national level. For example, in the Czech Republic these are determined on the basis of the "Rules for the design and execution of roofs" of the Guild of Plumbers, Roofers and Carpenters (CKPT) [12], and in Germany according

to the publication entitled "Deutsches Dachdeckerhandwerk – Regeln für Dachdeckungen" [13].

ARU based on microporous functional films have faced problems with premature degradation and loss of functionality almost from the very beginning. There are a number of cases where, due to the loss of this functionality, leaks have occurred in roof structures after only a few months of use. For this reason, the insufficient resistance of microporous ARU against the influence of the external environment has been a topic of discussion for many years. This issue was dealt with, for example, by [14], [15] or [16]. The expert public is in the midst of a debate as to whether the cause of premature degradation is non-compliance with the minimum quality of materials supplied to the European market, or whether the cause can be found in the excessive leniency of the test standard. We will try to find an answer to this question in this article.

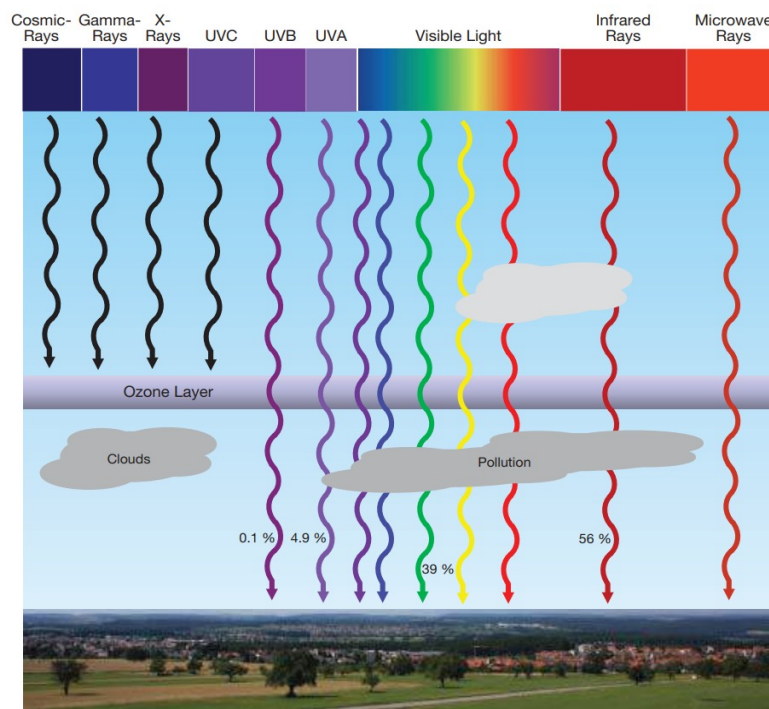


Figure 2. Detail of microporous functional film [5], [6].

Table 1. Selected properties of samples declared by manufacturers according to EN 13 859-1:2014.

Sample	Type of foil	Number of layers	Material of the functional layer	Material of protective layers	Imported from	Price including VAT [€/m ²]	Weight [g/m ²] EN 1849-2	Fire resistance [class] EN ISO 11925-2	Resistance against water penetration [class] EN 1928
1	microporous - multilayer	3	PP	PP	Germany	1,36	130 (+20;-10)	E	W1
2	microporous - multilayer	3	PP	PP	France	1,16	140 (+15;-15)	F	W1
3	microporous - multilayer	3	PP	PP	CR	1,16	140 (+-10)	E	W1
4	microporous - multilayer	3	PE	PP	—	1,40	135 (+-15)	F	W1
5	microporous - multilayer	3	PE	PP	Poland	0,80	150 (+-25)	F	W1
6	microporous - multilayer	3	PP	PP	Hungary	0,60	135 (+-20)	E	W1
7	microporous - multilayer	3	PP	PP	Austria	1,28	110 (+-10)	E	W1
— missing data									

Table 2. Selected properties of samples declared by manufacturers according to EN 13 859-1:2014 – continuation of Table 1.

Sample	Permeability (Sd) [m] EN ISO 12572	Tensile strength in longitudinal direction [N] EN 12311-1	Tensile strength in transverse direction [N] EN 12311-1	Elongation in longitudinal direction [%] EN 12311-1	Elongation in transverse direction [%] EN 12311-1	Tear resistance in longitudinal direction [N] EN 12310-1	Tear resistance in transverse direction [N] EN 12310-1
1	0.02 (+0.04;-0.01)	220 (+-20)	165 (+-15)	20-40	40-100	115 (+-25)	150 (+-30)
2	0.03 (+-0.015)	265 (+-50)	165 (+-50)	70 (+100;-40)	120 (+100;-70)	160 (+-50)	210 (+-60)
3	0.02 (-0.01;+0.015)	290 (+50;-30)	205 (+45;-30)	45 (+35;-15)	80 (+40;-25)	150 (+70;-40)	180 (+70;-50)
4	0.02 (+-0.019)	240 (+-85)	155 (+-85)	80	80	130 (+-90)	160 (+-90)
5	0.03 (+-0.015)	265 (+-50)	165 (+-50)	70 (+100;-40)	120 (+100;-70)	160 (+-50)	210 (+-60)
6	0.05 (+-0.015)	200 (+-40)	110 (+-28)	60	60	80 (+-20)	70 (+-18)
7	>2	200 (+-30)	135 (+-30)	—	—	135 (+-30)	160 (+-30)
— missing data							

MATERIALS

For the purpose of finding an answer to the above questions, a number of tests were carried out on various polymer films commonly used as ARU. Specifically, these were seven samples of lightweight foils based on microporous functional film, with a weight of 110-150 g/m², in the price range of 0.60-1.40 €. These samples then represented the most commonly used materials in the market. The selected properties of the material used can be seen in Table 1.

METHODS

If we want to verify whether the method of artificial ageing specified by the standard [11] corresponds to the real conditions that can realistically occur on the roof, it is easiest to compare these conditions with each other. Such a comparison can then be made on the basis of a comparison of the material

characteristics of the ARU exposed to these conditions.

For this purpose, a total of three test series bearing the designations A, B and C were assembled. Test series A consisted of seven test samples, while each test sample was represented by three test specimens for the longitudinal direction (parallel to the direction of production - LD) and three test specimens for the transverse direction (transverse to the production direction – TD). The size of the specimens was chosen with regard to the possibilities of clamping in the test device, namely 135 x 45 mm. These specimens were clamped in stainless steel holders (see Figure 3) and placed in an artificial ageing device in the form of a xenon test chamber, Xenotest Alpha+. The test itself was conducted in accordance with EN ISO 4892-2 [17] with modifications according to EN1297 [18] and EN 13 859-1 [11]. The test specimens were irradiated with a xenon lamp with a Xenochrome 300 filter, filtering its radiation,

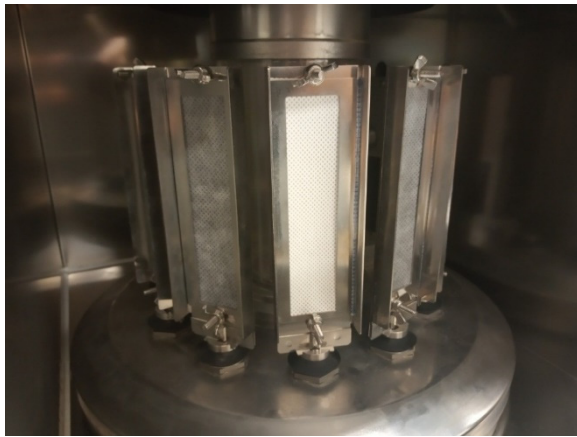


Figure 3. Test objects clamped into stainless steel holders.



Figure 4. Test specimens attached in wooden frames, placed in drying oven.



Figure 6. Image of sensor of solar radiation and UVA radiation.

Table 3. Relative spectral portion (RSP) of radiation energy.

XENOCROME 300		ISO 11341 (1) ISO 4892-2 (A)
Wavelength [nm]	RSP [-]	RSP [-]
<290	0,002	0,15
290-320	4,65	2,6-7,9
321-360	34,77	28,2-38,6
361-400	58,86	55,8-67,5
290-400	100	100

for radiation with a wavelength of 290-400 nm (the relative spectral radiation can be seen from Table 3). The test took place for 336 hours, at radiation intensity (45 ± 5) W/m², BST temperature ($20 +3/-0$) °C and relative humidity inside the chamber (10 ± 5) %. The sum of UVA radiation falling on the surface of the exposed specimens was 55 MJ/m².

After being exposed to UV radiation at an elevated temperature, the objects were taken from the holders and their size was adjusted to 121 x 35 mm, which corresponds to the size of the irradiated area of the object. The modified objects were attached to auxiliary wooden frames and placed into a drying oven according to EN 1296 [19]. Exposure to the elevated temperature took place in accordance with ČSN EN 13 859-1 [11], for a period of 90 days, at the temperature of (70 ± 2) °C, with the air exchange rate of 50 h⁻¹ (see Figure 4).

Test series B, with the same number of test specimens and bodies as series A, was subjected to natural ageing. The test samples were placed on the auxiliary structure (see Figure 5) and exposed to the effects of the external environment, with continuous recording of global solar radiation values and UVA radiation values, using calibrated sensors (see Figure 6). After reaching the total amount of UVA radiation on the exposed samples of 55 MJ/m², the material was removed and test specimens with dimensions of 121 x 35 mm were prepared. The accumulative UVA radiation by date, showing the daily differences, across the total exposure timeline, can be seen in Figure 7.

Test series C consisted of a total of seven test samples, while each test sample was represented by three test specimens for the longitudinal direction (parallel to the direction of production) and three test specimens for the transverse direction. This was a test series whose test samples were not subjected to any ageing and should therefore not show any changes in material characteristics. This series has been included purely for further comparison purposes.

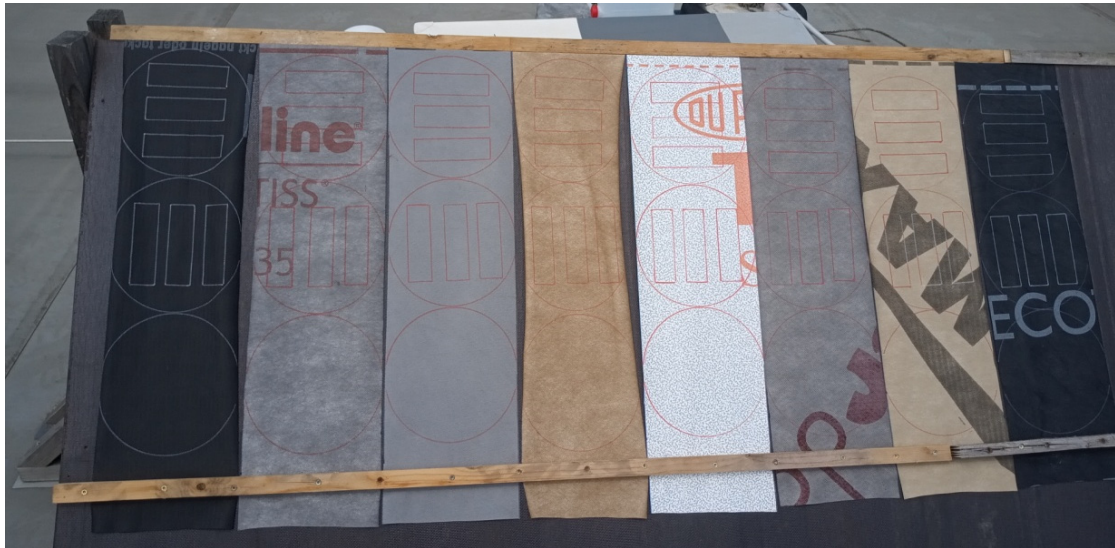


Figure 5. Test samples exposed to external factors.

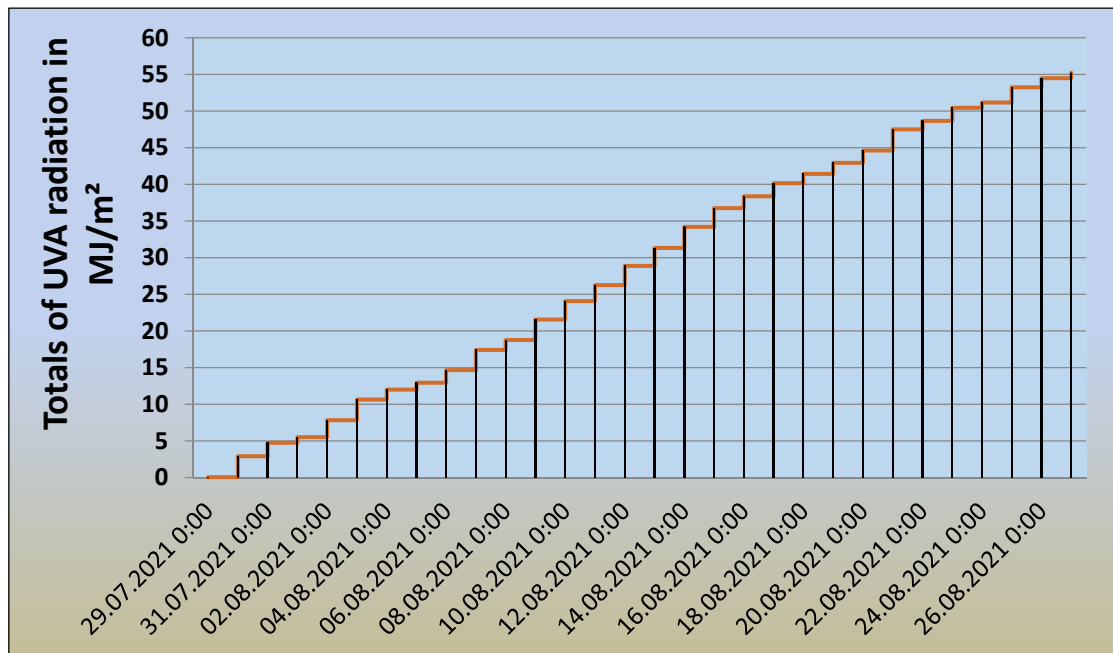


Figure 7. Daily totals of UVA radiation.

After the end of the exposure of the respective test series to artificial and natural aging, the tensile properties of the individual test specimens were verified. The tensile properties test was carried out in accordance with the guidelines of EN 13 859-1 [11], with some minor changes. The first change was the number of test specimens, which was reduced from the original five specimens for each direction (transverse and longitudinal to the production direction) to three test specimens. This reduction was made due to the limited number of exposures available in the Xenotest Alpha+. The second change was the size of the test bodies. While the test standard [11] speaks of test bodies of 100 x 200 mm (+double the length of the body clamping), for the purposes of this work, bodies of size 121 x 35 mm were used. The size of the test bodies was changed

again to ensure the possibility of clamping in the Xenotest Alpha+ test device.

In order to determine the difference between the effects of natural and artificial ageing according to EN 13 859-1 [11], the tensile properties of the tested materials were compared. The first variable compared was the tensile strength. The tensile strengths of the test specimens of series A and B were compared with the tensile strength of the corresponding specimens of the reference series C. The comparison of these strengths was made by determining the difference between the reference and measured values. This difference was then expressed as a percentage of the reference value, and subsequently converted to a point evaluation. The last step was to add up the point evaluations across the test series, whereby the greater the point

gain of the respective series, the greater the change in the tensile strength of the tested material and thus the greater the change in the material itself.

The second variable compared was the elongation (ductility) of the test specimens. The elongation of the individual specimens was first expressed as a percentage of the original length and was then again compared with the elongation values of the specimens of the reference test series C. This comparison was then carried out by determining the difference between the measured and reference values and expressing it in the form of a percentage relative to the higher of the elongation values. (While the tensile strength will decrease after exposure to external influences, due to the degradation of the material, the elongation (ductility) may in some cases also increase. However, this condition also points to a change in the material and should therefore be taken into account. From this the reason is the difference between the measured and reference values of elongation, always relative to the higher value, not always to the reference value.) In the final step of the extension evaluation, the above percentage was expressed as a point rating and all these ratings were summed across the test series. Again, the greater the point gain of the respective series, the greater the change in ductility of the tested material and the greater the change in the overall condition of the material. The last step of the evaluation was the summation of the results of the tensile strength and ductility test within the individual test series. However, it was not possible to simply add up the results of point evaluations. If, for example, the tensile strength results were in the order of hundreds and the elongation results were in the tens (in the

case of tensile strength, the point evaluation was based on the strength of the specimens in newtons, while in the case of ductility, the point evaluation was based on the percentage elongation), after adding up these results, distortion will occur. It was therefore necessary to find a way of expressing the results that would completely eliminate the risk of this distortion. For this reason, the results of point evaluations within the relevant test and the relevant series (e.g. the result of the point evaluation of ductility of series A) were expressed as a percentage of the sum of the results of the relevant test for both series A and B. Furthermore, these shares were added across the series and this sum was expressed as a point rating. By comparing the overall point evaluations of series A and B, the degree of effects of individual methods of exposure was determined.

RESULTS AND DISCUSSION

Figure 8 shows the mean values of the tensile strengths measured for individual test samples across the test series. Each test sample is then represented by two values, depending on the orientation of the test bodies (longitudinal and transverse direction). From this graph it can be seen that, in nine cases the largest strength drops occurred in test series A, in three cases the strength drop between series A and series B was comparable, and in two cases the highest strength drop was recorded in test series B. One of the cases (4TD) even exceeded the tensile strength reference value. However, this excess was only slight (approx. 2 N) and could therefore be characterized as measurement inaccuracy.

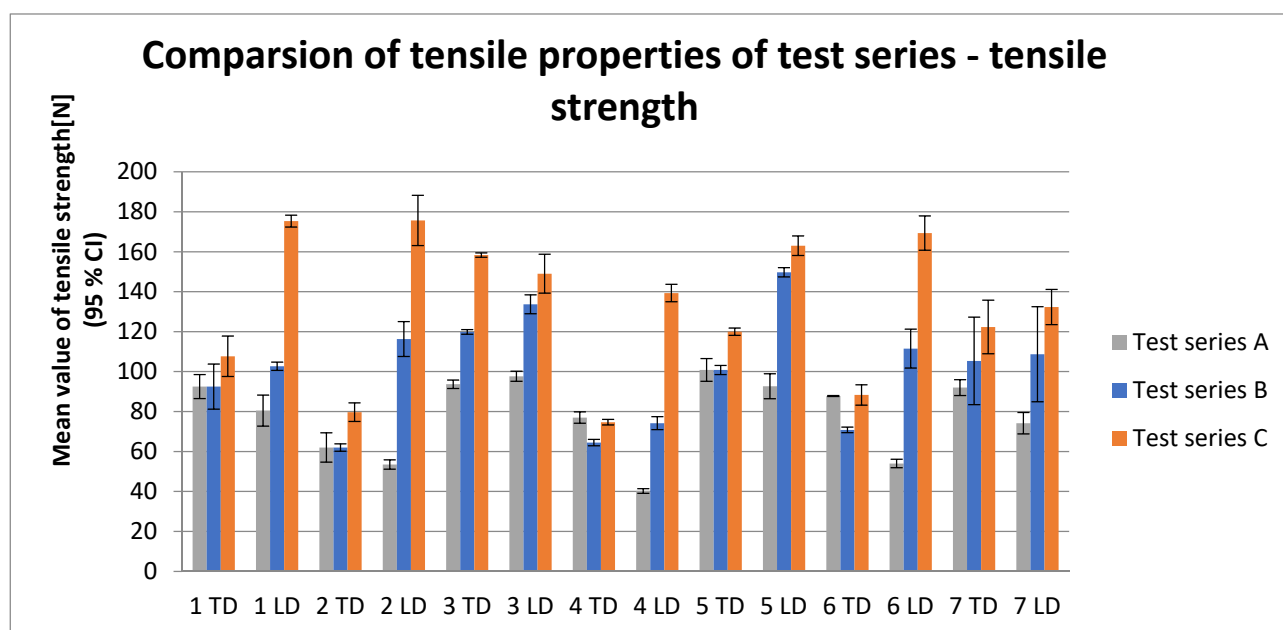


Figure 8. Tensile strength comparison.

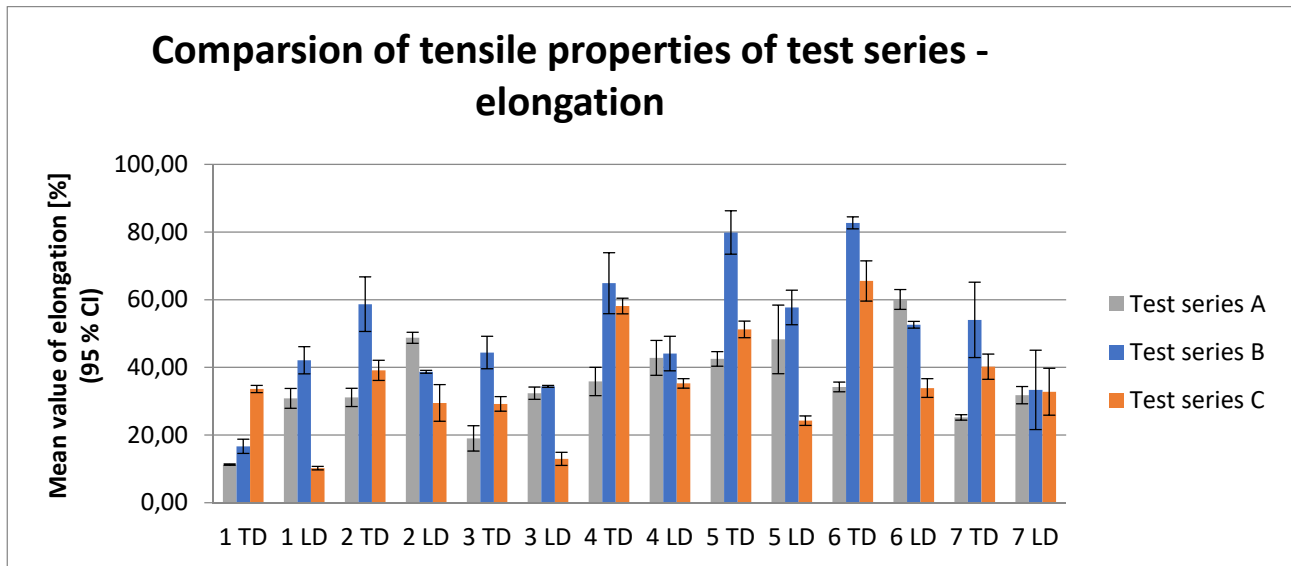


Figure 9. Elongation comparison.

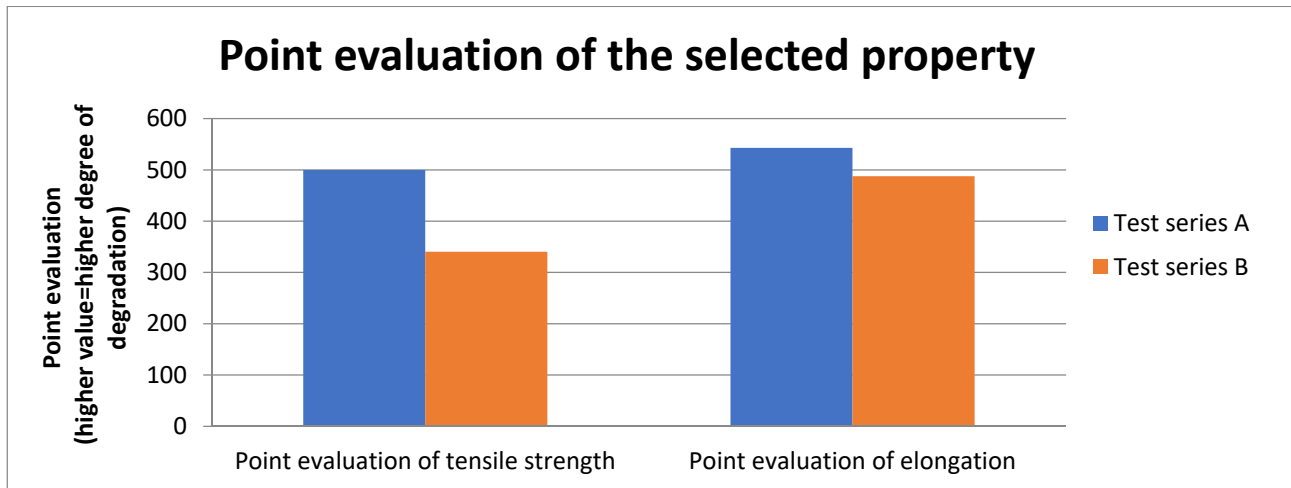


Figure 10. Comparison of point evaluation of tensile strength and elongation.

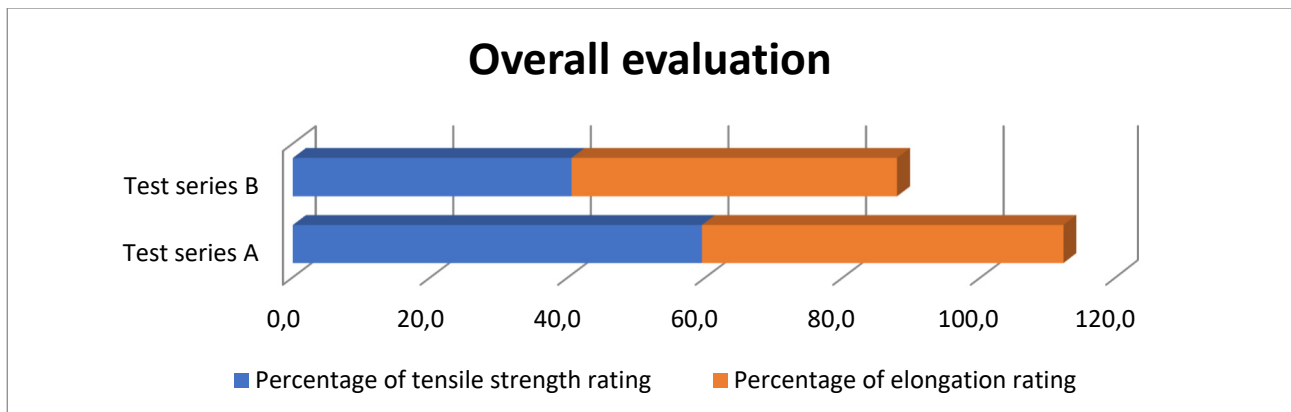


Figure 11. Overall evaluation of exposed ARU.

The elongation of test specimens of individual test samples and series can be evaluated in a similar way. Figure 9 shows the mean values of elongation of individual test specimens. It can be seen from this graph that while in some cases there was an increase in elongation, in some cases it was decreased. Both states are a change compared to the original state and can therefore be considered as indicators of the

influence of the relevant exposure on the ductility of the film.

The decrease in the strength of the test specimens of individual test series, as well as the change in elongation values, can be expressed as a percentage of the reference value (or the higher of the values). If we then convert these percentage shares into a point rating, we can determine the degree of influence of

the relevant exposure on the relevant property of the material by a simple sum of these ratings, across the test series. From Figure 10, it can be seen that test series A showed higher point gains than series B in the evaluation of tensile strength and in the evaluation of elongation, which points to a higher degradation of the material of series A. If we then express these gains as percentages of their sum and these shares are then added up in accordance with the methodology described above, we get the overall point rating of the individual test series and thus also the overall rating of the individual methods of exposure (see Figure 11).

Figure 11 shows that while the total score of the B test series was 87.8 (which accounts roughly for 44 %), the total point score of A test series was 112.2 (which accounts approximately for 56 %). It can thus be stated that the test objects in the A series showed tensile properties by 12 % lower than the objects in the B test series.

The A test series was exposed to artificial ageing according to EN 13 859-1 [11] (UV radiation with the total of 55 MJ/m² and others). The B test series was exposed to natural ageing, which simulated the exposure of the foil on the roof, where the foil was used for temporary covering of the structure. The total UV radiation on the foil surface was equal to the A series (i.e. 55 MJ/m²).

Based on the above, it can be stated that the conditions of artificial ageing determined by the aforementioned standard [11] are less favourable for ARU based on lightweight foil compared to the conditions the foils are normally exposed to in real life (the B test series was exposed to the conditions in summer, when the solar radiation shows the highest intensity. For more details, see e.g. [20]. If the exposure had taken place in a different season, it

would probably be prolonged due to lower daily amounts of radiation. Given the facts described above, the prolonged exposure should not lead to deterioration of material properties of the ARU tested compared to the ARU tested in the summer months for a shorter period of time. It can thus be said that the exposure of the B test series was the least suitable alternative of the above exposure to natural ageing.).

Therefore, if excessive leniency of standard requirements is excluded as a cause of the frequent premature degradation of ARU based on lightweight microporous foils, it can be stated that the only cause possible is an insufficient quality of these materials.

To be completely functional, ARU needs the correct design, and particularly correct installation. This issue has been often encountered in the case of flat roofs. For more details, see e.g. in [21].

In accordance with the aforementioned rules for design and construction of roofs [12], ARU can be divided into three quality classes marked A, B and C. A material that cannot be included in one of these classes is unsuitable to be used for ARU. The rules specify (among others) the tensile strength of material must be classified into one of the above classes (see Table 4), and that the maximum reduction in tensile strength both for transverse and longitudinal direction after the exposure to artificial ageing according to EN 13 859-1 [11] is 35% of the initial strength of the material (i.e. tensile strength of material must be at least 65 % of its initial values, see also Table 3). These rules further determine that the maximum change in the elongation of the material, after artificial aging, is 35% (that is, the elongation of the material must be at least 65% of its original value). The exact value of the permissible elongation is not determined (see Table 4).

Table 6. Requirements for individual qualitative classes of ARU.

Requirements for tensile strength according to EN 13 859-1			
	Class A	Class B	Class C
Before artificial ageing, longitudinal direction	≥250N/50mm	≥200N/50mm	≥120N/50mm
Before artificial ageing, transverse direction	≥200N/50mm	≥150N/50mm	≥110N/50mm
After artificial ageing, longitudinal direction	≥65% ⁱ⁾	≥65% ⁱ⁾	≥65% ⁱ⁾
After artificial ageing, transverse direction	≥65% ⁱ⁾	≥65% ⁱ⁾	≥65% ⁱ⁾
Requirements for elongation according to EN 13 859-1			
Before artificial ageing, longitudinal direction	Should be declared by manufacturer	Should be declared by manufacturer	Should be declared by manufacturer
Before artificial ageing, transverse direction	Should be declared by manufacturer	Should be declared by manufacturer	Should be declared by manufacturer
After artificial ageing, longitudinal direction	≥65% ⁱ⁾	≥65% ⁱ⁾	≥65% ⁱ⁾
After artificial ageing, transverse direction	≥65% ⁱ⁾	≥65% ⁱ⁾	≥65% ⁱ⁾

i) from initial values

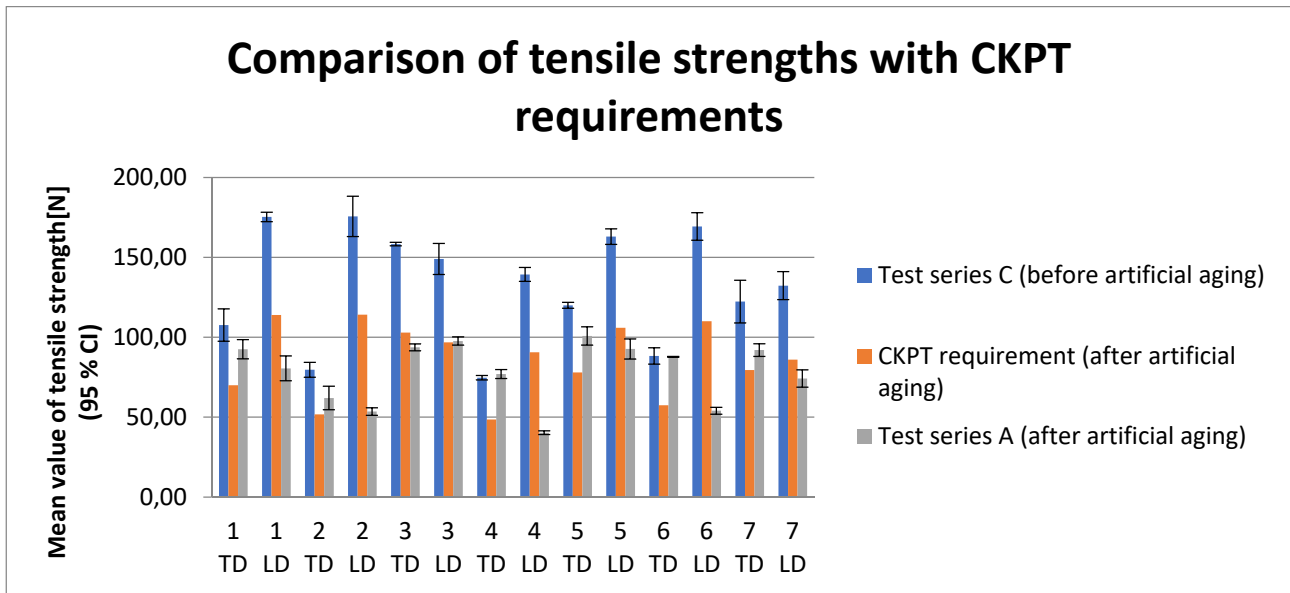


Figure 12. Comparison of tensile strength with CKPT requirements

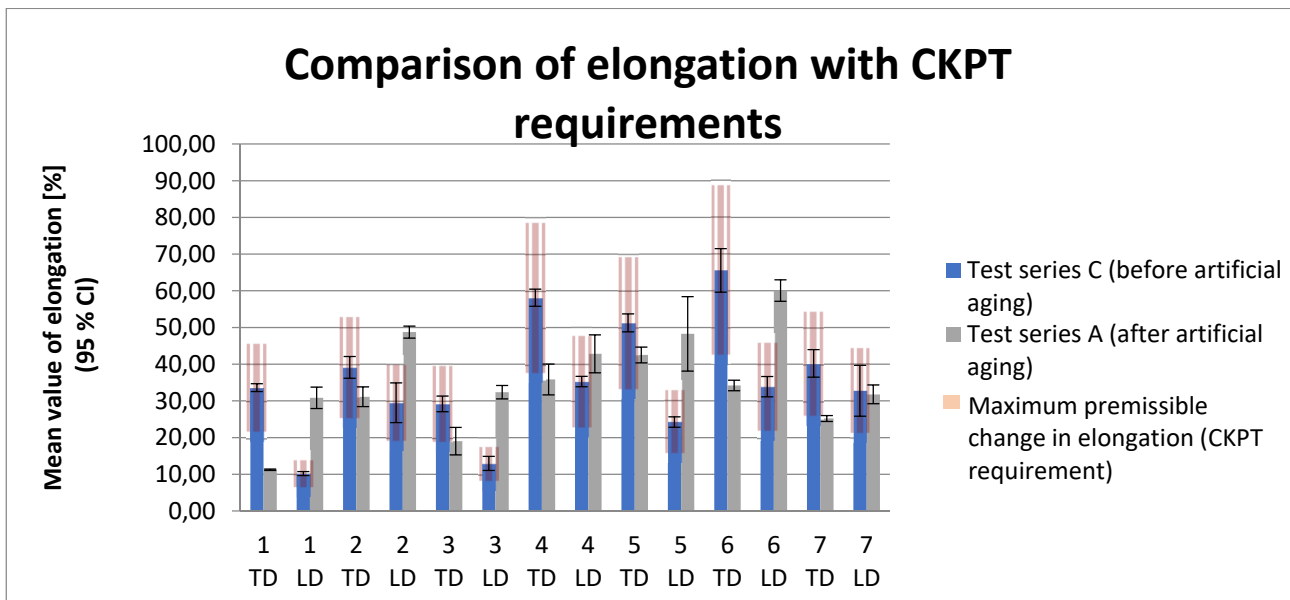


Figure 13. Comparison of elongation with CKPT requirements.

When comparing the required tensile strength values with the values declared by manufacturers, it turns out that two samples can be classified into Class C, four samples in Class B, and one sample in Class A. The comparison of initial tensile strength values (the C test series) and the values measured on test objects after their exposure to artificial ageing (the A test series) showed that none of the samples achieves the required 65 % of the initial values according to the standard (see Figure 12) and cannot thus be classified into one of the quality classes, which means they are not suitable to be used as ARU. The same evaluation of the samples can be done based on the elongation comparison. However, it follows from the facts described in the previous chapter that in the case of stretching, it is not always possible to evaluate only its reduction, but always only its overall change. If we then consider that the

maximum permissible change in material elongation is 35%, it can be said that even in the case of elongation evaluation, none of the test samples met the quality requirements, as well as for tensile strength (see Figure 13).

CONCLUSION

Additional roofing underlays based on lightweight polymeric foils with microporous functional film show a number of advantages, making them one of the most commonly used materials. Their main disadvantage is a limited durability connected with the low resistance against the effect of external factors, predominantly UVA radiation and high temperatures they are often exposed to. European testing standard EN 13 859-1 [11] determines the conditions of artificial ageing, which shall simulate the situation when ARU is embedded in roof cladding and thus

exposed to external factors. These conditions are relatively strict and less favourable than the conditions ARU in common roof cladding can be exposed to. The problem is thus not the leniency of the testing standard but the insufficient quality of the materials supplied to the market as ARU.

There are relatively big differences between individual materials in terms of quality, however final customers still choose a material primarily according to its price; at best (not ideal case), according to its weight. Materials of worse quality and often also cheaper materials do not show the necessary resistance against the effects of external factors and are thus unsuitable for ARU. Some leading manufacturers are aware of this fact and try to inform professionals and the non-expert public about it. However, even some materials from well-known manufacturers (usually, these are materials of the lowest price categories within the product range of a given manufacturer) are not capable of passing the test of artificial ageing and do not show material characteristics that would enable their classification into some of the quality classes applicable for the purposes of ARU.

REFERENCES

1. Kalibatis D., Kovaitis V.: Selecting the most effective alternative of waterproofing membranes for multifunctional inverted flat roofs, *Journal of civil engineering and management*, 23(5), 2017, pp. 650-660. <https://doi.org/10.3846/13923730.2016.1250808>
2. Černohorský M., Havrhlik M.: Water-resistance of nanofiber textiles, *Key Engineering Materials*, 731, 2017, pp. 55-59. <https://doi.org/10.4028/www.scientific.net/KEM.731.55>
3. Wu S., Lei C., Cai Q., et al.: Study of structure and properties of polypropylene microporous membrane by hot stretching, *Polymer bulletin*, 71(9), 2014, pp. 2205-2217. <https://doi.org/10.1007/s00289-014-1182-6>
4. Essah E.A., Sanders Ch., Baker P., et al.: Condensation and moisture transport in cold roofs: effects of roof underlay, *Building research and information*, 37(2), 2009, pp. 117-128. <https://doi.org/10.1080/09613210802645973>
5. Navara T.: Doplnkové hydroizolační vrstvy šikmých střech na bázi fólií lehkého typu, Master Thesis, Institute of Technology and Business in České Budějovice: České Budějovice, 2020.
6. Mazura M.: Ochranné vlastnosti podstřešních fólií. Master Thesis, Technical University of Liberec: Liberec, 2010.
7. Navara T.: Weather impacts on additional roofing underlays for sloping roofs, In proceedings of: 7th World Multidisciplinary Civil Engineering-Architecture-Urban Planning Symposium (WMCAUS 2022), 2022, In press.
8. Účinky zvýšené teploty na pojistnou hydroizolaci pod plechovou střešní krytinou. In: Doerken.com [online]. Praha: Dörkens.r.o. [cit. 2022-06-07]. Available at: https://www.doerken.com/media/docs/cz/05-prospekte/DOE-0000_THERM_Whitepaper_CZ_RZ2_screen.pdf
9. Designing the VEM6075 Into an Application. In: SparkFun Electronics [online]. Niwot, Colorado [cit. 2022-05-30]. Available at: <https://cdn.sparkfun.com/assets/3/9/d/4/1/designingvem6075.pdf>
10. Lewandowski S., Rejsek-Riba V., Bernes A. et al.: Influence of the environment during a photodegradation of multilayer films, *Journal of applied polymer science*, 133(41), 2016, pp. 1-7. <https://doi.org/10.1002/app.44075>
11. EN 13 859-1:2014: Flexible sheets for waterproofing - Definitions and characteristics of underlays: Part 1: Underlays for discontinuous roofing. Brusel: European Committee for Standardization, 2014.
12. CKPT - Cech klempířů pokrývačů a tesařů ČR: Pravidla pro navrhování a provádění střech: Základní pravidla pro provádění střech. Praha: Machart, 2014.
13. ZVDH, Zentral Verband des Deutschen Dachdeckerhandwerks: Deutsches Dachdeckerhandwerk - Regeln für Dachdeckungen. Köln: Rudolf Müller, 2022.
14. Fechner, O., Vogdt J.: Resistance to driving rain of pitched roof structures - German and European assessment methods for rain penetration into tiled roofs and the resistance to driving rain of covering underlays and self-supporting underlays, *Bauphysik*, 30(2), 2011, pp. 66-74. <https://doi.org/10.1002/bapi.200810011>
15. Lindfors T., Bjork F.: Performance of modern products for underlay in residential buildings, *Construction and Building Materials*, 11(2), 1997, pp. 109-118. [https://doi.org/10.1016/S0950-0618\(97\)00003-2](https://doi.org/10.1016/S0950-0618(97)00003-2)
16. Flaig, R.: Odolnost pojistných hydroizolačních fólií (DHV) proti stárnutí, *Střechy-Fasády-Izolace*, 2022(6), 2022, pp. 38-1.
17. EN ISO 4892-2: 2013 Plastics - Methods of exposure to laboratory light sources: Part 2: Xenon-arc lamps. Brusel: European Committee for Standardization, 2013.
18. EN 1297: 2004 Flexible sheets for waterproofing - Bitumen, plastic and rubber sheets for roof waterproofing: Method of artificial ageing by long term exposure to the combination of UV radiation, elevated temperature and water. Brusel: European Committee for Standardization, 2004.
19. EN 1296: 2001 Flexible sheets for waterproofing - Bitumen, plastic and rubber sheets for roofing.: Method of artificial ageing by long term exposure to elevated temperature. Brusel: European Committee for Standardization, 2001.
20. Plachý J., Vysoká J.: Surface temperature of flat roofs with waterproofing polymer membranes, *Materials Science and Engineering*, 728, 2020. <https://doi.org/10.1088/1757-899X/728/1/012006>
21. Šutliak, S., Plachý J.: Diagnostics of Flat Roofs with Flexible Sheets for Waterproofing. *Materials Science and Engineering*, 728, 2020. <https://doi.org/10.1088/1757-899X/728/1/012004>

TEAR AND TENSILE STRENGTH OF 100% COTTON WOVEN FABRICS' BASIC STRUCTURES: REGRESSION MODELLING

HOSSAIN, MOHAMMAD MOBARAK^{1*}; ALIMUZZAMAN, SHAH² AND AHMED, DEWAN MURSHED²

¹ Department of Textile Engineering, Jashore University of Science and Technology (JUST), Jashore, Bangladesh

² Department of Fabric Engineering, Bangladesh University of Textiles (BUTEX), Dhaka, Bangladesh

ABSTRACT

This research paper aims to estimate the tear and tensile strength of woven fabrics while considering a number of construction factors. Construction variables include ends per cm (EPCm), picks per cm (PPCm), an overall configuration of yarn, and fabric's areal density or grams per square meter (GSM). While the statistical relationship in deciding the fabric strength is very complicated considering all variables, the correlation-regression model is used to explain the influence of structural parameters on the tear and tensile strength of various fundamental fabrics' designs. With different thread densities varying reed counts, and heald count using 100 percent cotton yarn having 36.9 tex, eight different designs of plain, twill, and sateen are prepared for the study. Four regression models, built to predict the tear and tensile strength of the sample woven fabrics, are vital components of this research. It is noticed that the setting of yarn affects the tensile strength of the fabrics, and the fabric pattern determines the tear strength of the fabrics. For higher tear strength, matt weave, and tensile strength, a twill structure is desired within this scope of the fabric structures.

KEYWORDS

Tear; Tensile; Strength; Woven; Regression; Modelling, Prediction.

INTRODUCTION

Strength is the first property that has the most significant effect when choosing the necessary fabrics to produce clothing or apparel. These are based mainly on the expected end-use [1]. The tensile and tear behavior of the fabric depends not only on the strength of the yarn alone but also on other variables, including the use of fiber or blend form, twist amount, twist angle, yarn count, spinning systems, yarn bending behavior, frictional properties, interlacement pattern, fabric construction parameters, series of warp and weft, finishing treatment etc. [2]. The geometry of the fabric, thread density, and weaving design also have a significant effect on the strength of the fabrics. The strength also be influenced based on the production state during wet processing and finishing treatment [3-5]. Also, test conditions such as temperature, humidity, loading time, loading quantity, jaw distance, and measuring methods often influence the difference in the intensity of the fabric value. For all these controllable and uncontrollable variables relevant to fiber, yarn, and fabric during production cycles, creating a simple direct quantitative connection between the yarn's intensity and the fabric's corresponding strength is quite complicated. In this respect, it is crucial to identify the right ways to decide

the parameters before manufacturing fabrics to ensure the tremendous loss of supplies, time, electricity, labor, and money [2-6].

Different fabric manufacturing processes, such as spinning, knitting, non-woven, and braiding, are available [7]. Strong dimensional stability and good cover are seen between them by woven fabric. Strength is one of the most significant features of woven fabric [8]. In stretching a test piece to a breaking point, the highest tensile force measured is called tensile strength or breaking strength. Tearing intensity is the average force needed to continue a tear already begun in a fabric [9]. During the tearing test, threads break singly or in small clusters. Threads that have been twisted skew and slide. The strain is first carried by a few strands. The adjacent yarn also fails. Yarns may cluster around the tear due to increased extensibility or fewer frictional restrictions, however yarn strength may not improve tear strength. Again, breaking force is determined by area. Tensile force at the point of rupture is referred to as tenacity. Tensile strength of fabrics is affected by yarn density and cross-section of fabrics itself and yarn from which it is composed of. Thread density and oblique yarn orientation need more efforts to balance the weight. Crimping causes yarn to stretch. More crimp extends the cloth. Floats increase thread density while

* Corresponding author: Hossain M.M., e-mail: mobaraknits89@gmail.com

Received October 8, 2022; accepted February 3, 2023

decreasing extension. Weaving decreases fabric extensibility by tightening the warp and weft and tensile strength fell [10].

These two strengths (tear and tensile) had different application in the textile field to produce fabrics considering wear and tear resistance and produce higher tensile strength in technical textiles manufacturing. However different research approached are done in predicting these strength properties in different way. Multiple linear regression (MLR), artificial neural network (ANN), Automated Machine Learning (AutoML), and Fuzzy techniques are some preferred tools that have been used to predict the strength of the fabric of composite fabric considering different variations in count, thread density (warp and weft), inter- yarn friction, float length, interlacing points, design (plain, twill, matt), loading direction (uniaxial or biaxial), fiber composition (single or blends), fiber composition (single/blends), spinning (ring/rotor), yarn strength transfer efficiency etc. [11-14]. When utilizing hidden layers in prediction models, machine learning approach outperformed regression method in prediction using learnt data [15]. However, the input parameters consideration and design variation cannot be included as a whole in modeling for incapability in numerical or weighted value expression. Because various weave designs might have the same float length or yarn densities [10].

To know the effect of design variation (basic plain, twill and sateen) on tensile and tear strength of woven fabrics having similar loom setting and yarn properties within the smallest repeat sizes, this experiment is performed. Although machine learning approach is better this experiment only used multiple linear regression tool primarily to investigate the found result from testing the sample fabrics produced in this study with the relation of considered parameters. Here, the primary objective of this research is to forecast woven fabrics considering various construction variables. Ends per cm (EPCm), picks per cm (PPCm), maximum yarn setting, and cloth areal density in gram per square meter (GSM) are considered to be primary factors. At the same time, numerous researchers have established different fabric weaving factors [10, 16]. But there are too many considerations linked to the strength of the fabric, such as yarn count, twist, fiber fineness, rigidity, fiber density, the shape of the fabrics, cover, yarn density, layer number, tightness factor, and so on [17].

The objectives of the study are to develop four regression models to predict both warp and weft way tear strength as well as warp and weft tensile strength of woven fabrics having eight different weave structures of plain, twill, and sateen. The objectives of the study are mentioned below:

- To explore the effect of loom settings on output variables warp way (Y1) and weft way (Y2) tear strength and warp way (Y3) and weft way (Y4) tensile strength.
- To explore the effect of design types on output variables warp way (Y1) and weft way (Y2) tear strength and warp way (Y3) and weft way (Y4) tensile strength.
- To investigate the effect of "EPCm, PPCm, Law's maximum thread density and GSM with output variables warp way (Y1) and weft way (Y2) tear strength and warp way (Y3) and weft way (Y4) tensile strength.

Due to the difficulty of integrating all those variables to represent the configuration of the weave, the correlation-regression tool and ANOVA are used to explain the influence of structural parameters of fabrics on the tear and tensile strength of fabrics with various fundamental designs. Regression tools are used to evaluate study theories that have been established from literature reviews [18]. And after checking approaches [19], the impact of yarn environment and design styles on the intensity of fabrics is observed. Finally, predictors such as PPCm, EPCm, GSM, and Law's maximum yarn setting of the sample woven fabrics are provided by four regression models. Here following effects in alternate hypothesis statements are analyzed statistically:

H1-H8: There is a significant difference in yield of warp way tear strength (Y1), weft way tear strength (Y2), warp way tensile strength (Y3), and weft way tensile strength (Y4) for different loom settings (H1,H2, H3, H4 respectively) and similarly across design types (H5, H6, H7, H8 respectively).

H9-H12: EPCm (H9), PPCm (H10), Law's max yarn set (H11), and GSM (H12) have significant effect on warp way tear strength (Y1).

H13-H16: EPCm (H13), PPCm (H14), Law's max yarn set (H15), and GSM (H16) have considerable impact on weft way tear strength (Y2).

H17-H20: EPCm (H17), PPCm (H18), Law's max yarn set (H19), and GSM (H20) have significant effect on warp way tensile strength (Y3).

H21-H24: EPCm (H21), PPCm (H22), Law's max yarn set (H23), and GSM (H24) have considerable impact on weft way tensile strength (Y4).

EXPERIMENTAL METHODOLOGY

Materials

36.9 Tex, 100% cotton rotor yarn is used to manufacture woven fabrics. It has a lea strength of 81.93 kg at 25 0C with 78% relative humidity in the testing lab. Single yarn strength is 5.6 N, with 6.9%

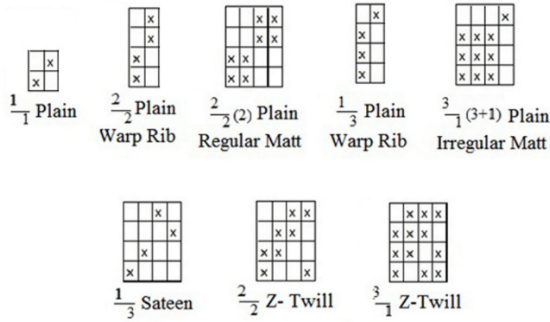


Figure 1. Fabrics' design repeats used in this experiment.

breaking extension and tenacity is 15 cN/Tex. As the interlacement ratio of plain, twill, and satin fabric differs in various way, and their stiffness are affected by the angle of weaving, in this experiment, fabrics structures for eight woven designs, namely $\frac{1}{3}$ sateen, $\frac{2}{2}$ z-twill, $\frac{3}{1}$ z-twill, $\frac{1}{1}$ plain, $\frac{2}{2}$ plain warp rib, $\frac{2}{2}(2)$ plain regular matt, $\frac{3}{1}$ plain warp rib and $\frac{3}{1}(3+1)$ plain irregular matt are prepared. For data processing in the statistical tools following descriptions are used to represent types of fabrics (Fig. 1).

Finally, 8 (Designs) \times 3 (Loom Setting) = 24 samples are being tested according to the testing methods. To produce these fabrics, 40 Stockport reed drawing 2 in a dent (40 heald count) and 60 Stockport reed drawing 1 in a dent (30 heald count), and 2 in a dent

(60 heald count) in Automated Sampling Rapier Loom (CCI Tech Inc.). For collecting tear ($5 \times 2 \times 24 = 240$) and tensile strength ($5 \times 2 \times 24 = 240$) in both warp and weft direction " $240 + 240 = 480$ " specimens are produced, tested and average values are recorded in Table 2.

Instruments

Lea strength tester, single yarn tester (Pytan), Automated Sampling Rapier Loom (CCI Tech Inc.), universal tensile tester (Titan 500 Newton) and Elma tear tester (133 N), wrap reel and weight balance (yarn count test method), and twist tester are used in this experiment. All data is recorded in a single working sheet then the relation among the factors of fabrics is analyzed using a graphical method, SPSS 23, and R-Studio software.

Standards and methods for testing

Single yarn strength, fabrics' tear, and tensile strength are tested as ASTM D2256/D 2256M:2010 [20], Elma Tear with max load 133 N as ISO 13937-1:2000 [21], and Universal Tensile Tester as ISO 13934-2:2014 [22] respectively. 5 breaks are performed both for warp and weft direction with similar setting and speed. The machine speed of tensile testing is 50 mm/min. After enzymatic desizing, washing for 25 min at 50 °C temperature with 1 ml detergent, the samples were dried and relaxed for 72 hours before testing.

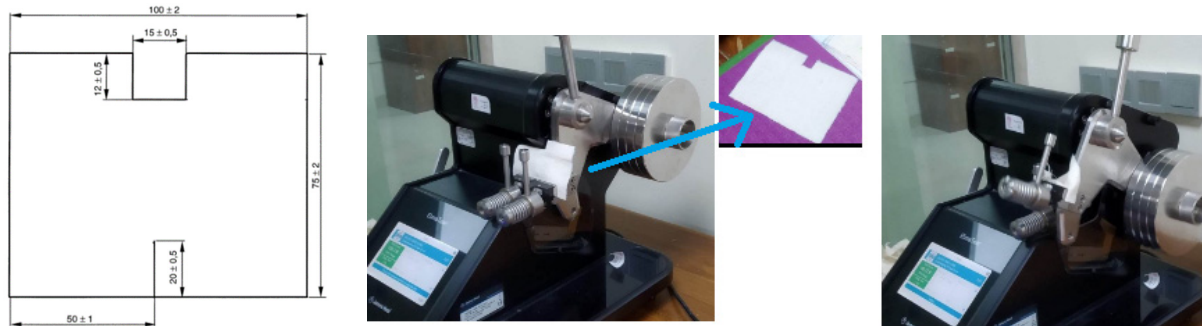


Figure 2. Fabric tear strength testing specimen size and testing [21].

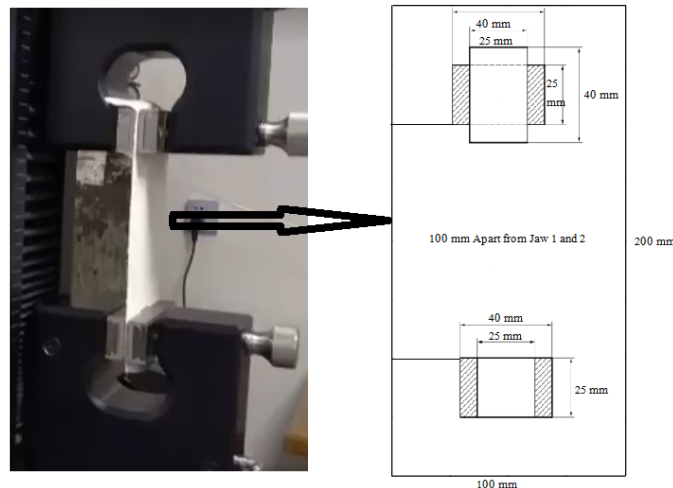


Figure 3. Fabric tensile strength testing specimen size and testing [22].

Table 1. Some symbols and their meanings in this experiment.

Y_i	Warp way tear strength (Y1), Weft way tear strength (Y2), Warp way tensile strength (Y3), Weft way tensile strength (Y4)	$laws_{yarnset}^{max}$	$S(yN)^{1/2}$ Where, S= setting ratio varying with weave upto 4 float, y =cloth setting constant depends on yarn numbering system, N indirect count of yarn	F	t-test value
β_{0-4}	Constant for regression models	gsm	Gram per squar meter (GSM)	p	Probability value
ϵ	Error term	R and Adjusted R^2	Reliability of the beta values	H1-H24	Research Hypothesis
EPCm	Ends per centimeter	W	Shapiro-Wilk values		
PPCm	Picks per centimeter	df	Degree of freedom		

Variables

Dependent variables are warp way (Y1) and weft way (Y2) tear strength and warp way (Y3) and weft way (Y4) tensile strength of the fabrics. Again, independent variables are EPCm, PPCm, GSM, and Law's max yarn set. $\frac{1}{1}$ plain, $\frac{2}{2}$ plain warp rib, $\frac{2}{2}$ (2) plain regular matt, $\frac{3}{1}$ plain warp rib, $\frac{3}{1}$ (3 + 1) plain irregular matt, $\frac{2}{2}$ z-twill, $\frac{3}{1}$ z-twill, and $\frac{1}{1}$ sateen structure of fabric 1/1P, 2/2P, 2/2(2)P, 3/1 P, 3/1(3+1)P, 2/2T, 3/1T, and 1/3S are used respectively for software processing in R-studio 3.6 and SPSS 23. Some symbols and their meaning are enlisted in Table 1.

Statistical methods

Following statistical analyses were conducted throughout this study:

1. The level of significance for all hypotheses was taken as $\alpha = 5\%$. A p-value less than α indicates the test's significance (i.e., reject the null hypothesis).
2. Shapiro -Wilk test was performed to check whether response/output variables and residuals of the regression model are normally distributed or not.

The hypothesis statement of the Shapiro -Wilk test is given below:

H_0 : Variable or data is normally distributed

H_a : Variable or data is NOT normally distributed

3. Two-way ANOVA was conducted to understand the effect of fabric setting and design type on output variables. A p-value less than α indicates a significant impact.
4. Multiple linear regression techniques were applied to assess the effect of five predictor variables like EPCm, PPCm, Laws maximum yarn setting, and GSM on output variables. A p-value less than α indicates the model's significance and significant individual effect of each predictor variable. For four response variables, four separate regression models was developed:

$$Y_i = \beta_0 + \beta_1 (\text{EPCm}) + \beta_2 (\text{PPCm}) + \beta_3 (\text{Law's maximum yarn setting}) + \beta_4 (\text{GSM}) + \epsilon; i = 1, 2, 3, 4 \quad (1)$$

where in each model, the error term ϵ is assumed to be normally distributed with mean 0 and constant variance σ_e^2 .

RESULTS AND DISCUSSION

In this section effect of the design or changing of fabrics' structures and loom settings on tear and tensile strength are tested by two-way ANOVA. Then, by regression analysis four specific models are prepared using EPCm, PPCm, Law's maximum yarn setting, and GSM as influencing factors of the fabrics where other factors assumed constant during production of the fabrics samples. Considering constant yarn properties like yarn count, fiber consumptions, twist per inch the loom setting changed within Stockport reed count 30 with 1 and 2 yarn per dent, and Stockport reed count 40 with single yarn drawn per dent. The data set is summarized in Table 2.

Two-way ANOVA of strength (Y1-Y4) for loom setting and design name

A two-way ANOVA was conducted to determine if there is a difference in average "OUTPUT" with loom setting and design type (derivatives of plain, twill and sateen) which is mentioned as 'design_name' variable here from 'table 3' to 'table 6'. Since there are four output variables warp way tear strength (Y1), weft way tear strength (Y2), warp way tensile strength (Y3), and weft way tensile strength (Y4) in this study, so four two-way ANOVA have been performed separately.

Table 3 indicates that the loom setting's main effect is insignificant, $F(2, 14) = 0.92$, $p = 0.42$, which means that the average warp way tear strength (Y1) is almost the same for the three loom setting. The main effect of the fabric design is significant, $F(7, 14) = 2.89$, $p = 0.04$; that is average warp way tear strength (Y1) differs significantly from design to design, and the highest average of warp way tear strength (Y1) was yielded for design $\frac{2}{2}$ (2) plain matt.

Table 2. Data summary for tear and tensile strength in warp and weft way due to different design and loom setting.

Loom Setting	Design Name	EPCm	PPCm	Law's Max Thread Density	GSM	Tear Strength (N)*		Tensile Strength (N)*	
						Warp way	Weft Way	Warp way	Weft Way
Reed Count (Stock Port) 60 and Heald Count 30	$\frac{1}{1}$ Plain	15	14	22	132.47	56.390	64.011	158.678	159.551
	$\frac{2}{2}$ Plain Warp Rib	14	14	30	128.95	92.132	78.373	144.548	130.681
	$\frac{2}{2}$ (2) Plain Regular Matt	16	13	30	135.49	100.950	103.010	141.525	111.855
	$\frac{3}{1}$ Plain Warp Rib	15	14	33	143.98	62.296	76.838	155.143	115.397
	$\frac{3}{1}$ (3+1) Plain Irregular Matt	17	14	33	147.29	75.424	70.724	159.277	104.566
	$\frac{2}{2}$ Z-twill	16	14	30	143.28	80.386	88.242	142.465	132.514
	$\frac{3}{1}$ Z-twill	15	14	33	134.27	84.252	88.754	138.579	123.679
	$\frac{1}{3}$ Sateen	17	14	33	146.97	81.405	92.152	142.964	136.200
Reed Count (Stock Port) 40 and Heald Count 40	$\frac{1}{1}$ Plain	19	17	22	158.68	39.681	48.406	252.439	239.639
	$\frac{2}{2}$ Plain Warp Rib	21	18	30	179.08	105.640	85.288	238.676	187.382
	$\frac{2}{2}$ (2) Plain Regular Matt	20	17	30	169.26	106.390	102.505	209.917	194.409
	$\frac{3}{1}$ Plain Warp Rib	20	18	33	181.52	108.470	84.684	242.757	184.091
	$\frac{3}{1}$ (3+1) Plain Irregular Matt	21	18	33	178.73	93.060	95.304	209.777	184.762
	$\frac{2}{2}$ Z-twill	20	18	30	171.35	96.719	100.558	233.029	208.370
	$\frac{3}{1}$ Z-twill	20	18	33	179.17	83.534	90.806	230.675	216.376
	$\frac{1}{3}$ Sateen	21	18	33	183.73	72.418	85.810	207.945	238.204
Reed Count (Stock Port) 60 and Heald Count 60	$\frac{1}{1}$ Plain	25	24	22	218.11	18.858	32.798	405.833	338.846
	$\frac{2}{2}$ Plain Warp Rib	26	25	30	219.36	63.872	56.667	428.512	341.938
	$\frac{2}{2}$ (2) Plain Regular Matt	25	25	30	210.38	100.408	104.193	371.480	333.181
	$\frac{3}{1}$ Plain Warp Rib	26	25	33	215.67	122.200	64.117	388.311	330.500
	$\frac{3}{1}$ (3+1) Plain Irregular Matt	27	26	33	220.32	132.810	129.400	357.948	357.381
	$\frac{2}{2}$ Z-twill	26	26	30	224.45	59.613	72.977	392.879	366.607
	$\frac{3}{1}$ Z-twill	26	25	33	223.05	47.421	48.136	319.733	440.507
	$\frac{1}{3}$ Sateen	27	26	33	229.65	41.407	71.366	374.405	360.847

Note: * mean values are taken from 5 tests.

From 'Table 4' it is seen that as weft way tear strength (Y2) the main effect of loom setting is not significant, $F(2,14)=1.59$, $p=0.24$, implying that average weft way tear strength (Y2) does not differ significantly across loom setting. Whereas the main effect of the fabric design is significant, $F(7,14)=3.20$, $p=0.03$. So, it can be said that design has an impact on weft way tear strength (Y2) and design $\frac{2}{2}$ (2) plain matt had the highest average yield.

In the same procedure, two-way ANOVA was carried out, and the result is displayed in 'table 5'. The main effect of the loom setting is very significant on the yield of Y3, $F(2,14)=316.9$, $p=0.00$. The highest average of warp way tensile strength (Y3) is obtained for loom setting 2. On the other hand, the fabric design effect is insignificant; the average yield of warp way tensile strength (Y3) is almost the same for eight designs with same loom setting, $F(7,14)=2.07$, $p=0.12$.

Table 3. Response variable warp way tear strength (Y1).

Source of variation	Df	Sum Square	Mean Square	F	p
Loom Setting	2	903.99	451.99	0.92	0.42
design_name	7	9963.02	1423.29	2.89	0.04
Residuals	14	6890.9	492.21		
Total	23	17757.9			

Table 4. Response variable weft way tear strength (Y2).

Source of variation	Df	Sum Square	Mean Square	F	p
Loom Setting	2	862.7	431.34	1.59	0.24
design_name	7	6064.3	866.33	3.20	0.03
Residuals	14	3791.0	270.79		
Total	23	10718.0			

Table 5. Response variable warp way tensile strength (Y3).

Source of variation	Df	Sum Square	Mean Square	F	p
Loom Setting	2	222090.7	111045.3	316.9	0.00
design_name	7	5084.9	726.4	2.07	0.12
Residuals	14	4906.3	350.5		
Total	23	232081			

Table 6. Response variable weft way tensile strength (Y4).

Source of variation	Df	Sum Square	Mean Square	F	p
Loom Setting	2	222103	111052	210.45	0.00
design_name	7	7252	1036	1.96	0.13
Residuals	14	7388	528		
Total	23	236743			

Thus, from Table 3 to Table 6 hypotheses H3, H4, H5 and H6 are accepted. On the other hand, hypotheses H1, H2, H7, and H8 are rejected. Thus it is proved that loom setting variation in yarn setting influences the tensile strength of fabrics and design variation influences the tear strength of the fabrics. Thus, an increase in the yarn setting greatly affects the fabric's tensile strength change. The more yarn present in the fabric tensile strength will be high. Again, whether the number of yarns more or less design variation influences its tear strength. The more floats of yarn are present in the fabrics, the more the tear strength. It also supports the result found by Eryuruk S.H. and Kalaoğlu F. [23] that weft tearing strength values found greater than the warp tearing strength and change in tear strength as the number of threads per metre in either direction. Again the thread densities improves the tensile strength [24-25].

As a result of the inability to present fabric design in numerical numbers such as EPCm, PPCm, and

GSM, Law's maximum thread density in 'table 1' is the term used in regression models due to its consideration of fabric design in its formula to limit the maximum yarn density for specific yarn count and fabric design. A drawback of the research is that the fundamental design and its derivatives cannot be separated with distinct justified numerical values to consider in the regression models which is a scope of further research. Thus, design parameters and their numerical expression needs to be further analyzed. Law's max yarn set is the term that consider both the yarn representing unit and basic fabric design variation that improves the model prediction strength in this regard [10].

Regression models with ANOVA

Regression Model 1: Dependent variable warp way tear strength (Y1)

$$\hat{Y}_1 = 16.367 + 20.629 * \text{EPCm} + 2.46 * \text{PPCm} + 4.695 * \text{laws}_{\text{max yarnset}} - 3.095 * \text{gsm} \quad (\text{A})$$

Regression Model 2: Dependent variable weft way tear strength (Y2)

$$\hat{Y}_2 = 33.258 + 13.816 * \text{EPCm} + 0.754 * \text{PPCm} + 3.509 * \text{laws}_{\text{max yarnset}} - 2.015 * \text{gsm} \quad (\text{B})$$

Regression Model 3: Dependent variable warp way tensile strength (Y3)

$$\hat{Y}_3 = -20.290 - 2.102 * \text{EPCm} + 16.877 * \text{PPCm} - 4.549 * \text{laws}_{\text{max yarnset}} + 0.755 * \text{gsm} \quad (\text{C})$$

Regression Model 4: Dependent variable weft way tensile strength (Y4)

$$\hat{Y}_4 = -84.04 - 1.665 * \text{EPCm} + 18.872 * \text{PPCm} - 2.729 * \text{laws}_{\text{max yarnset}} + 0.419 * \text{gsm} \quad (\text{D})$$

Regression Model 5: Dependent variable log weft way tensile strength (log(Y4))

$$\log(\hat{Y}_4) = 1.753 + 0.006 * \text{EPCm} + 0.022 * \text{PPCm} - 0.009 * \text{laws}_{\text{max yarnset}} + 0.002 * \text{gsm} \quad (\text{E})$$

From Table 7, the overall impact of independent variables significantly impacts warp way tear strength (Y1). However, the estimated model can explain a 79.7% variation in warp way tear strength (Y1). The model residuals are also normally distributed, $W=1.880$, $p=0.009$, which indicates the excellent fit of the model.

Again, The overall model 2 (model B) is significant, $F(4,19)=4.579$, $p=0.009$. The estimated model can explain a 70.1% variation of weft way tear strength (Y2). The model residuals are also normally distributed, indicating a well-fitted model, $W=2.238$, $p=0.018$.

Table 7. ANOVA for regression models.

ANOVA for regression	Source of variation	Df	Sum Square	Mean Square	F value	Model Summary
Model 1 of Y1 (A)	Regression	4	8729.966	2182.491	4.593	R=0.701, Adjusted R ² =0.385, W = 1.880, p-value = 0.009
	Residuals	19	9027.946	475.155		
	Total	23	17757.912			
Model 2 of Y2 (B)	Regression	4	4813.391	1203.348	3.872	R=0.670, Adjusted R ² = 0.333 , W = 2.238, p-value = 0.018
	Residuals	19	5904.616	310.769		
	Total	23	10718.007			
Model 3 of Y3 (C)	Regression	4	223540.839	55885.210	124.32	R= 0.981, Adjusted R ² =0.955, W = 2.036, p-value = 0.000
	Residuals	19	854.991	449.526		
	Total	23	232081.830			
Model 4 of Y4 (D)	Regression	4	222607.584	55651.896	74.804	R=0.970, Adjusted R ² =0.928, W = 1.066, p-value = 0.000
	Residuals	19	14135.373	743.967		
	Total	23	236742.957			
Model 5 of Y5 (E)	Regression	4	0.821	0.205	75.45	R= 0.97, Adjusted R ² = 0.928, W = 1.427, p-value = 0.000
	Residuals	19	0.052	0.003		
	Total	23	0.873			

On the other hand, to investigate the overall impact of EPCm, PPCm, Law's maximum yarn setting, GSM on warp way tensile strength (Y3); model 3(C) has been fitted. The fitted model is highly significant, $F(4,19)=124.32$, $p=0.000$. The $R=0.981$ implies that the fitted model can predict a 98.1% variation in warp way tensile strength (Y3). The model's residual (C) is normally distributed, $W=2.036$, $p=0.000$.

Though, model 4 (D) is overall significant, $F(4,19)=74.804$, $p=0.000$, but the residuals are not normally distributed, $W=1.066$, $p=0.000$. This may be due to functional misspecification of the model. So, another model is developed taking the logarithm of weft way tensile strength (Y4). Now, semi-log model 5 (Model E) is highly significant, $F(4,19)=75.45$, $p=0.000$ and the model's residuals are also normally distributed, $W=1.427$, $p=0.000$. The estimated model can explain 97.0% variation in weft way tensile strength (Y4).

Table 8 indicates that EPCm has a positive and very significant effect on warp way tear strength (Y1), $t(19)=2.547$, $p=0.020$. The impact of the law's maximum yarn setting on warp way tear strength (Y1) is positive and highly significant, $t(19)=3.490$, $p=0.002$. The effect of GSM on warp way tear strength (Y1) is negative and highly significant, $t(19)=-2.892$, $p=0.009$. Moreover, PPCm has positive impact but is not statistically significant. Thus, hypotheses H9, H11, and H12 are accepted, whereas H10 is rejected. But their overall effect made the model satisfactory with the goodness of fit.

Again, EPCm, Law's maximum yarn setting, and GSM significantly affect weft way tear strength (Y2) ($p=0.048$, 0.004 , 0.031 , respectively). Thus,

hypotheses H13, H15, and H16 are accepted, whereas H14 is rejected. But their overall effect made the model satisfactory with the goodness of fit.

On the other hand, it also indicates that PPCm has a significant positive effect, and Law's maximum yarn setting significantly negatively impacts warp way tensile strength (Y3) where $p=0.003$, $p=0.003$, respectively. Other variables' impacts are not significant. Thus, hypotheses H18 and H19 are accepted, whereas H17 and H20 are rejected. But their overall effect made the model satisfactory with the goodness of fit.

The interpretation of the estimated coefficient of the semi-log model differs from the linear model. "Table-8" implies that the yield of weft way tensile strength (Y4) increases at a rate of 0.022 for a unit of PPCm, or 2.2%. Interpretation of other coefficients is in the same manner. Again, the yield of weft way tensile strength (Y4) decreases at a rate of 0.009 for a unit of Law's max yarn setting or 0.9%. But they have a very significant effect on the yield of weft way tensile strength (Y4). Thus, hypotheses H22 and H23 are accepted, whereas hypotheses H21 and H24 are rejected. But their overall effect made the model satisfactory with the goodness of fit.

Fractional changes of strength based on design

According to float length, it can be said that the float length of the fabric significantly affects tear strength. With the increased float length, more yarns are close to each other, thus increasing tear strength. But, it is not clearly said from the data the effect of change in float length how the tensile strength changes as it

Table 8. Regression coefficients for models.

Regression coefficients	Variables/predictor	Estimate	Std. Error	t value	Pr(> t)
Model Y1 (A)	(Intercept)	16.367	46.293	0.354	0.728
	EPCm	20.629	8.101	2.547	0.020**
	PPCm	2.460	5.037	0.488	0.631
	laws_max_yarn_set	4.695	1.345	3.490	0.002***
	gsm	-3.096	1.071	-2.892	0.009***
Model Y2 (B)	(Intercept)	33.258	37.438	0.888	0.385
	EPCm	13.816	6.551	2.109	0.048**
	PPCm	0.754	4.073	0.185	0.855
	laws_max_yarn_set	3.509	1.088	3.225	0.004***
	gsm	-2.015	0.866	-2.327	0.031**
Model Y3 (C)	(Intercept)	-20.290	45.027	-0.451	0.657
	EPCm	-2.102	7.879	-0.267	0.793
	PPCm	16.877	4.899	3.445	0.003***
	laws_max_yarn_set	-4.549	1.308	-3.477	0.003***
	gsm	0.755	1.041	0.725	0.478
Model Y4 (D)	(Intercept)	-84.040	57.926	-1.451	0.163
	EPCm	-1.665	10.137	-0.164	0.871
	PPCm	18.872	6.302	2.994	.007***
	laws_max_yarn_set	-2.729	1.683	-1.621	0.121
	gsm	0.419	1.340	0.312	0.758
Model Y5 (E)	(Intercept)	1.753	.111	15.823	.000
	EPCm	.006	.019	.319	.753
	PPCm	.022	.012	1.805	.087*
	laws_max_yarn_set	-.009	.003	-2.713	.014**
	gsm	.002	.003	.647	.525

Note: *p<0.1; **p<0.05; ***p<0.01

didn't show any clear indication due to the fluctuation of the tensile strength much with the change of the design of the fabrics and yarn set [23-25].

For distinct heald counts, rib, matt, twill, and sateen show greater warp way tear strength than plain fabric in Fig. 4. Similar result found for twill weave by Asaduzzaman M. et al. [26], and the strength increases with the increase of heald counts that supports the result found by Malik Z.A. et al. [25]. Matt fabric with a similar float length shows greater strength than rib, twill, and sateen (Fig. 2) which further shows different from Asaduzzaman M. et al. [26] due to the change is weave design of plain structure.

For different heald counts, it is seen that rib, matt, twill, and sateen showed greater weft way tear strength than plain fabric. And the strength increases with the increase of heald counts. The tear strength of matt fabric is higher than that of rib, twill, and sateen, with a similar float length (Fig. 5). These also supported by result found in work of Asaduzzaman M. et al. and Malik Z.A. et al. [25-26]. Thus contact between warp and weft yarn or interlacement pattern or variation in weave design plays a vital role in warp

and weft tear strength which is also supported by Radwan S.S. [27].

It is found in Fig. 6 that matt, twill, and sateen show lower warp way tensile strength than that of plain fabric except $\frac{2}{2}$ plain warp rib and $\frac{2}{2}$ z-twill. But, the change is not very continuous except $\frac{3}{1}$ z-twill structures in this experiment which are similar found by Asaduzzaman M. et al. [26].

Fig. 7 demonstrates that the tensile strength of the rib, matt, twill, and sateen fabric is lower than that of the plain structure. However, the strength of these fabrics becomes greater with the increase of the heald count and demonstrates more than that of plain construction. Concerning plain fabric construction, twill and sateen fabric change is more regular than rib and matt. Here with the increase of yarn densities below the optimum level the weft way tensile strength of twill and sateen was found lower than plain weave that supports the result found by Asaduzzaman M. et al. [26] but at the optimum level the strength become higher than the $\frac{1}{1}$ plain weave which is again support the theoretical context of Gokarneshan N. [28].

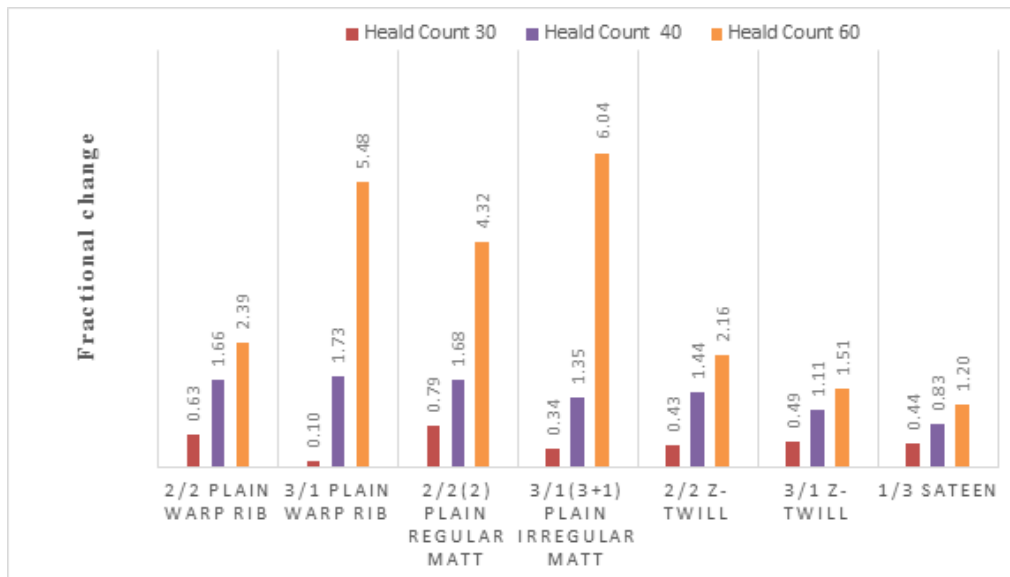


Figure 4. Fractional change in warp way tear strength from the plain weave

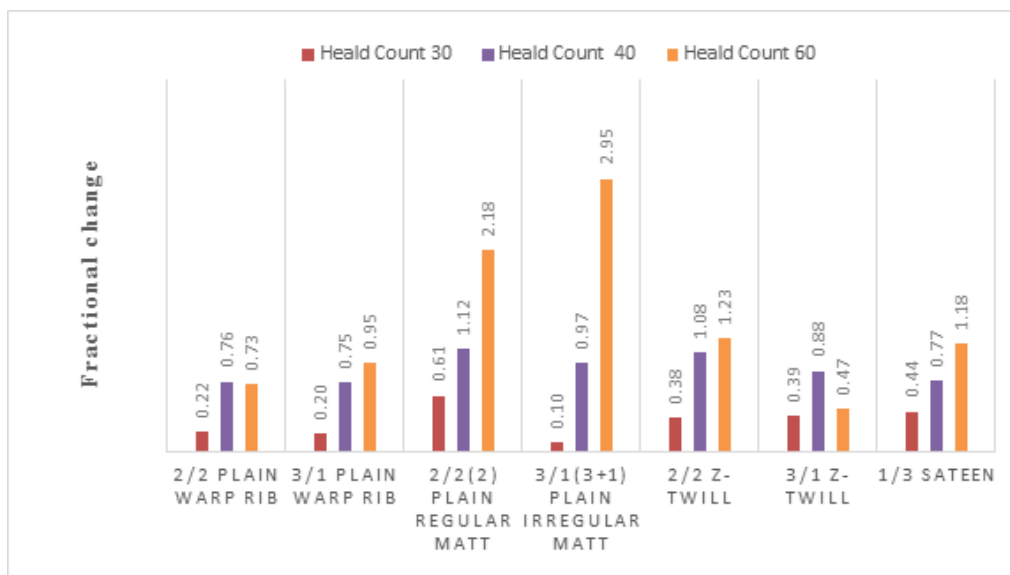


Figure 5. Fractional change in weft way tear strength with respect to plain weave.

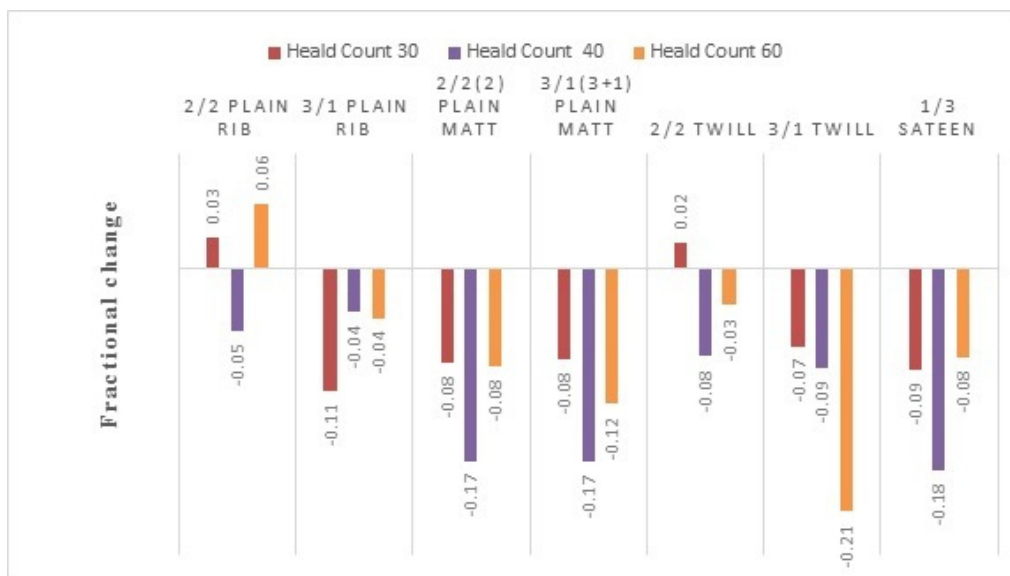


Figure 6. Fractional change in warp way tensile strength with respect to plain weave structure.

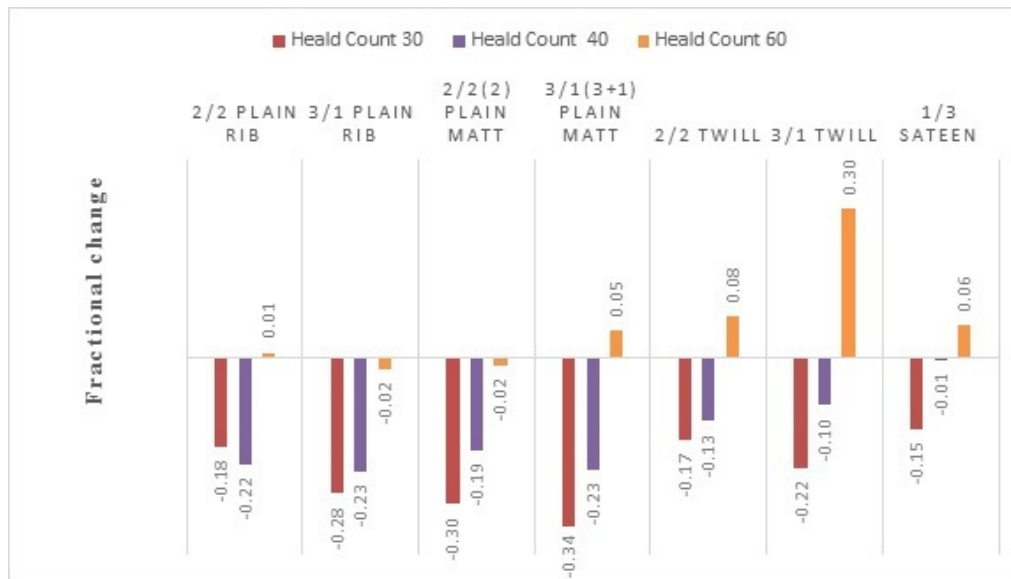


Figure 7. Fractional change in weft way tensile strength from the plain weave structure.

The four regression models can precisely predict the values using EPCm, PPCm, and Law's maximum yarn setting as influencing factors. As the yarn used in this research is one thus, fiber composition and yarn properties remained constant in this study. It was most challenging to find out the relation of these factors with the tear and tensile strength and consider design variation in the prediction model. Law's maximum yarn setting parameters use the float length and yarn count during measurement and are statistically significantly related to tear and tensile strength. As float length is still the same for different weave designs thus, there are still spaces to improve this model. This study also uses graphical representations to understand the variation of tear and tensile strength with design variation.

This study found that all models can predict the tear and tensile strength with accuracy from 70.1% to 97.3% at a 5% significance level considering EPCm, PPCm, Law's maximum yarn setting, and GSM as independent variables. Among these parameters, the most significant factor for tear strength is EPCm and PPCm for tensile strength. It is also observed that design variation significantly influences tear strength, and fabric setting or yarn density greatly varies the tensile strength of the fabric. Thus, hypothesis testing shows changing yarn density in fabric structure does not influence tear strength, but yarn floating or weave design significantly influences the tear strength of the fabrics. On the other hand, design change or weave interlacement does not considerably change the tensile strength of the fabrics. Other hypothesis testing shows that EPCm, Law's maximum yarn setting, and GSM significantly influence warp and weft tear strength. On the contrary, PPCm and Law's maximum yarn setting significantly affect warp and weft way tensile strength.

This research's hardest part was considering weave factors in prediction models. As most of the weave

factors have high inter-correlation. They cannot be viewed in a single model; only Law's maximum yarn setting is considered in prediction models. To understand effect of float length and comparison with basic plain structure for tear and tensile strength, a graphical representation was the only option that authors found during this study. The float length of the fabric significantly affects tear strength. With the increased float length, more yarns are close to each other, thus increasing tear strength. But, it is not clearly said from the data the effect of change in float length how the tensile strength changes as it didn't show any clear indication due to the fluctuation of the tensile strength much with the change of design of the fabrics and yarn set.

It is also found that the tear strength increases with the increase of heald counts. The tear strength of matt fabric is higher than that of rib, twill, and sateen, with a similar float length. At the same time, twill and sateen show lower warp way tensile strength than that of plain fabric, except $\frac{2}{2}$ warp rib, $\frac{2}{2}$ z-twill and $\frac{3}{1}$ z-twill structures in this experiment.

The tensile strength of the rib, matt, twill, and sateen fabric is lower than that of the plain structure. However, the strength of these fabrics becomes greater with the increase of the heald count and demonstrates more than that of plain construction. With regard to plain fabric construction, the change in twill and sateen fabric is more regular than rib and matt.

CONCLUSION

Mathematical models concentrating on the fundamentals of woven textiles may struggle to provide adequate findings since all of the model's uncertainties cannot be accounted for. Due to the accuracy required, mathematical modeling of fabric constitutive equations necessitates the use of a

specialist approach. Certain variables are used as assumptions for prediction in predictive, descriptive, and computational models. Mathematical approaches are also case-specific. Four variables, EPCm, PPCm, GSM, and Law's maximum yarn setting, are utilized to generate four regression models to predict fabric strength in the sample to understand the effect of these parameters on the tear and tensile strength of the 100% cotton woven fabrics. Combining yarn composition, textile structure, twisting, and test techniques in a single formula is difficult. This research determines the optimum parameters and statistical representation to predict fabric strength. Floating parameters impact test performance and parameters like elongation. Such variables are omitted from regression models to avoid ambiguity. Research shows that thread setting and fabric design influence tear and tensile strength. As yarn properties such as single yarn power, fiber, twist, count, lea strength, etc., are the same, they dramatically alter the design result's tear strength. Thread density affects tensile strength more than design, however. Four regression models might be used within the scope of the design and yarn properties, and more research could be done with more yarn variation. Despite certain disadvantages, four regression models fit well (67%-98.1%) in this case. Here, the matt and twill weave structure showed more tear strength and tensile strength respectively. So, these structures can be the best choice for specific strength in technical textile production for higher tear and tensile strength. The prediction models can be adjusted with consideration of other parameters and more design structures. Therefore in models, GSM had a negative impact on weft way tear strength, EPCm and PPCm on warp way tensile strength, and PPCm on weft way tensile strength, which might be due to woven fabric relaxation and design variation or floating of warp and weft threads. The impact of other parameters positively on tear and tensile strength also might be balancing the negative influence of those parameters in respected cases. As, design of the fabric cannot be expressed in the numerical value as like other parameters (EPCm, PPCm, Law's Max Yarn setting and GSM) the models did not consider the design variables. Design variables as categorical or ordinal variables are needed to adjust the models with various designs. Again, Choosing fibers other than 100% cotton and yarn count other than 36.9 Tex will enhance the possibility of versatile technical applications from lower strength to higher strength. Thus, stiffness and other properties will be another option in proper selection of the fabric design to meet the technical requirements.

Funding: *The work is financed by author throughout the experiment, sample preparation, raw material purchase, and manpower recruitment. Authors took help from numerous skilled colleagues and took assistance without financial benefits. This complete work is done without any organizational funding.*

Acknowledgement: *We like to thank Bangladesh University of Textiles (BUTEX) and Bangladesh University Business and Technology (BUBT) for doing the test required for the experiment and all its staff. Special thanks to Prof. Engr. Masud Ahmed, Kazi Sayadul Alam, Rina Alam, Sheuli Aktar, Salma Akter, Kazi Md Mosharraf Hossain, Md. Mozzammel Hossain, Md. Nazim Uddin, Md. Shahin Alam, Md. Ali Akbar, Md. Shofiqul Islam, Md. Abul Hasan and Md. Enamul Hasan.*

REFERENCES

1. Realf M.L., Boyce M.C. and Backer S.: A micro-mechanical model of the tensile behavior of woven fabric, *Textile Research Journal*, 67, 1997, pp. 445-459. <https://doi.org/10.1177/0040517597067006>
2. Chattopadhyay R.: Design of apparel fabrics: Role of fiber, yarn and fabric parameters on its functional attributes, *Journal of Textile Engineering*, 54, 2008, pp. 179-190. <https://doi.org/10.4188/jte.54.179>
3. Sharma I.C., Deshpande S.D., Jaiswani O.P., et al.: Effect of wet processing on the tearing strength of polyester/viscose rayon blended fabrics, *Indian Journal of Textile Research*, 9, 1984, pp. 106-111.
4. Rafique S., Khattak S.P., Hussain T., et al.: Impact of functional finishes on the tensile and tear strength properties of pigment dyed P/C fabrics by post & meta finishing modes of application, *Journal of Science and Technology University Peshawar*, 37(2), 2013, pp. 71-83.
5. Gupta P., Roy M.D., Ghosh S.: Effect of finishing chemicals on tearing strength of plain-woven cotton fabric, *Research Journal of Textile and Apparel*, 24(3), 2020, pp. 229-243. <https://doi.org/10.1108/RJTA-09-2019-0043>
6. Gabrijelcic, H., Cernosa, E., Dimitrovski, K.: Influence of weave and weft characteristics on tensile properties of fabrics, *Fibres & Textiles in Eastern Europe*, 2(67), 2008, pp. 45-51.
7. Lopez V.M., Carou D., Cruz S.F.A.: Feasibility study on the use of recycled materials for prototyping purpose: A comparative study based on the tensile strength, *Proceedings of the Institution of Mechanical Engineers, Part B: Journal of Engineering Manufacture*, 46(19), 2022, pp. 9187-9193. <https://doi.org/10.1177/0954405422111337>
8. Zhang X., Wu M.: Modified stress field model for critical tearing strength of architectural coated fabrics, *Journal of Industrial Textiles*, 51(4), 2022, pp. 5560S-5591S. <https://doi.org/10.1177/15280837221106232>
9. Sinclair R.: *Textiles and Fashion: Materials, Design and Technology*, Woodhead Publishing, 2014, pp. 705-737. <https://doi.org/10.1016/C2013-0-17410-7>
10. Hossain M.M., Datta E., Rahman S.: A Review on different factors of woven fabrics' strength prediction, *Science Research*, 4(3), 2016, pp. 88-97. <https://doi.org/10.11648/j.sr.20160403.13>
11. Ahirwar M., Behera B.K.: Prediction of tear strength of bed sheet fabric using machine learning based artificial neural network, *The Journal of The Textile Institute*, 2022. <https://doi.org/10.1080/00405000.2022.2150960>
12. Ribeiro R., Pilastrri A., Moura C., et. al: Predicting the tear strength of woven fabrics via automated machine learning: An application of the CRISP-DM methodology. In *Proceedings of the 22nd International Conference on Enterprise Information Systems*, 1, 2020, pp. 548-555. <https://doi.org/10.5220/0009411205480555>
13. Hossain K., Anwar M., Samani S.: Regression and artificial neural network models for strength properties of engineered cementitious composites, *Neural Computing and Applications*, 29, 2018. <https://doi.org/10.1007/s00521-016-2602-3>
14. Singh N.: *Weave factors of different woven constructions*, Delhi: IIT, 2007. B. Tech Project Report.
15. Elkateb S.N.: Prediction of mechanical properties of woven fabrics by ANN, *Fibres & Textiles in Eastern Europe*, 30(4), 2022, pp. 54-59. <https://doi.org/10.2478/ftce-2022-0036>

16. Shahpurwala A., Schwartz P.: Modeling woven fabric tensile strength using statistical bundle theory, *Textile Research Journal*, 59(1), 1989, pp. 26-32.
<https://doi.org/10.1177/004051758905900104>
17. Hu J., *Fabric Testing*. Cambridge: Woodhead Publishing Limited, 2008, pp. 92-104.
18. Mishra, S.: Prediction of yarn strength utilization in cotton woven fabrics using artificial neural network, *Journal of the Institute of Engineers, Series E*, 96(2), 2014, pp. 151-157.
<https://doi.org/10.1007/s40034-014-0049-6>
16. Morino H., Matsudaira M., Furutani M.: Predicting mechanical properties and hand values from the parameters of weave structures, *Textile Research Journal*, 75(3), 2016, pp. 10-82.
<https://doi.org/10.1177/004051750507500>
20. ASTM D2256/D 2256M:2010. Standard Test Method for Tensile Properties of Yarns by the Single-Strand Method.
21. ISO 13937-1:2000. Textiles - Tear Properties of Fabrics - Part 1: Determination of Tear Force Using Ballistic Pendulum Method (Elmendorf)
22. ISO 13934-2:2014. Textiles - Tensile Properties of Fabrics - Part 2: Determination of Maximum Force Using the Grab Method.
23. Eryuruk S.H., Kalaoğlu F.: The effect of weave construction on tear strength of woven fabrics, *AUTEX Research Journal*, 15(3), 2015, pp. 207-214.
<https://doi.org/10.1515/aut-2015-0004>
24. Nasrun F.M.Z., Yahya M.F., Ghani S.A., et al: Effect of weft density and yarn crimps towards tensile strength of 3D angle interlock woven fabric, *AIP Conference Proceedings*, 1774, 2016, 020003.
<https://doi.org/10.1063/1.4965051>
25. Malik M.H., Hussain T., Ali, Z.: Effect of fabric count on the tensile strength of blended woven fabrics, *Journal of Engineering and Applied Science*, 28(2), 2009, pp. 23-29.
<https://doi.org/10.25211/JEAS.V28I2.297>
26. Asaduzzaman M., Hasan A.K.M.M., Patwary M.M., et. al: Effect of weave type variation on tensile and tearing strength of woven fabric, *Technium*, 2(6), 2020, pp. 35-40.
<https://doi.org/10.47577/technium.v2i6.1409>
27. Radwan S.S.: Effect of plain rib direction on fabric properties, *International Design Journal*, 4(4), 2014, pp. 179-185.
28. Gokarneshan N.: *Fabric structure and design*, New Delhi: New Age International Publishers, 2020, pp. 1-184.

STATE PROBLEM OF BALANCING SEWING LINE OF INDUSTRIAL KNITTED PRODUCTS

THAO, PHAN THANH^{*}; MY, PHAM THI LE AND PHAN, DUY-NAM

School of Textile – Leather and Fashion, Hanoi University of Science and Technology, Hanoi 10000, Viet Nam

ABSTRACT

Line balancing is always a big problem appearing in industrial production. Manual balancing of industrial sewing products takes a long time to give results, which depends on the experience of the sewing line manager, moreover, the efficiency is not necessarily optimal. Digital conversion will help find a solution to balance the sewing line more quickly, accurately, and optimally. This study presents the statements of the problem of balancing knitted garment lines in the industry with the line balancing process according to the method of Hanoi University of Science and Technology (HUST) and BSL-HUST-1 software, which is the software designed and built by our research group. For the balancing calculation, three groups of input data were defined for the comparison of balancing efficiency among the HUST method, the software method, and the method used traditionally by the companies. The line's capacity is determined as the total production amount in a shift, and the shift time is figured accordingly following each factory's rules. The total number of workers is an essential factor. Also, the cycle time is one of the important factors for balancing the sewing line.

KEYWORDS

Line Balancing; Sewing Line Balancing; Knitted Garments.

INTRODUCTION

2022 is the time when textile enterprises gradually recover after two years of being heavily affected by the global Covid-19 pandemic. In the first six months of 2022, textile and garment export turnover is estimated at 22.3 billion USD, increasing 17.7% compared to the same period in 2021. While the main export items are garments with a turnover of 16.94 billion USD, up 19.5% over the same period; fabric export reached 1.4 billion USD, up 20.8%; fiber exports reached USD 2.76 billion, up 4.4%; export of textiles and garment accessories reached USD 734 million, up 22.3%; exports of nonwovens reached US\$452 million, up 25.5%. The total import turnover of textile raw materials and accessories in the first six months of 2022 was estimated at 13.4 billion USD, up 9.8% over the same period in 2021. The trade surplus reached 8.86 billion USD, up 32% compared to the first six months of 2021. It can be seen as a great effort of Vietnamese textile and garment enterprises in the context of the world's economic difficulties [1]. The outbreak of Covid 19 has caused many Vietnamese businesses to fall into difficulties, the digital transformation becomes a "survival" opportunity to restore business and increase the possibility of breakthroughs. The program "Supporting businesses in digital transformation for

the period 2021-2025" of the Ministry of Planning and Investment aims to promote digital transformation in enterprises through technology integration and application to improve production and business activities, capacity, and competitive advantage [2].

In the garment industry, line balancing is always a big problem that needs to be addressed. When the sewing line is balanced, the product creation process is a continuous flow, wastes will be gradually eliminated, creating fairness in labor, increasing worker productivity and quality garment products. The development of information technology and mathematics effectively supports solving practical problems in life in general and in industrial garment production in particular, particularly in production conditions in Vietnam. Various IoT-based monitoring solutions have been developed recently to monitor individual workers. The data was transmitted to computers using a Wi-Fi connection to optimize smart garment manufacturing at a real-time scale and reduce cost levels [3]. In 2021, Phan Thanh Thao, Le Thi Mai Anh, et al. [4] conducted research and applied five methods: ranked position weighted method (RPW), probabilistic line balancing technique (PLB), longest task time method (LTT), most following tasks method (MFT), and the most reasonable line balancing method of Hanoi University of Science and

^{*} Corresponding author: Thao P.T., e-mail: thao.phanthanh@hust.edu.vn

Received November 21, 2022; accepted February 24, 2023

Technology with T-Shirt products. In February 2021, Phan Thanh Thao and other researcher [5] established, modeled, and proposed algorithms for three optimization problems of sewing line balance: given capacity, given the number of workers, and the cycle time to maximize the line balancing efficiency and minimize the number of workers. The sewing line balance software was developed at that time called ALBS V1.0 built especially for Polo-Shirts.

Following that development trend, this study will provide the results of stating the problem of sewing line balancing of knitted products based on real-life conditions of garment industry products such as customers' requirement for the number of products; order and delivery time, the number of workers, or the characters of each sewing products. We propose suitable algorithms and design the sewing line balancing software with each input parameter. Other authors have stated the problem and built a sewing line balancing software with various drawbacks, solving that this software used the method and process of line balancing according to the Hanoi University of Science and Technology principles, which are different from previous research [5]. This research result will be an important reference in the group of studies promoting digital transformation in the garment industry to help Vietnamese garment enterprises develop sustainably in the trend of integration and globalization.

EXPERIMENTAL

Research subjects

The sewing line is the production line of the technological process of sewing products, which is a basic stage in the garment industry. It is a form of organizing the process of sewing products, thereby creating a workstation system that is unified in terms of time or capacity.

Workstations are arranged to be performed simultaneously at the workplaces, by the technological sequence. Semi-finished products are moved from one job site to another at equal intervals of time using manual or motorized transport. Tasks are the basic unit of the technological process of sewing products, which is completed continuously and completely in one workplace. Workstations are organized in coordination with one or several tasks.

+ Single workstation: This is the production process performed by one worker at one workplace.

+ Multi-workstation: It is a production process performed by several workers at several workplaces.

Standardization

Documentary research methods

Synthesize and analyze published documents related to the research problem, as a basis for developing research contents.

Methods of designing and balancing sewing lines [4], [5], [6]

Calculation of sewing line parameters [4], [5], [6]

- Product processing time:

T_{sp} is determined as follows:

$$T_{sp} = \sum t_i [s] \quad (1)$$

where t_i is the processing time of task i , T_{sp} is product sewing time.

- Cycle time

Cycle time is the average time between two products leaving the line, or after which the production steps are repeated and a product is produced. Cycle time is one of the important data to balance the sewing line. The symbol is R . The formula for calculating cycle time:

+ $R = T_{sp} / N [s]$ with N is the total number of workers.

+ $R = (T_{sx} \times 3600) / P [s]$ with $T_{sx} [h/day]$ total working time in a day, P [products/day] total production amount in a day.

- The fluctuation of the cycle time ΔR depends on the organizational form of the chain of each enterprise, which is the initial data of the problem.

+ The sewing line has a tight cycle time:

$$0 \leq \Delta R \leq 0.05 R \quad (2)$$

$$R_{min} = 0.95R; R_{max} = 1.05R$$

+ The sewing line has a free cycle time:

$$0.10 R < \Delta R \leq 0.15 R \quad (3)$$

$$R_{min} = 0.9 R; R_{max} = 1.15R$$

The sequence of designing and balancing the sewing line

It is carried out according to the method currently being researched and taught at the Department of Garment Technology & Fashion, School of Textile – Leather and Fashion, Hanoi University of Science and Technology [4], [5], [6] including the following steps:

- Preliminary determination of the parameters of the line.

- Building the diagram of production and processing production and line balancing.

- Accurate parameters of the line.

- Workplace planning and line layout.

- Calculate the economic - technical indicators of the line.

Principles when organizing the tasks into workstations.

- Ensure the path of semi-finished products line is straight and the shortest technological journey:

+ Requirement 1: To comply with the maximum technological sequence, follow the principle of serialization coordination of serial tasks on the same processing branch.

+ Requirement 2: Follow the principle of parallelism pairing tasks on different processing branches but without affecting the technological sequence. The tasks have not been assigned are selected into workstation, which does not affect the technological sequence.

Note:

+ Prioritize the pairing of tasks according to the principle of serialization.

+ When joining tasks according to the principle of parallelism (joining operations on different detail groups should only combine tasks in the same detail group – e.g., front, back, neck, brace, arm), no tasks on the processing branches should be coupled with tasks on the assembly branches because the semi-finished products will be upstream of the transport and thus will violate the principle of straight-line technology.

- Requirements for machines and operation grade:

+ Requirement 1: Coordinate the tasks with the same equipment, and the same worker's rank or take the highest grade.

+ Requirement 2: Can coordinate tasks using equipment with manual tasks.

+ Requirement 3: Each workstation has a maximum of 2 different types of equipment.

- Ensuring the time conditions of the workstations:

$$u.R_{min} \leq t_{sxj} \leq u.R_{max} \quad (4)$$

where t_{sxj} : the time of the j workstation

+ Requirement 1: Select the workstations having t_{sxj} satisfy the condition $u = 1$, $u = 2$ and $u = 3$. u is the number of workers.

+ Requirement 2: Each workstation allows maximum three workers.

+ Requirement 3: Each workstation is allowed to be formed from a maximum of three tasks.

+ Requirement 4: To avoid the phenomenon of production process being stalled or stopped, priority should be given to under-loaded workstations rather than overloaded ones.

+ Requirement 5: However, it is necessary to limit the organization of a workstation from many tasks or has multiple workers, which is lower the specialization, coordination of semi-finished products and line layout complicated.

Parameters of workstations [4], [5], [6]:

$$t_{sxj} = \sum_{i=1}^{m_i} t_{ij} \text{ [s]} \quad (5)$$

where m_i is the number of tasks forming the j workstation, t_{ij} is the time of i task allocated to the j workstation.

- The number of workers for each workstation is N_j calculated by the formula: $N_j = t_{sxj}/R$

- Choose the number of j workstation according to the rounding principle, N_{cj} is the number of workstation selected, m is the integer part of N_{ij}

+ If $N_j \leq 1$, choose $N_{cj}=1$

+ If $m \leq N_j < (m+0.5)$, then choose $N_{cj} = m$

+ If $(m+0.5) \leq N_j \leq (m+1)$, then choose $N_{cj} = m+1$

- The cycle time of workstation j is R_j calculated by the formula: $R_j = t_{sxj}/N_{cj}$ [s]

The total number of workers needed after combining is:

$$N = \sum_{i=1}^n N_{cj} \text{ [worker]} \quad (6)$$

Indicators to evaluate the effectiveness of sewing line balancing [4], [5], [6], [7]:

In this paper, the following criteria are used to evaluate the efficiency of sewing line balancing:

+ The ratio of the number of workstations having their specific cycle time lied within the allowed interval of cycle time, K is calculated by the formula:

$$K = \frac{k_1}{k} \times 100 \text{ [%]} \quad (7)$$

where K : Balance efficiency, k_1 : Number of balance workstations, k : Total number of workstations.

$K \geq 60\%$, the line is balanced. $K < 60\%$, the line is not balanced, it is necessary to carry out balancing the line according to the new plan [6].

+ Line efficiency H is in the range of 98% to 102% is the optimum:

$$H = \frac{\sum t_i}{N \times R} \times 100\% \quad (8)$$

where H is line efficiency, $\sum t_i = T_{sp}$ - Product sewing time [s], N is Total number of workers, R is Cycle time [s].

Sewing line balancing optimization algorithm

Dinh Mai Huong [8], [9] proved that the Meta-Heuristic algorithm is suitable to solve the problem of balancing sewing lines for garment products in general and knitted products in particular. The authors Dinh Mai Huong [8], [9] used Meta-Heuristic algorithms including Tabu Search (Tabu), Genetic Algorithms (GA), Simulated Annealing Algorithm (SA) and binary search algorithm used in sewing line balancing studies. Special attention is paid to SA algorithm first introduced by S. Krikpatrick et al. [10].

In order to create a basis for choosing algorithms and learning algorithms suitable for sewing line balancing problems, the authors will focus on establishing the content of the statement of the problem of balancing the sewing line of knitted products, including objectives, content and sequence of steps to solve the problem with clear descriptions of constraints and performance conditions. The problem statement in a professional manner taking into account factors in the production practice of the garment industry, building input data, and determining the output requirements of the sewing line balancing problem will help to choose effective learning algorithms and be the basis for designing line-balanced software, including designing functional modules, interfaces, database, system security and user manual.

Table 1. Implementation steps of a problem of type 1 given P or R ($N_{sx} \rightarrow$ Min optimum).

No.	Content
1	<ul style="list-style-type: none"> - Style's basic information: + Section "Detailed style" includes: style name, Product name, Product description. + Section "Operation breakdown" includes: Number, Tasks name, Description, Machine, Time [s], Operation grade. + Section "Constraints sequence" includes: table, diagram, photo showing the binding sequence of tasks sewing products.
2	<ul style="list-style-type: none"> - Step 1: User assigns total working time in one day T_{sx} [h/day], total production amount in a day P [product/day], $\Delta R = 5, 10, 15, 20$ [%] - Step 2: From $P \Rightarrow$ Calculate R ($R = T_{sx}/P$), and ΔR [$R_{min}; R_{max}$]. - Step 3: combine tasks into workstations in the sewing line according to the principle of organizing and coordinating workstations as above. Calculate the workstations time and R_j. - Step 4: Draw the load graph of the workstations with the vertical axis being the cycle time R_j of workstations, and the horizontal axis is the ordinal numbers of workstations. - Step 5: Test if K is optimal + Calculate the number of balance workstations + Calculate the balance efficiency $K\%$ with the numerator is the number of workstations having their specific cycle time lied within the allowed cycle time interval [$R_{min}; R_{max}$], and the denominator is the total number of workstations. + If $K \geq 60\%$, then conclude the sewing line balancing \Rightarrow Go to step 6. + If $K < 60\%$, return to step 1, enter other parameters. - Step 6: Correct the sewing line's parameters $P, R, R_{min}, R_{max}, N$.
3	<ul style="list-style-type: none"> - The software returns the results in the order of priority: + Level 1: $K = 60\%$, and N_{min} + Level 2: $K_{max} < 60\%$ is not optimal, and N_{min} \Rightarrow Software gives notice "The line has not balanced in terms of load Go back to the previous step to change the parameters"
	\Rightarrow The software gives calculation results: $K, H, T_{sp}, P, N, R, R_{min}, R_{max}$

Table 2. Implementation steps of the problem of type 2 given N ($K \geq 60\%$, $P_{sx} \rightarrow$ Max optimum).

No.	Content
1	<ul style="list-style-type: none"> - Style's basic information: + Section "Detailed style" includes: style name, Product name, Product description. + Section "Operation breakdown" includes: Number, Tasks name, Description, Machine, Time [s], Operation grade. + Section "Constraints sequence" includes: table, diagram, photo showing the binding sequence of tasks sewing products.
2	<ul style="list-style-type: none"> - Step 1: User assigns total working time in one day T_{sx} [h/day], number of workers N, $\Delta R = 5, 10, 15, 20$ [%]. - Step 2: Using the Binary Search algorithm, find R in the range of values from $T_{min} = 0$ to $T_{max} = T_{sp}$ (Normal product processing time according to the operation breakdown table $T_{sp} = \sum t_i$, the case sewn by only one person), calculate ΔR [$R_{min}; R_{max}$]. + Step 2.1: $T_{mean} = (T_{min} + T_{max})/2$ and $R = T_{mean}$. + Step 2.2: From the operation breakdown and binding the sequence of combining tasks to workstations in the full line according to the principle of organizing and coordinating the operations as the P problem. + Step 2.3: The total number of workstations is N_1. If $N_1 = N$ does not exist \Rightarrow Assign $T_{min} = T_{mean} \Rightarrow$ Go back to step 2.1 If exists $N_1 = N \Rightarrow$ Assign $T_{max} = T_{mean} \Rightarrow$ Go back to step 2.1 The algorithm will run until $(T_{min} + \alpha) > T_{max} \Rightarrow$ Go to step 3. - Step 3: Draw the load graph of the workstations with the vertical axis being the cycle time R_j of workstations, and the horizontal axis is the ordinal numbers of workstations. - Step 4: Test if K is optimal + Calculate the number of balance workstations + Calculate the balance efficiency $K\%$ with the numerator is the number of workstations having their specific cycle time lied within the allowed cycle time interval [$R_{min}; R_{max}$], and the denominator is the total number of workstations in full-line. + If $K \geq 60\%$, then conclude that N_1 is the number of workers on the line \Rightarrow Go to step 5. + If $K < 60\%$, go back to step 1 and enter another parameter. - Step 5: Correct the sewing line's parameters $P, R, R_{min}, R_{max}, N$.
3	<ul style="list-style-type: none"> - The software returns the results in the order of priority: + Level 1: R-value at which $N_1 = N$, $K = 60\%$, and P_{max} + Level 2: R-value at which $N_1 = N$ and $K_{max} < 60\%$ is not optimal. Give the corresponding P-value result. \Rightarrow Software gives notice "The line has not balanced the load. Return to the previous step to change the parameter".
	\Rightarrow The software gives calculation results: $K, H, T_{sp}, P, N, R, R_{min}, R_{max}$.

Table 3. Implementation steps of type 3 problem ($K \geq 60\%$ optimization).

No.	Content
1	<ul style="list-style-type: none"> - Style's basic information: + Section "Detailed style" includes: style name, Product name, Product description. + Section "Operation breakdown" includes: Number, Tasks name, Description, Machine, Time(s), Operation grade. + Section "Constraints sequence" includes: table, diagram, photo showing the binding sequence of tasks sewing products.
2	<ul style="list-style-type: none"> - User assigns total working time in one day T_{sx} [h/day] - Select line type: + Conjugate line. + Group conjugation line.

3	Conjugate line: => Draw the norm time chart of the whole line tasks.	Group conjugate line: => The staff chooses the tasks in the assembly group from the full-line operation breakdown table. => Draw the norm time chart of the assembly group's tasks.
4	In full-line, the processing time of tasks runs from $[T_{min}; T_{max}]$. Corresponding to this period, the power domain of the line will be $[P_{Tmax}; P_{Tmin}]$.	The assembly group's tasks rated time runs from $[T_{lmin}; T_{lmax}]$. Corresponding to this period, the power domain of the assembly group will be $[P_{Tlmax}; P_{Tlmin}]$.
5	<p>Method 1:</p> <ul style="list-style-type: none"> - Step 1: In the range $[P_{Tmax}; P_{Tmin}]$, choose one P value (usually in the middle of this range determined by the user) => Calculate R, and cycle time interval $[R_{min}; R_{max}]$ ($\Delta=5, 10, 15, 20\%$ - asked and assigned the value by the user). - Step 2: combine tasks into workstations in the sewing line according to the principle of organizing and coordinating workstations as the N or P problem. Calculate the rated time of workstations and R_j. - Step 3: Draw the load graph of the workstations with the vertical axis being the cycle time R_j of workstations, and the horizontal axis is the ordinal numbers of workstations. - Step 4: Test if P is the optimal capacity + Calculate the number of balance workstations + Calculate the balance efficiency $K\%$ with the numerator is the number of workstations having their specific cycle time lied within the allowed cycle time interval $[R_{min}; R_{max}]$, and the denominator is the total number of workstations in full-line. + If $K \geq 60\%$, then the conclusion P is the optimal capacity => Go to step 5. + If $K < 60\%$, then choose P again (greater or smaller value) => Return to step 1. - Step 5: Correct the sewing line's parameters $P, R, R_{min}, R_{max}, N$. 	<p>Method 1:</p> <ul style="list-style-type: none"> - Step 1: In the range $[P_{Tlmax}; P_{Tlmin}]$, choose one P value (usually in the middle of this range determined by the user) => Calculate R, and cycle time interval $[R_{min}; R_{max}]$ ($\Delta=5, 10, 15, 20\%$ - asked and assigned the value by the user). - Step 2: combine tasks into workstations in the sewing line's assembly group according to the principle of organizing and coordinating workstations as the N or P problem. Calculate the rated time of workstations in the assembly group and R_j. - Step 3: Draw the load graph of the assembly group's workstations with the vertical axis being the cycle time R_j of workstations, and the horizontal axis is the ordinal numbers of workstations. - Step 4: Test if P is the optimal capacity of the assembly group. + Calculate the number of balance workstations in the assembly group. + Calculate the balance efficiency of the assembly group. $E [\%] = \frac{e_1}{e_2} \times 100 [\%]$ with numerator e_1 is the number of workstations lied within the allowed cycle time interval $[R_{min}; R_{max}]$, and denominator e_2 is the total number of workstations in the assembly group. + If $e \geq 60\%$, then the conclusion P is the optimal capacity of the assembly group => Go to step 5. + If $e < 60\%$, then choose P again (greater or smaller value) => Return to step 1. - Step 5: Correct the assembly group's parameters $P, R, R_{min}, R_{max}, N$ of the assembly group => Go to step 6.
6	<p>Method 2:</p> <p>The algorithm runs to find P in the range of P values so that $K \geq 60\%$</p>	<p>Method 2:</p> <p>The algorithm runs to find P in the range of P values so that $e \geq 60\%$.</p>
7		<ul style="list-style-type: none"> - Step 6: combine tasks into workstations in the sewing line's detail group according to the principle of organizing and coordinating workstations as the N or P problem. Calculate the rated time of workstations in the detail group and R_j. - Step 7: Draw the load chart of the detail group's workstations. - Step 8: Test if P is the optimal capacity of the whole line. + Calculate the number of workstations lied within the allowed cycle time interval $[R_{min}; R_{max}]$ in the detail group. + Calculate the balance efficiency of the detail group $f [\%] = \frac{f_1}{f_2} \times 100 [\%]$ with numerator f_1 is the number of workstations lied within the allowed cycle time interval $[R_{min}; R_{max}]$, and denominator f_2 is the total number of workstations in the detail group. + Calculate $K [\%] = \frac{k_1}{k} \times 100 [\%]$ $= \frac{e_1+f_1}{e_2+f_2} \times 100 [\%]$ + Simultaneous test K and f values: If $K \geq 60\%$ and $f \geq 60$ (level 1), then P is the optimal => Go to step 9. If $K \geq 60\%$ and $f < 60\%$ (level 2) => Temporarily save the result. If $K < 60\%$, then choose P again (greater or smaller value) => Return to step 1. - Step 9: Correct the detail group's parameters (N of detail group). (It is essentially a given problem P)
8		<p>Full line</p> <ul style="list-style-type: none"> - Step 10: Draw the load chart of the full line - Step 12: Accurate parameters of the full line $P, R, R_{min}, R_{max}, N$ of the full line.
9		<p>Note: algorithm priority</p> <ul style="list-style-type: none"> + Level 1: $K \geq 60\%$; $e \geq 60\%$ and $f \geq 60\%$ + Level 2: $K \geq 60\%$; $e > 60\%$ and $f < 60\%$
	=> The software gives calculation results: $K, H, T_{sp}, P, N, R, R_{min}, R_{max}$.	

Table 4. Algorithms for sewing line balancing problems

No.	Sewing line balancing problem		Algorithm
	Input	Optimal Priority Order	
1	Given P or R	$K \geq 60\%$, and N_{min}	SA
2	Given N	$N_{found} = N_{input}$, $K \geq 60\%$, and P_{max}	Binary Search and SA
3	R value optimization problem	$K \geq 60\%$, N_{min}	SA

RESULTS AND DISCUSSION

Objectives of the sewing line balancing problem

The purpose of the study is to optimize the sewing line balance in industrial production in real conditions with three groups of input data:

Type 1: the capacity of the line given is determined as the total production amount in a shift from which the cycle time is figured. Objective: Minimum number of workers, $N_{sx} \rightarrow \text{Min}$.

The problem assumes that the worker's capacity and ability to work are the same, regardless of the influence of the operation grade.

Type 2: Having the total number of workers from which to calculate the cycle time. Objective: Maximize total production amount in a day, $P_{sx} \rightarrow \text{Max}$.

Type 3: Balancing the sewing line according to the characteristic's product regardless of the number of workers N or total production amount in a day. Objective: Optimizing the cycle time R to ensure the line is balanced (K maximum and $\geq 60\%$) and effectively using the number of workers on the line $N_{sx} \rightarrow \text{Min}$ as well as total production amount in one day is the largest $P_{sx} \rightarrow \text{Max}$.

The results of the statement of the sewing line balancing problem

Not only do base on the method of designing and balancing the sewing line being researched and taught at the Department of Garment & Fashion Technology, School of Textile – Leather & Fashion, Hanoi University of Science and Technology [4], [5],

[6], but it also establishes the requirements of the sewing line balancing problem presented in section 2 above, the team has conducted to demonstrate their problems include the contents and process of performing steps to solve three types of statements of balancing the sewing line of industrial knitted products. The results are displayed in Tables 1, 2 and 3.

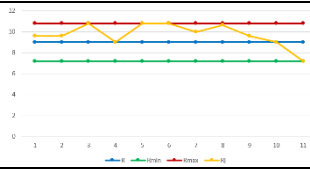
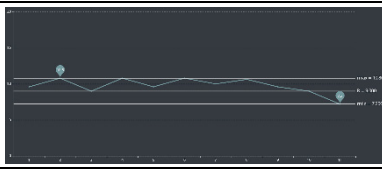
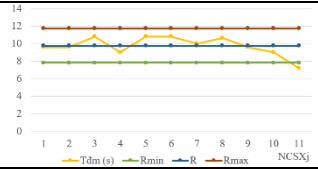
Algorithms

This paper proposes to specifically apply the algorithm in the Meta-Heuristic group corresponding to the three problems of balancing the knitted product line in the garment industry, see Table 4.

We have applied the line balancing software for 14 knitting production lines, and the actual set of data for T-Shirt and Polo-Shirt at 03 factories were collected and analyzed. The Vietnamese factories are Ha Nam - HANOSIMEX Company Limited, Star Fashion Company Limited, and Regent Garment Factory Limited. The collected results of balancing the sewing line for T-Shirt and Polo-Shirt products using the software BSL-HUST-1, 2, 3 were compared with the method invented by Hanoi University of Science and Technology, and the conventional sewing line balancing method from the factories. In the following Figure 1, we represent a T-Shirt code T08 balancing process presented on our software.

The methods to balance the production line according to the principles from Hanoi University of Science and Technology and using BSL-HUST-1 software are calculated independently but given the same results. All three methods present good results with $K \geq 60\%$, but the first two methods are better than the company's one. Similarly, parameters P , and H calculated by the method of Hanoi University of Science and Technology are larger than those of the company. Looking at the load chart of the whole line generated by the software, there are no under-loaded or overloaded production steps, whereas the company's method has an under-loaded step. The same number of workers are required for production among all methods, the R parameter decreases leading to the H parameter increases.

Table 5. Comparing the load chart of the sewing line code T08.

	Hust balancing method	BSL-HUST-1 Software	Regent Garment Factory Limited's method
Load chart of the sewing line T08			
Comment	From the load graph, all manufacturing steps have their own spans in the range ΔR .		From the load chart, there is 1 manufacturing step underload.

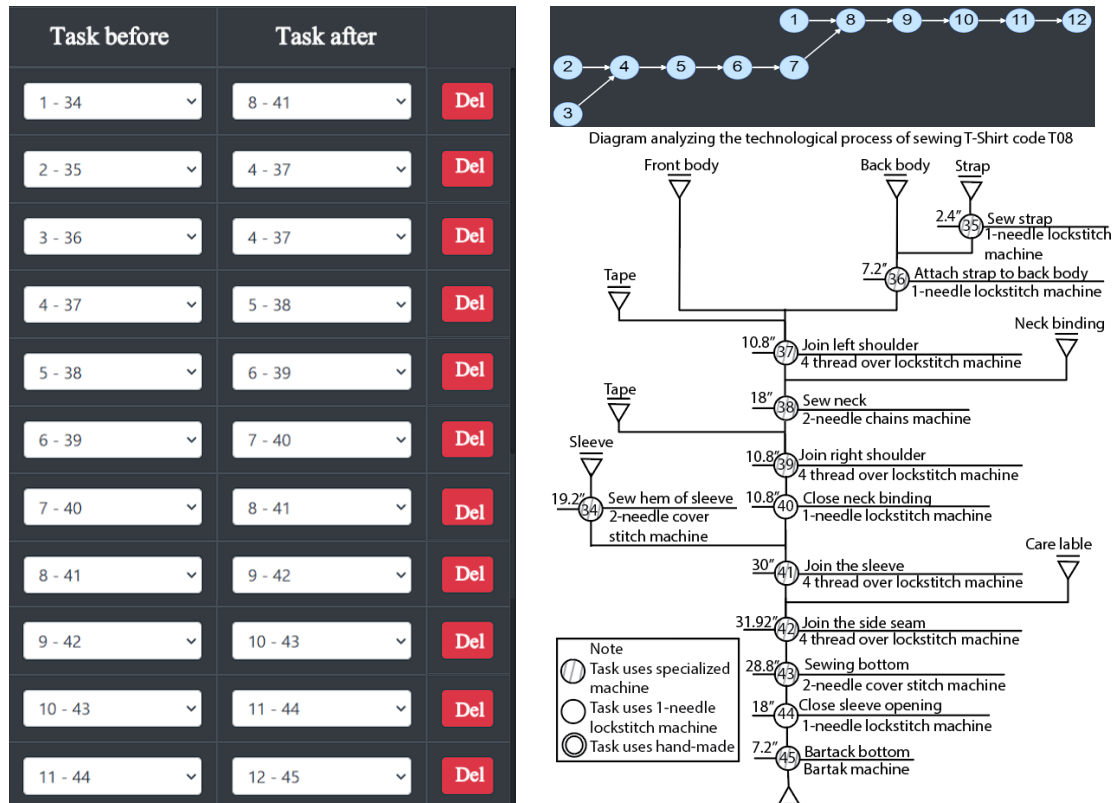


Figure 1. Representative photo of the BSL-HUST software balancing for production line code T08.

Table 6. Comparing the layout diagram of the sewing line T08 between varied methods.

	The layout diagram of the T08 sewing line	Layout form
HUST balancing method		Horizontal arrangement, semi-finished products moved with zigzag routes using container.
BSL-HUST-1 software		Zigzag lines
		U lines
		'Cell' line (perpendicular sitting position)
		'Cell' line (opposite sitting position)
Line balancing design of Regent Garment Factory Limited.		Horizontal layout, semi-finished products transported in a straight line, with semi-automatic hanging lines

Table 7. Comparing sewing line parameters for T08 production line.

	K%	P [product/shift]	N [person]	R [s]	H%
HUST balancing method	100	3200	20	9	108.4
BSL-HUST-1 software	100	3200	20	9	108.4
Line balancing results from Regent Garment Factory Limited's methods.	90.909	2952	20	9.756	100

The layout of the sewing lines in three relatively similar ways is all horizontal. However, there is a difference: the company's line is a line with a series of machines, in reality, the production of T-Shirt products at Regent Garment Factory Limited paired two lines to run the same product, using the line for transporting semi-finished products to preserve production area and improve labor productivity. The software BSL-HUST-1 supports more U-shaped line layouts and cell lines. From here, it can be seen that the determination of a reasonable capacity to effectively ensure the balance of the sewing line by BSL-HUST-1 software is completely reasonable and can be applied to actual production.

CONCLUSION

Based on the actual requirements of garment industry production and the process of line balancing according to the method of Hanoi University of Science and Technology, this study has stated the sewing line balancing problem of knitted products through concrete, explicit and coherent steps whereas giving suggestions for choosing suitable algorithms for each problem. It is one of the initial steps contributing to developing sewing line balancing software applied to solve the sewing line balancing problem in industrial production.

Acknowledgement: *This study was carried out within the framework of the topic Science and Technology 01C-02/04 – 2019 – 3. We would like to thank the Ha Noi Department of Science and Technology, Hanoi University of Science and Technology for supporting us in completing this study.*

REFERENCES

1. Alam F.B. and Hasan M.M.: Analysis on SMV to increase productivity in sewing section: a case study on T-shirt manufacturing in Bangladesh, *International Journal of Research in Engineering and Science*, 6(8), 2018, pp. 18-24.
2. Rahman H., Roy P.K., Karim R. et al.: Effective way to estimate the standard minute value (SMV) of a t-shirt by work study, *European Scientific Journal*, 10(30), 2014, pp. 196-203.
<https://doi.org/10.19044/esj.2014.v10n30p%25>
3. Jung, W.K., Kim H., Park Y.C., et al.: Smart sewing work measurement system using IoT-based power monitoring device and approximation algorithm, *International Journal of Production Research*, 58(20), 2020, pp. 6202-6216.
<https://doi.org/10.1080/00207543.2019.1671629>
4. Thao P.T., Anh L.T.M., Phan D.N., et al.: Researching the optimal method of balancing the sewing line with T-shirt product in the garment industry in Vietnam, *ECS Transactions*, 107(1), 2022, pp. 7869-7887.
<https://doi.org/10.1149/10701.7869ecst>
5. Thao P.T. and Huong D.M.: Research on apply of polo-shirt assembly line balancing methods in Vietnam garment industry, In: *Proceedings the 2st National Scientific Conference on Textile, Apparel and Leather Engineering*, 2021, pp. 307-318.
6. Thao P.T., Long T.V., Huong D.M., et al.: Apply genetic algorithm to solve assembly line balancing problem, In: *Proceedings the 2st National Scientific Conference on Textile, Apparel and Leather Engineering*, 2021, pp. 254-260.
7. Eryuruk S.H., Kalaoglu F., Baskak M.: Assembly line balancing in a clothing company, *FIBRES & TEXTILES in Eastern Europe* January, 16(1), 2008, pp. 93-98.
8. Dinh M. H., Nguyen V.D., Truong, V.L., et al.: Cycle time enhancement by simulated annealing for a practical assembly line balancing problem, *Informatica*, 44(2), 2020, pp. 127-138.
<https://doi.org/10.31449/inf.v44i2.3083>
9. Huong D.M., Long T.V., Thuan D.P., et al.: Application of exhaustive search for optimization assembly line balancing in garment industry, *Journal of Science & Technology Technical Universities*, 141, 2020, pp. 34-41.
10. Kirkpatrick S., Gelatt C.D., and Vecchi M.P. Optimization by Simulated Annealing. *Science*, New Series 220(4598), 1983, pp. 671-680.
<https://doi.org/10.1126/science.220.4598.671>

A 2D CELLULAR AUTOMATON MODEL OF LIQUID ABSORPTION INTO PAPER FIBERS WITH HYDROPHOBIC TREATMENT

KŘÍŽ, VÍTĚZSLAV¹; KŘÍŽOVÁ, HANA^{2*}; KOCICH, MARTIN¹ AND DALÍKOVÁ, JOHANA⁴

¹ Faculty of Information Technology, Brno University of Technology, Božetěchova 1/2, 612 00 Brno, Královo Pole, Czech Republic

² Technical University of Liberec, Institute for Nanomaterials, Advanced Technologies and Innovations, Studentská 1402/2, 461 17 Liberec, Czech Republic

³ Faculty of Mathematics and Physics, Charles University, Ke Karlovu 207/3, 120 00 Prague, Czech Republic

ABSTRACT

In this work, the issue of applying water or a homogeneous aqueous suspension with a uniform size of (nano)particles (e.g., ink) to the surface of SBSK (southern bleached softwood kraft) paper with randomly arranged local hydrophobic treatment is investigated and then simulated. Based on the two investigated models, various simulation approaches were compared, an own simulation model was created, and its validity was subsequently demonstrated on the experiments performed.

KEYWORDS

Cellular automaton; Water absorption simulation; Cellulose fibers; Paper pulp, C++ language.

INTRODUCTION

There are a lot of reasons for studying and simulating the absorption of water into hydrophobically treated paper. Some possible reasons include: to understand the mechanisms by which hydrophobic treatment affects the absorption of liquids into paper; to predict the rate and extent of liquid absorption into different types of paper with different hydrophobic treatments; to optimize the hydrophobic treatment of paper for specific applications, such as in packaging or in sanitary products; to investigate the potential of using hydrophobic treatment as a way to improve the strength, durability, and other properties of paper; to compare the performance of different hydrophobic treatments in terms of their ability to reduce liquid absorption in paper, and more.

The professional literature on simulations using a cellular automaton is mostly focused on the interaction of inks, colors, and pigments with paper fibers [1-4]. These simulations are partially applicable to textiles and composites containing fibers. The creation of other simulation programs describing the behavior of fluids in contact with textiles and fibrous formations is desirable regarding the development of medical materials, hygiene supplies, agrotiles, geotiles, etc.

CONCEPTS AND APPROACHES

Paper

Paper is a material made from cellulose fibers, typically derived from wood, rags, or grasses. Paper is made by mechanically or chemically separating the fibers from the raw material, and then forming the fibers into a mat or sheet. The mat is then pressed and dried to remove any remaining moisture, resulting in a sheet of paper. Paper can be treated in various ways to improve its strength, durability, and other properties, such as by adding chemicals or other treatments to make it water-resistant or hydrophobic. Paper is commonly used for writing, printing, and packaging, it can also be used for artistic purposes (painting, origami), to produce hygiene items, disposable dishes for fast food and even for building purposes. The specific conditions of the paper production vary depending on its desired properties and use.

SBSK paper

Southern bleached softwood kraft (SBSK) is a type of paper that is made from pulp obtained from southern bleached softwood trees. The production of SBSK paper involves several steps, including logging, pulping, bleaching, and drying. The pulp obtained from the kraft pulping process is typically bleached using chlorine-based chemicals to produce a bright

* Corresponding author: Křížová H., e-mail: hana.krizova@tul.cz

Received December 20, 2022; accepted February 24, 2023

white color. The pulp is then formed into sheets of paper, which are dried and pressed to remove excess moisture.

The pressing conditions for SBSK paper typically involve the application of heat, pressure, and time. The specific conditions used can vary depending on the desired properties of the paper and the type of equipment being used. In general, SBSK paper is pressed at temperatures of around 120-180 degrees Celsius [5]. The paper is typically pressed for a period of 5-10 minutes, although longer pressing times may be used for certain applications. The pressure applied to the paper during pressing can range from 1-3 bars [6], depending on the specific equipment being used. These pressing conditions are designed to remove excess moisture from the paper and to compact the fibers, which helps to give the paper its strength and durability. The specific conditions used can be adjusted to achieve the desired properties of the finished paper, such as its thickness, density, and smoothness.

The length and thickness of SBSK paper fibers, as well as their distribution, are important factors in determining the properties of the paper. In general, the fibers used to make SBSK paper are obtained from softwood trees, such as pine or spruce. These fibers are typically long and thin, with an average length of 1-3 millimeters and an average thickness of 0.01-0.02 millimeters [6] [7]. The distribution of fibers in SBSK paper is typically uniform, with the fibers evenly distributed throughout the sheet of paper. This helps to give the paper its strength and durability, and it allows it to withstand high levels of stress without tearing or breaking.

Cellular automaton

A two-dimensional cellular automaton is a type of mathematical model that is made up of a grid of cells (lattice), each of which is represented by a set of numerical parameters or simple state from a set of finite number of states (such as "on" or "off", or "1" or "0") [8].

The neighborhood of a cell is the set of cells that are neighboring to that cell, and it is a key factor in determining how the cell will behave and it can have a significant impact on the overall behavior of the system. For example, a cell's neighbors can include cells that are diagonal to the cell, or cells that are a certain distance away from the cell.

The rules of a cellular automaton specify how each cell should behave at each time step. These rules typically depend on the current state of the cell and the states of its neighbors, and they determine how the state of the cell should change at the next time step. The cells interact with each other based on a set of rules, and the resulting patterns that emerge over time can be used to model studied phenomena.

C++ programming language

C++ is a general-purpose programming language. It was designed to be an extension of the C programming language, and it adds support for object-oriented programming, generic programming, and other features. C++ is often used for building large-scale applications, such as operating systems, web browsers, and games. It is also commonly used in the development of high-performance systems, such as those found in the fields of finance, engineering, and scientific computing [9].

C++ is a compiled language, which means that it needs to be converted into machine code before it can be executed. This typically involves using a compiler to translate the C++ code into an executable program. One of the main advantages of C++ is that it is a statically typed language, which means that most errors can be caught at compile time rather than runtime. This can make it easier to debug and maintain large code bases. Additionally, C++ is a highly efficient language, which makes it well suited for applications that need to run quickly and efficiently, such as those that require real-time performance [10].

General simulation procedure

The simulation process included these main steps [11] [12]:

- Experiments to obtain the data from which the simulation is based.
- Analysis, evaluation, and processing of the conceptual design of two published models to point out the possible risks and pitfalls of simulation process.
- Creation of an abstract model: Formation of a simplified description of the investigated system.
- Creation of a simulation model: Writing an abstract model in the form of a program.
- Verification and validation: Verification of the correctness of the model.
- Simulation: Experimenting with a simulation model.
- Analysis and interpretation of the results: gaining new knowledge about the investigated system.

Description of the applied procedures

In this study, a 2D cellular automaton is used for computer simulation because it allows to see how the system behaves over time [13]. The von Neumann neighborhood was used [14], that means a cell's neighbors are the cells that are directly above, below, to the left, and to the right of the cell.

The program was implemented in the C++20 language using the functions of the standard library without the use of third-party libraries, due to the possibility of a higher degree of customization and optimization of the program. CMake tools were used to translate the source files.

The structure of the program was designed in such a way that it was possible to change the used cell classes, their fields, and the rules for them with minimal intervention in the structure of the program. The principles of designing a cellular automaton were freely taken from [15] but were modified due to the use of the C++ language and own experience with the design of cellular automata.

Theoretical analysis of physical processes influencing the water absorption into paper

Paper is a thin, smooth material made by compacting fibers. The fibers used are cellulose-based, and their length, thickness, and placement usually define the structure and other physical properties of the paper [6]. Liquids deposited on such a surface are subject to several physical processes, which are mostly caused by capillary phenomena [1]. Specifically, these are:

- Soaking of liquids into the surface (influenced by the degree of hydrophobicity)
- Particle movement caused by capillary pressure equalization and non-zero particle velocity
- Sedimentation of solids (for example in the case of fine ink, it is affected by the size of the particles)
- Evaporation (depends on the temperature and relative atmospheric humidity around the paper)
- Capillary diffusion of liquids below the surface of the paper

ANALYSIS OF PUBLISHED MODELS

Model 1

The first tested conceptual model (Fig. 1) was based on a study investigating the application of Japanese Nijimi ink on traditional paper [2]. The paper is described as a 2D lattice of cells, each cell is a quadruplet of parameters $[B, C, W, I]$, where B is the thickness of the paper, C is the maximum height of the trapped water column, W is the number of virtual water particles in that cell, and I is the number of virtual particles of ink in the cell. At each discrete time step, the height difference of neighboring water columns is calculated for all cells and the proportional part of the water column without ink deposition is moved.

The advantage of this model is the structure of the paper, which is simulated by creating random lines representing individual cellulose fibers. These fibers affect the thickness of the paper and the maximum amount of water trapped in the water column.

Problem of the model 1

The model does not work with real quantities, the structure of the paper is not well defined, and the main function of the automaton (spreading water) does not even remotely match the experiments carried out.

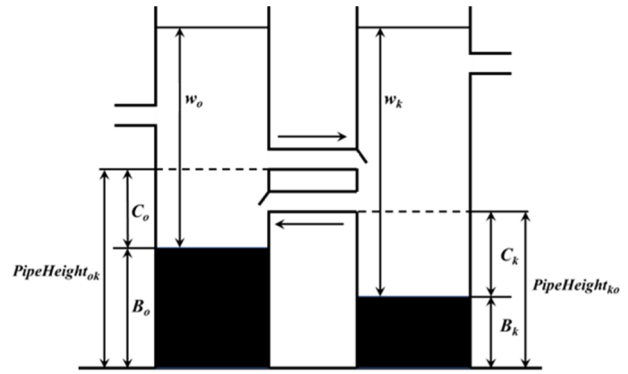


Figure 1. Visualization of the Model 1 [2].

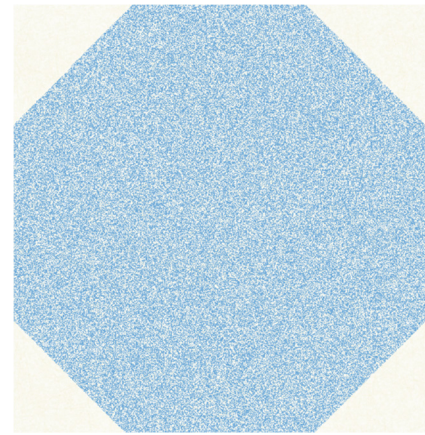


Figure 2. Problem of the Model 1.

When "laying" a circular seed representing a drop of water, after several iterations the state of the automaton is very far from reality (Fig. 2). At the same time, the model does not allow the extension of hydrophobic surface treatment, which was a fundamental problem for our study.

Model 2

The second conceptual model tested [1] was based on a published article on the use of cellular automata for simulating the diffusion of watercolors for computer-generated paintings. In this model, the paper is also described as a 2D lattice of cells, but in contrast to Model 1, each cell is represented as more complex tens $[hx, hy, c, u, v, p, gk, dk, s, m]$, where hx is the direction of paper height between neighboring cells on x-axis, hy is direction of paper height between neighboring cells on y-axis, c is maximum holding capacity of fluid in cell, u is the velocity of fluid flow on x-axis, v is the velocity of fluid flow on y-axis, p is the water pressure in the cell, gk is the amount of pigment in the upper layer of water, dk is the amount of deposited pigment, s is the quantity indicating the saturation level of the paper and m is the mask delimiting the wet part of the paper. Pseudocode describing the behavior of the cellular

```

proc UpdateVelocities(M, u, v, p):
  (u,v)  $\leftarrow$  (u,v) - h
   $\Delta t \leftarrow 1/[\max_{i,j} \{|u|, |v|\}]$ 
  for t  $\leftarrow$  0 to 1 by  $\Delta t$  do
    for all cells (i,j) do
       $A \leftarrow u^2_{i,j} - u^2_{i+1,j} + (uv)_{i+5,j-5} - (uv)_{i+5,j+5}$ 
       $B \leftarrow (u_{i+1.5,j} + u_{i-5,j} + u_{i+5,j+1} + u_{i+5,j-1} - 4u_{i+5,j})$ 
       $u'_{i+5,j} \leftarrow u_{i+5,j} + \Delta t(A - \mu B + p_{i,j} - p_{i+1,j} - \kappa u_{i+5,j})$ 
       $A \leftarrow v^2_{i,j} - v^2_{i,j+1} + (uv)_{i-5,j+5} - (uv)_{i+5,j+5}$ 
       $B \leftarrow (v_{i+1,j+5} + v_{i-1,j+5} + v_{i,j+1.5} + v_{i,j-5} - 4v_{i,j+5})$ 
       $v'_{i,j+5} \leftarrow v_{i,j+5} + \Delta t(A - \mu B + p_{i,j} - p_{i,j+1} - \kappa v_{i,j+5})$ 
    end for
    (u,v) (u',v')
    EnforceBoundaryConditions(M,u,v)
  end for
end proc

```

Figure 4. Pseudocode of the UpdateVelocities procedure.

automaton is described in Fig. 3. (Note: all pseudocodes in this paper are framed.)

The advantage of Model 2 is that the system works with velocities, pressure and constants describing the viscosity of fluids. Due to the complex concept of capillary phenomena, this model is probably very close to reality with a small degree of abstraction.

Problem of the model 2

During the application of the Model 2, several calculation errors were discovered already in the MoveWater procedure, specifically in its UpdateVelocities sub procedure (Fig. 4).

The error lies in the concept of fluid propagation speed with a quadratic dependence of its slope on the current difference of neighboring cells. In addition, the formulas incorrectly favor calculating the pressure in only two quadrants ([+x, +y] and [-x, -y]). This leads to the errors shown in Figures 5 and 6.

```

proc MainLoop(M,u,v,p,g1,...,gn,d1,...,dn,s):
  for each time step do:
    MoveWater(M,u,v,p)
    MovePigment(M,u,v,g1,...,gn)
    TransferPigment(g1,...,gn,d1,...,dn)
    SimulateCapillaryFlow(M,s)
  end for
end proc

```

Figure 3. Pseudocode describing the behavior of the Model 2 [1].

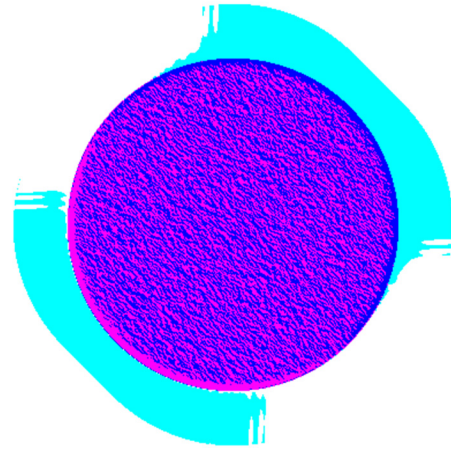


Figure 5. Non-uniform velocity distribution (*u* = purple, *v* = blue), state after 10 iterations.

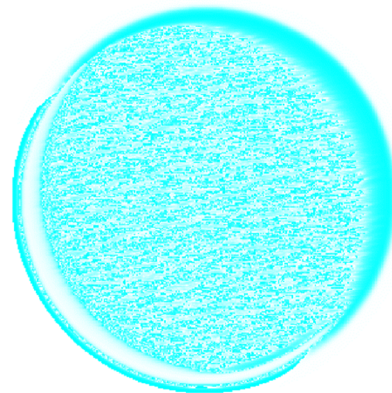


Figure 6. Non-uniform capillary pressure distribution, state after 10 iterations.

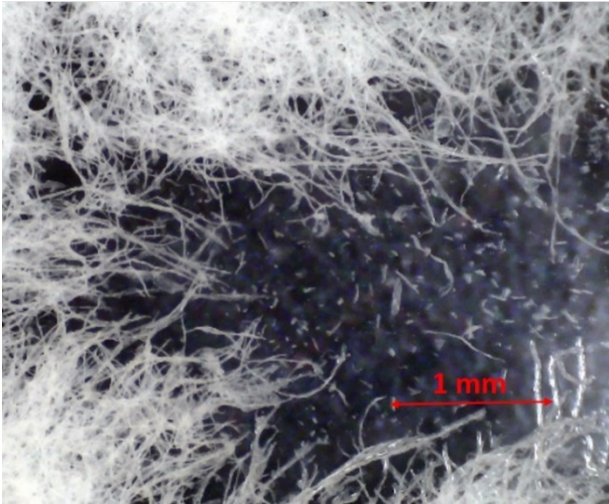


Figure 7. Softwood pulp before papermaking.

CREATION OF ABSTRACT MODEL

Experimental data and observations

The paper used corresponds to the SBSK (southern bleached softwood kraft) type with surface weight 82 g/m², average fiber length 2.8 mm and, average fiber diameter 20 μ m (Fig. 7).

The paper was experimentally coated with hydrophobic spots of mean size of 300 μ m. The surface was hydrophobized using polypropylene dissolved in toluene. This gel solution was applied by spraying, and after evaporation of the solvent and thermal fixation, randomly distributed hydrophobic porous structures resembling aerogel were formed. Water soaks into the paper through these spots at a minimum, but after a certain time the upper wet layer connects with the paper base without hydrophobization. As soon as this happens, the canals formed in this way subsequently absorb more water thanks to capillary phenomena and thus effectively bypass the hydrophobic protection in the

upper layer of the paper. At the same time, the water spreads in the bottom layer of the paper due to capillary phenomena and this causes further water seepage.

An aqueous suspension of pink ink with a uniform particle size of approximately 165 nm was used to visualize the spreading (absorption) of a drop of water into paper with randomly distributed hydrophobic spots (Fig. 8).

Hypothesis: after flowing through the hydrophobic layer and creating continuous canals through which the water seeps into the paper, the entire area under the hydrophobic spot gets wet.

Paper model design

The paper represents the basic state of a 2D cellular automaton. The cells are arranged in a square grid, where the size of one cell corresponds to 20 μ m. This size was chosen based on [2] to accurately create the corresponding paper structure. The second component simulating the structure of the paper are surface irregularities, which simply describe the geometric curvature of the surface.

Bresenham's algorithm [16] for rasterized drawing of lines was used to generate paper fibers. The length of the angle is chosen randomly; the length of the lines corresponds to 2 mm of the real size. In the cells through which the fiber passes, its virtual thickness is increased.

The geometric curvature is like fiber generation simplified by a random process as a depth function of 2D Perlin noise [17]. This depth is an abstract quantity in the range $<0, 1>$ and determines the maximum amount of water trapped in the cell. Real values are greatly simplified by this concept. A graphical visualization of the paper surface is shown in Figure 9.

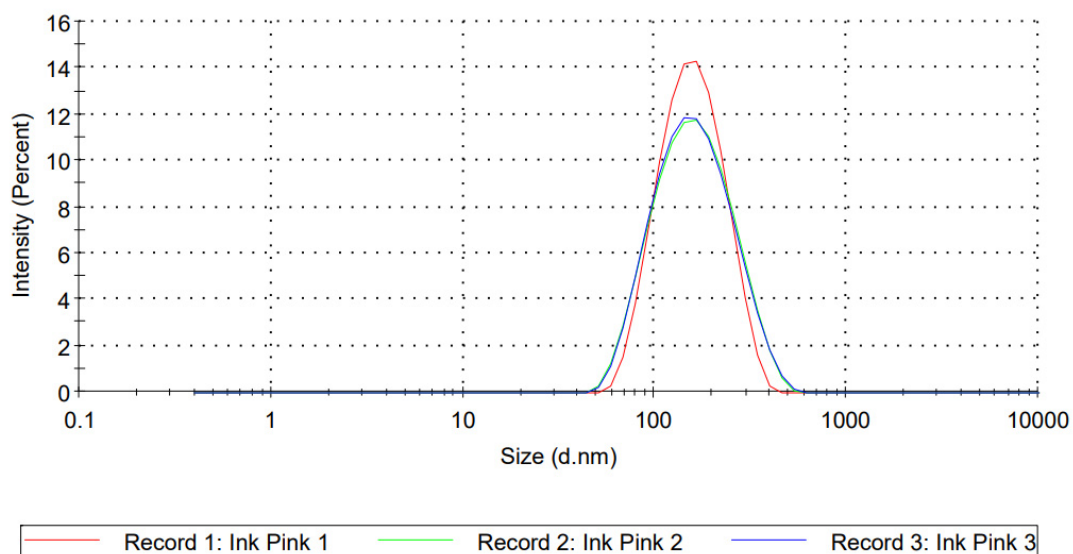


Figure 8. Particle size distribution of the test pink ink as measured by the Zetasizer.

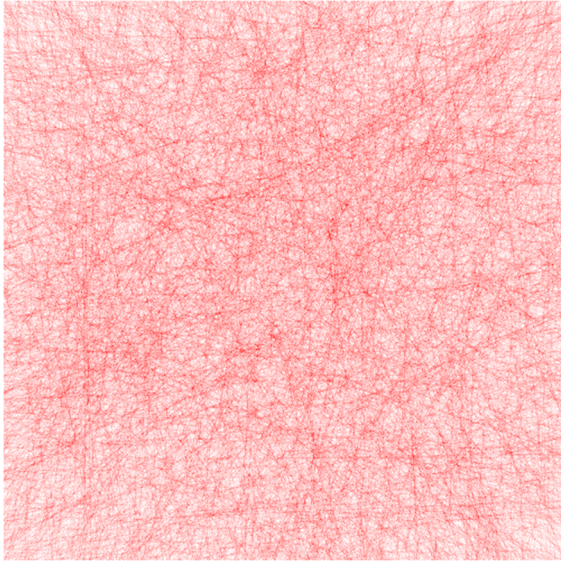


Figure 9. Graphic representation of the h parameter on the generated paper

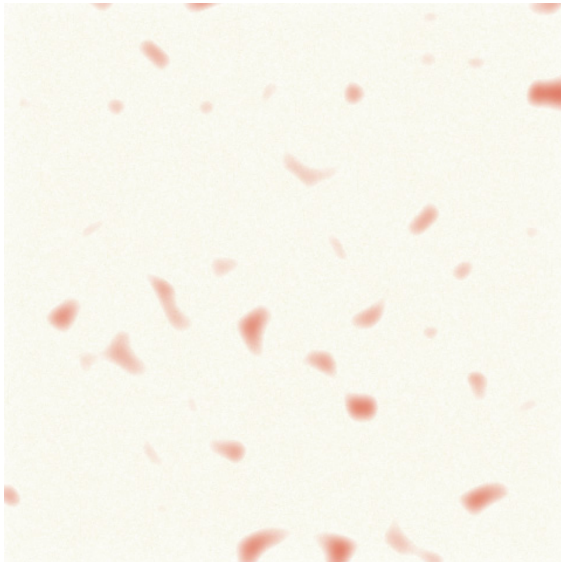


Figure 10. Graphic representation of hydrophobic spots added to paper.

Hydrophobic paper treatment

For the random distribution of hydrophobic spots, the depth function of 2D Perlin noise [17] was again used. As hydrophobically marked islands, noise values with a value of 0.5 were marked and subsequently scaled so that their size corresponded to the mean value of the spots from the measurement (Fig. 10).

Applying a drop of water

The final step in cell preparation was to place an initial drop of water on the paper. Since the applied droplet has a spherical shape, the initial amount of water in the water columns of the cells was determined as the depth of the spherical canopy of the virtual sphere placed below the surface of the paper. For a sphere centered at the point (x_0, y_0) this function has the prescription (1):

$$w = \sqrt{r^2 - (x - x_0)^2 - (y - y_0)^2} - \frac{r}{2} \quad (1)$$

This simplification was created by the authors of the work using an analytical method.

Cell definition

With respect to the parameters specified above, the cell in this model is described as a quintuple $[h, a, p, w_s, w_a]$, where:

h is the "height" of the paper, describing its surface structure and the maximum amount of captured water (dimensionless), a is the mask bounding the wet part of the paper, p is the degree of hydrophobicity belonging to the given cell (dimensionless), w_s is the amount of water in the upper part of the paper (μg) and w_a is the amount of water absorbed in the paper (μg).

Transition function

In each discrete time step Δt , the following transition function (2) is performed for all active cells o to state S_o :

$$S_o(t + \Delta t) = f(S_o(t), S_k(t) \mid k \in \text{Neighbour}) \quad (2)$$

Where $S_o(t)$ is the state of the cell at time t , given as (3):

$$\begin{aligned} S_o(t) &= (\text{activateNearby} \circ \text{absorbWater} \\ &\circ \text{spreadWater} \circ \text{flowWater} \\ &\circ \text{vaporizeWater})(S_o, S_k) \end{aligned} \quad (3)$$

Step 1: activation of neighboring cells

To save computing time, processes are calculated only in active cells. In the initial state, the active cells are under a drop of water, see Fig. 11.

Step 2: absorption of water into the paper

Following capillary phenomena, the water absorption process was approximated by a curve composed of two graphs, as can be seen in Fig. 12. The graph in Fig. 12 is realized by pseudocode shown in Fig. 13. Coefficients $[A, B, C]$ were chosen based on experiments as $[50, 0.05, 0.001]$. This function is intended to simulate the slow "onset" of absorbed water, which accelerates exponentially with its amount, dampens at higher saturation, and at the same time the overall process is delayed due to the hydrophobicity value in the given cell.

```

proc activateNearby( $a$ ):
  for cell in neighbours:
     $a \leftarrow a$  or  $a_{\text{cell}}$ 
  end for
end proc

```

Figure 11. Pseudocode extending the active simulation zone to neighbouring cells.

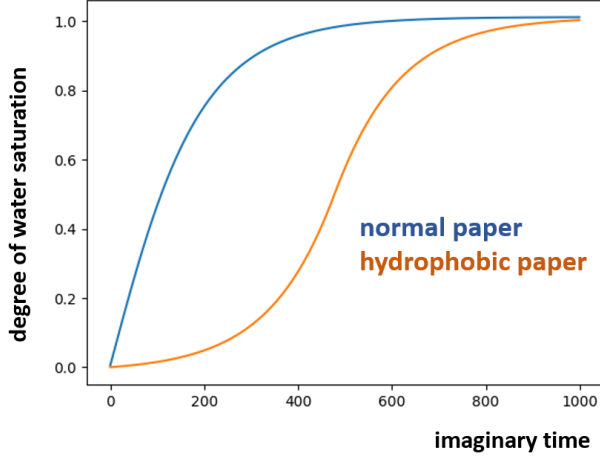


Figure 12. Approximation of the process of absorption of water into paper in time.

```

proc absorbWater(h, p, ws, wa):
    abs_force ← 0.01 +  $\frac{w_s}{A}$ 
    if (wa < p) then
        absorbe ← min(B
            · sin( $\frac{\pi}{2} \cdot \frac{w_a}{h}$ ) + C, ws)
            · abs_force
    else then
        absorbe ← min(B
            · sin( $\frac{\pi}{2} \cdot (h - \frac{w_a}{h})$ )
            + C, ws) · abs_force
    end if
    ws ← ws - absorbe
    wa ← wa + absorbe
end proc
    
```

Figure 13. Pseudocode for calculation of the amount of absorbed water.

```

proc spreadWater(h, wa):
    saturation ←  $\frac{w_a}{h}$ 
    wout ← 0
    for cell in neighbours:
        saturationcell ←  $\frac{w_{a_{cell}}}{h_{cell}}$ 
        wout
            ← wout
            +  $\left( \frac{saturation - saturation_{cell}}{2} \right) \cdot h \cdot D$ 
    end for
    wa ← wa - wout
end proc
    
```

Figure 14. Pseudocode for the calculation of the amount of water transferred to other cells by capillary diffusion.

```

proc flowWater(h, ws):
    wout ← 0
    for cell in neighbours:
        flowcell ←  $\frac{w_s - w_{s_{cell}}}{2} \cdot E \cdot (1$ 
            + (p - pcell))
        wout ← wout + flowcell
    end for
    ws ← ws - wout
end proc
    
```

Figure 15. Pseudocode for the calculation of the amount of water transferred to other cells based on hydrophobicity and water column balancing.

Step 3: water diffusion in the bottom layer

The diffusion of water in the lower layer, which is otherwise caused by capillary attractiveness, was simplified in the proposed model to the process of gradually equalizing the degree of saturation of the lower layer with other cells, see Fig. 14.

The amount of water that moves between the cells through this process is not affected by the surface treatment of the paper because it no longer extends to this depth.

Based on testing, the value of 0.1 was chosen as the *D* coefficient.

Step 4: water diffusion in the top layer

This step in which the error was found in Model 2 is essentially the same as in Model 1. The amount of water moved in each step corresponds to equalizing the water columns of neighboring cells, as described in the pseudocode in Fig. 15.

During this process, the hydrophobicity of the cells is considered (water prefers to flow into a cell with a lower *p*-value). Based on testing, the coefficient *E* was set to 0.25.

Step 5: water evaporation

This process removes water from the system with the assumption that the water in the upper layers evaporates faster than the absorbed water. Based on testing, the values [0.001, 0.01] were chosen for the [*F*, *G*] coefficients, see Fig. 16.

IMPLEMENTATION DETAILS

Multithreading

Computer programs are composed of instructions, which are run sequentially. A thread is a flow of execution of such instructions. However, modern computers can run multiple threads (hence the term Multithreading) at the same time, which allows for a faster parallel execution.

The simulation is divided into horizontal rectangles. Each rectangle is processed by one thread. During processing, the edge of the image (2 cells) and

```

proc vaporizeWater( $w_a, w_s$ ):
   $v \leftarrow F$ 
  if ( $w_s > v$ ) then
     $w_s \leftarrow w_s - v$ 
     $v \leftarrow 0$ 
  else then
     $w_s \leftarrow 0$ 
     $v \leftarrow v - w_s$ 
  end if
   $v \leftarrow v \cdot G$ 
  if ( $w_a > v$ ) then
     $w_a \leftarrow w_a - v$ 
  else then
     $w_a \leftarrow 0$ 
  end if
end proc

```

Figure 16. Pseudocode for the calculation of the amount of evaporated water.

inactive cells are omitted to maintain fast processing and correct memory access. At each time step, logical functions that provide the cell simulation logic will execute for all cells in the cellular automaton and wait for all threads to complete. This way, the program can utilize the full processing power of given program environment and thus causing the simulation to run quickly even for sizes of millions of cells.

Implementation

The cellular automaton uses the 2D field abstraction for simulation. In the source code, the 2D field is implemented as a 1D field indexed by $[x + y * W]$, where W is the width of the field. The field itself does not contain specific elements, but pointers to the given cells to enable caching.

The simulation itself uses two of these fields, which it switches between during the simulation. The 1st field is read-only and contains the old state, which is used to calculate the new state. The 2nd field is intended for storing the new state of the simulation. Two functions are implemented to manipulate these fields: the flip function, which swaps pointers to these fields, and the mirror function, which creates a deep copy of the new field into the old one.

Pointer swapping is fast but cannot be used in all cases. If only parts of the model are updated (for example speed of water movement, amount of water after transfer), data inconsistency may arise. Therefore, this method should only be used after completing the entire simulation step.

Creating a deep copy provides a safe way to manipulate data without possible inconsistency but creating a copy of the data itself is very time consuming compared to changing two pointers.

The implementation of individual models is separated into individual components according to the given model.

VERIFICATION AND VALIDATION OF THE MODEL

The validity of the model could be verified visually by comparison with laboratory results. The output of the simulation is an animated .gif file, which shows the time course of water spreading in the bottom layer of paper. The key points of this simulation are shown in Figure 17.

We managed to verify the main researched hypothesis through simulation. Figure 11 shows how the water gradually spread to the lower layer through the created channels and within a few seconds of their introduction, it was fully saturated. This result, after the optimal determination of the parameters A-G, corresponds to the physical results with which the output of the model was compared (Fig. 18).

CONCLUSION

We managed to detect errors and inaccuracies in two published simulation models and successfully design our own simplified model, thanks to which it is possible to parameterize and visualize water absorption on specially treated paper.

Such a simulation can be used, for example, for artistic needs, but also for simulating the absorption behavior of various liquids and the rate of paper seepage depending on the change of some parameters, especially the thickness of the paper (parameter h), the distribution of hydrophobic areas (parameter p) or specific behavior of the liquid (parameters w), etc.

As non-woven fabrics, for example, have a similar structure and fiber arrangement to paper, this model is also suitable for textile structures where wetting processes, liquid distribution, etc. are very important, e.g., for hygiene products.

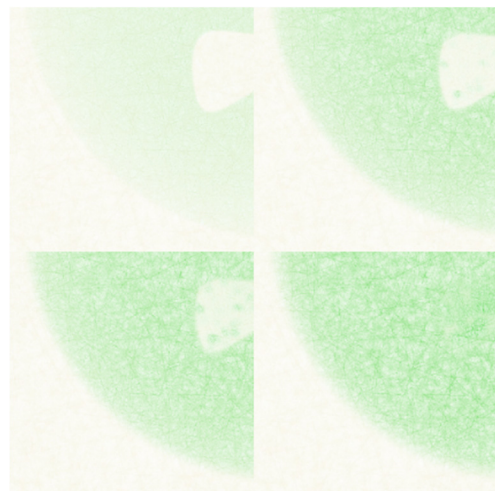


Figure 17. Degree of paper saturation with water at times 3 s, 12 s, 18 s, 26 s.



Figure 18. Three samples made at a time interval of 10 s on paper with surface hydrophobization using a spray-applied hydrophobic varnish: left with incipient surface absorption, middle with visible hydrophobic defects, right almost absorbed.

Acknowledgement: *This work was supported by Iceland, Liechtenstein and Norway through the EEA Grants and the Technology Agency of the Czech Republic within the framework of project “inherently Flexible Aerogels for energy efficient structurES (i-FACES)” (Grant number TO01000311).*

REFERENCES

1. Curtis C.J., et al.: Computer-generated watercolor. In: Proceedings of the 24th annual conference on Computer graphics and interactive techniques, 1997, pp. 421-430
2. Zhang Q., et al.: Simple cellular automaton-based simulation of ink behaviour and its application to Suibokuga-like 3D rendering of trees, The Journal of Visualization and Computer Animation, 10(1), 1999, pp. 27-37.
[https://doi.org/10.1002/\(SICI\)1099-1778\(199901/03\)10:1<27::AID-VIS194>3.0.CO;2-C](https://doi.org/10.1002/(SICI)1099-1778(199901/03)10:1<27::AID-VIS194>3.0.CO;2-C)
3. Small, D.: Simulating watercolor by modeling diffusion, pigment, and paper fibers. In: Image Handling and Reproduction Systems Integration. SPIE, 1460, 1991, pp. 140-146.
<https://doi.org/10.1117/12.44417>
4. Ren, Y., et al.: Ink diffusion simulation in Chinese calligraphy using navier–stokes equation. In: Simulations, Serious Games and Their Applications. Springer, Singapore, 2014, pp. 15-29.
https://doi.org/10.1007/978-981-4560-32-0_2
5. Roberts J. C.: The chemistry of paper, Royal Society of Chemistry, 2007, 204 p.
6. De Assis T., et al. : Comparison of wood and non-wood market pulps for tissue paper application, BioResources, 14(3), 2019, pp. 6781-6810.
<https://doi.org/10.15376/biores.14.3.6781-6810>
7. Zambrano F., et al.: Upcycling strategies for old corrugated containerboard to attain high-performance tissue paper: A viable answer to the packaging waste generation dilemma, Resources, Conservation and Recycling, 175, 2021, 105854.
<https://doi.org/10.1016/j.resconrec.2021.105854>
8. Codd E. F., Ashenurst R. L.(ed.): Cellular automata, Academic press, 2014, 132 P.
9. Stroustrup B.: An overview of the C++ programming language. Handbook of object technology, CRC Press LLC, Boca Raton, 1999, 23 p.
10. Soulié, J.: C++ Language tutorial, 2008, online: <http://www.cplusplus.com/doc/tutorial> [cit. 14.12.2022]
11. Zeigler B.P, et al.: Theory of modelling and simulation, 3rd edition, Elsevier, 2018, 435 p.
12. Fishwick P.A.: Simulation model design and execution: Building Digital Worlds, Prentice-Hall, 1995, 448 p.
13. Chopard B., Droz M.: Cellular automata. Modelling of physical, Cambridge University Press, 1998, 341 p.
14. Wolnik B., et al.: Number-conserving cellular automata with a von Neumann neighborhood of range one. Journal of Physics A: Mathematical and Theoretical, 50(43), 435101.
<https://doi.org/10.1088/1751-8121/aa89cf>
15. Shiffman D.: Chapter 7: Cellular automata. Nature of Code, 2012.
16. Koopman P.: Bresenham line-drawing algorithm. Forth Dimensions, 8(6), 1987, pp. 12-16.
17. Hart J. C.: Perlin noise pixel shaders. In: Proceedings of the ACM SIGGRAPH/EUROGRAPHICS workshop on Graphics hardware, 2001, pp. 87-94.2022.

ELECTRIC HEATING CLOTHING FOR MOTORCYCLISTS

ARABULI, ARSENI; ARABULI, SVITLANA*; KYZYMCHUK, OLENA AND MELNYK, LIUDMYLA

Kyiv National University of Technologies & Design, Nemyrovycha-Danchenko str. 2, 01011 Kyiv, Ukraine

ABSTRACT

In recent years motorcycling becomes more and more popular. It is known that even in relatively warm weather, moving air is cooler and constant exposure to wind when riding may cause a chilling effect that leads to hypothermia. Motorcyclists may lose the ability to concentrate and react on changing traffic conditions when they have hypothermia. We propose the use of electric heating elements in the jacket so that motorcyclist comforts increase. This element receives the energy from the worked engine of the motorcycle. It is located between the two fabrics layers (top and lining) and is made of nichrome wire. The heating is carried out by connecting this element with the power supply system of the motorcycle. In research, we use two types of packages that differ by top fabrics and two connection circuits. The studies were carried out in three different environmental conditions (air temperature, wind speed, and air humidity). Standard test methods were used for performance testing. The effectiveness of electric heating elements used in underwear space for increasing the thermal properties of motorcyclist clothing is proven. It was established that the use of an electric heating element is effective only with a thermocontroller in the electrical circuit. The results of our investigation confirmed the effectiveness of electric heating elements being used in motorcyclist jackets.


KEYWORDS

Motorcyclist clothing; Hypothermia; Heating element; Comfort.

INTRODUCTION

The riding gear market studied was valued at USD 10.65 billion in 2020, and it is projected to be worth USD 15.84 billion by 2026, registering a compound annual growth rate (CAGR) of 6.84% during the forecast period [1]. The increasing demand for premium motorcycles has led to an increase in spending on motorcycle clothing as well as protective gear such as helmets, gloves, jackets, knee and elbow guards, spine guards, pants, and footwear. Over the next three years, motorcycle clothing will record a 3,8% growth rate in terms of revenue, the size of the global market will reach \$ 117.90 billion in 2026 [2]. Moreover, protective gears are thicker than conventional clothing with waterproof closures and pockets, zips, higher collars, and are even fitted out with armor. Demand for innovative products that offer efficient use and safety features is growing among the consumers that leading to increases in spending on R&D to offer innovative products with added safety features [3].

Today there is known a wide range of motorcyclists clothing designs which depends on the type of motorcycle (for a certain kind of sports or used in everyday life). Clothing for motorcyclists is classified into 3 groups:

1. Nonprotective (clothing creates a barrier against weather conditions: wind, rain, snow, etc.);
2. Nonprotective but clothing is equipped with protectors marked  on the shoulder, knee, back, or cubits;
3. Protective (clothing with protection by the use of plastic protectors, connected to each other).

There are some basic requirements for motorcyclists' clothing. First of all, clothing should be reliable, because of increasing human traumatism during competitions, accidents, and falls. Nowadays, the requirements of reliability are provided by the protective inserts and technological elements of clothing (silhouette, shape, cut) [4, 5]. Protective gear has a second important purpose - comfort. Uncomfortable gear can distract from riding but properly fitting protective gear will help to stay comfortable when encountering various riding conditions. Ergonomic requirements in terms of comfort, fit, and ease of movement should not create safety hazards. For example, jackets with external pockets or straps may snag on the motorcycle or other vehicle in a crash [6].

It is essential to design/develop the right clothing for motorcycle riders. Very little research is being carried out in this field. The invention is more concerned with

* Corresponding author: Arabuli S., e-mail: arabuli.si@knu.edu.ua

Received June 13, 2022; accepted March 9, 2023

society, reducing injuries during accidents, safeguarding the lives of the people, protecting animals (minimizing the usage of leather), motivating interdisciplinary projects, and preferably for the wellbeing of humans [7]. Most research in motorcyclist clothes is related to development the helmet [8], to improving the visibility [9, 10] and safety [11] of bicyclists. Some papers report the effect of protective clothing on wear comfort [12, 13]. They are emphasis on improving the protective fabric's resistance with better comfort properties [14] such as permeability, moisture management and thermal resistance.

Thermal comfort is one of the essential components of motorcyclist wear. Even in relatively warm weather, moving air is cooler and constant exposure to wind when riding may cause a chilling effect that leads to hypothermia [15]. Hypothermia is a condition of subnormal body temperature that can cause loss of concentration, slowed reactions, and loss of smooth, precise muscle movement. It's possible to lose the ability to concentrate and react to changing traffic conditions. From the other point clothes that are just right for cold weather may be too hot once you stop.

Thus, an improvement of the clothing for motorcyclist thermal properties is important. As the result of literature analysis for the project by the Centre for Accident Research & Road Safety [16] the key elements to be considered in evaluating the weather protection provided by motorcycle clothing was established. The main ones are the provision to allow insulation from cold temperatures and ventilation in heat and the design and fit to reduce flapping and wind buffeting which forces warm air out. Still there is a gap in investigation the possible ways to increase the thermal resistance of clothes for motorbikers.

There are four types of personal heating garment: electrical heating garment (EHG), phase change material (PCM) garment, chemical heating garment (CHG), and fluid/air flow heating garments [17, 18]. Currently, the personal heating garment has some visible drawbacks, e.g., battery performance cannot meet the requirements of long exposure in cold conditions in EHG; the temperature cannot be controlled in chemical heating pads; released latent heat has little effect on the human body in both microencapsulated and packaged PCM heating garments; and liquid/air flow heating systems limit human activities. Compared with other types EHG are expected to have a promising future.

There are several papers presenting research results in heating garment development regarding clothes design as well as heating elements creation and production.

Song et al [19] study the possibility to use electrically and chemically heated garments in order to improve

the thermal comfort of university students in a cold classroom. For EHG, five electrical heating pads were attached to the inner side of the vest (two at the waist, two at the scapula, and one at the lower back), and two additional heating pads were located in the kneecaps. It was found that heated clothing ensembles could significantly improve both the overall-body thermal comfort (evidenced by the significantly elevated mean skin and body temperatures and improved the whole-, upper- and lower-body thermal and comfort sensations) and the local-body thermal comfort (evidenced by the significantly elevated finger temperature, finger blood flow, and finger dexterity, and improved thermal sensations at hands and feet).

The development in the electrical heating garment is going in the direction of wearable heating systems [20-22]. The flexibility of the heating system is very important since the users'/system structures are mostly irregular shaped. Heating with non-flexible systems may cause great heat losses due to less contact. For this reason, textile-based heating systems are an added advantage because of the efficient heat delivery mechanism by wrapping the structure due to its flexibility. For example, knitted heating fabrics of plain, rib, and interlock structure were designed and fabricated by using silver plating compound yarns and polyester staple fiber spun yarns [23]. By taking and analyzing infrared temperature images strong linear correlations can be observed between surface maximum equilibrium temperature and power consumption density as well as between power consumption density and inner equilibrium temperature of mimetic clothing. Such materials will have wide application prospects in the active warming field because of a lot of advantages, such as an even surface temperature field in the heating process, structure simplicity, flexibility, etc.

Havelka et al [24] focused on the possibilities of the application of electric heating built directly into clothing for seniors, especially for clothes designed for a cold environment. The proposed heating system based on embroidery with using hybrid threads can be used especially in winter clothing, but can also be used for home-use clothing or everywhere it is disadvantageous or inappropriately to increase the ambient temperature.

The purpose of the work is to create a wind-, water-resistance, and heat protective jacket for a motorcyclist not only due to the properties of textile materials. We propose a method of increasing the thermal properties of motorcyclists' clothing, namely, through the use of electric heating element in the suit. This element receives the energy from the worked engine.

Table 1. Characteristics of textiles.

Textile code	Fabric structure (weave)	Material composition [%]	Weight (Areal density) [g/m ²]	Thickness [mm]	Count [warp · weft/cm]	Fineness of yarn (linear mass), warp/weft, [tex]
Top fabric						
T1	twill2/2	PES – 100	145	0.18	75/41	9.7/12.1
T2	multiple twill	PES – 100	180	0.32	65/43	20.4/13.3
Lining fabric						
L	twill2/1	PES – 100	99	0.15	65/39	8.3/8.3

MATERIALS AND METHODS

Textile materials

This paper deals with clothing for motorcyclists of the first group – “non-protective” – clothing that creates a barrier against only weather conditions: wind, rain, snow, etc. As the top layer, polyester fabric used for clothing was selected. Top fabrics have water repellency treatment. Characteristics of textiles are shown in Table 1.

Electric heating element

Ukrainian assortment of jackets for motorcyclists with a warming lining does not allow provide comfortable conditions that satisfy ergonomic requirements (boundary temperature range of the human body from 36.8°C to 37.2°C [25]; a temperature of the underwear space from 29°C to 32°C). If the temperature goes beyond these limits, it leads to various physiological and behavioral changes in the human body, which are aimed at resuming the boundary temperature [26-28].

We propose to use the electric heating element in the jackets. The size of each heating element is 10x16 cm. This element is located between two layers of lining fabric and is made of nichrome wire. A nichrome spiral is a heating element in the form of a wire twisted in a spiral for compact placement. The wire is made of nichrome, a precision alloy, the main components of which are nickel (80%) and chromium (20%). The length of the nichrome wire is 2.0 m, the diameter is 0.8 mm, it is folded in a zigzag (spiral). The minimum temperature parameter of the heating element is 30°C, and the maximum is 50°C. During

washing, the heating element is pulled out. The heating is carried out by connecting this element with the power supply system of the motorcycle. In research, we use 2 connection schemes (Fig. 1(a, b)) of the heating element to supply system, which is shown in Fig. 2.

Connection scheme №1 (Fig. 1(a)): heating element is connected to the motorcycle battery using electric wires, through a tumbler switch and a resistor.

Connection scheme №2 (Fig. 1(b)): heating element is connected to the motorcycle battery using electric wires, through a tumbler switch and thermocontroller. TCXRE digital thermocontroller was used. The thermocontroller allows regulating the temperature of the heating element. This, in turn, allows to control and give the air temperature in the underwear space.

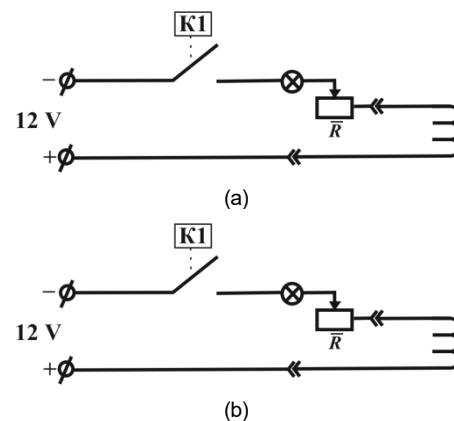


Figure 1. Connective scheme of the electric heating element with a power supply system of the motorcycle: (a) connection scheme №1; (b) connection scheme №2.



Figure 2. Connection of the electric heating element with a power supply system of the motorcycle.

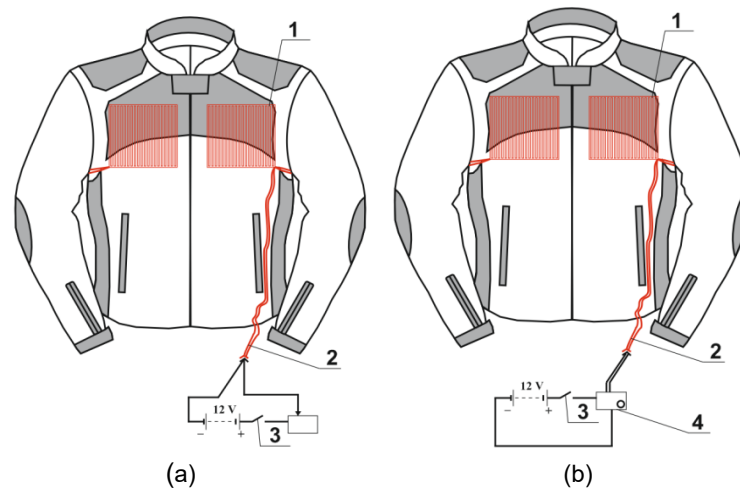


Figure 4. Design of motorcyclist's jacket with electric heating element: (a) connection scheme №1 (1 - heating element; 2 - wire; 3 - tumbler switch), (b) connection scheme №2 (1 - heating element; 2 - wire; 3 - tumbler switch, 4 - thermocontroller).

Textile packages

Two types of packages that differ of top fabrics were investigated (Fig. 3):

- package A – T1 + (L + electric heating element + L);
- package B – T2 + (L + electric heating element + L).

The electric heating element is located between the two layers of lining fabrics L.

Design of motorcyclist's jacket

The design of the motorcycle jacket is shown in Fig. 4(a, b). The heating element (1) is located at the top of the front of the motorcycle's jacket. Using electric wires (2), through a tumbler switch (3) and a thermocontroller (4) (in case of Connection scheme №2) it is connected to the motorcycle battery. This arrangement of the heating element in the jacket is due to the fact that during the movement of the motorcycle, the cold air flow through the front of the jacket partially penetrates under the space between the jacket and the body of the motorcyclist and cools it (Fig. 5). The presence of a heating element in the jacket heats the air under the jacket. Cold air, which partially penetrates through the jacket while the motorcycle is moving, mixes with the heated air. This avoids hypothermia in the motorcyclist. However, the presence of a heating element without a thermocontroller can lead to overheating of the space under the jacket. To prevent this phenomenon, a thermocontroller was connected to the electrical circuit (Fig. 4 (b)).

Methods

Structural parameters. Studies of the structural parameters of the fabrics were conducted according to standard methods:

- ISO 3801:1977. Textiles — Woven fabrics — Determination of mass per unit, length, and mass per unit area [29]

- ISO/TR 11827:2012 Textiles — Composition testing — Identification of fibers. [30]

Spray test. The spray method is a primary technique for the evaluation of water repellency of fabric as per ISO 4920:2012 Textile fabrics — Determination of resistance to surface wetting (spray test) [31]. A spray test of fabric samples subjected to waterproofing treatment was evaluated using a spray-type water repellency tester. For tests, 5 samples were taken from different places of the textile material without wrinkles. Each test specimen was conditioned at 21 ± 1 °C and $65 \pm 2\%$ relative humidity for a minimum of 4 h before testing. Each specimen was assigned a rating corresponding to the nearest level on the rating chart (Fig. 6).

Air permeability. The air permeability [mm/s] of fabrics was determined and calculated by the equation according to ISO 9237:1995 [32]. Ten parallel measurements were carried out for each fabric variant. The mean values are used for the analysis.

The fabric samples were placed in the standard atmosphere, which was 21 ± 1 °C and $65 \pm 2\%$ relative humidity, for 24 h.

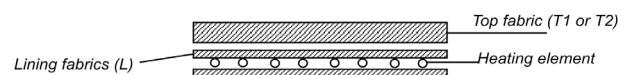


Figure 3. Scheme of the package of the motorcycle jacket.

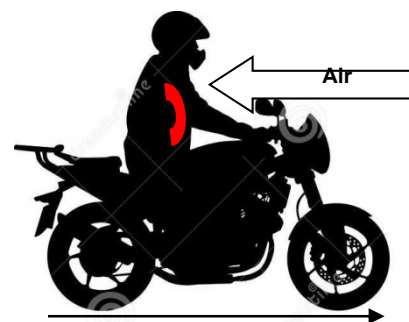


Figure 5. Scheme of motorcyclist movement.

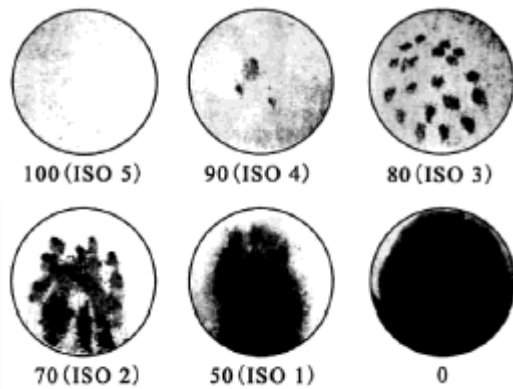


Figure 6. Standard spray test ratings [31]: 100 (ISO 5) No wetting of the specimen face; 90 (ISO 4) Slight random wetting of the specimen face; 80 (ISO 3) Wetting of specimen face at spray points; 70 (ISO 2) Partial wetting of the specimen face beyond the spray points; 50 (ISO 1) Complete wetting of the entire specimen face beyond the spray points; 0 Complete wetting of the entire face of the specimen.

Table 2. Air permeability and water resistance of textiles and packages.

Textile code	Air permeability, [mm/s]	Water repellency
<i>Top fabric</i>		
T1	3.1±0.1	80 (ISO 3)
T2	2.9±0.1	90 (ISO 4)
<i>Package</i>		
package A	2.9±0.1	-
package B	2.4±0.1	-

Air temperature. The temperature in the underclothing space was determined under real conditions: at night; motorcycle Yamaha YZF-R6; the road with asphalt covering. Driving speed was varied from 10 to 60 km/h. Air temperature was varied from 10 to 20 ± 2°C with an interval of 5°C, wind speed ranging from 0 to 4 m/s. The temperature in the underclothing space was measured by a thermocouple, which is connected to the digital thermometer WSD-10. The thermocouple was located at the level of the upper part of the front in the area of the heating element. Ten parallel measurements were carried out for each fabric variant. The average values are used for the analysis.

RESULTS AND DISCUSSION

Air permeability and water repellency of fabrics

According to the requirements for motorcycle jackets, the air permeability of the top fabric should be minimal and provide a barrier to cooling the space under the clothes and the body of the motorcycle rider. It can be seen from the results in Table 2 that the top fabric T2 has a low level of air permeability compared to fabric T1.

The water repellency of top fabrics was measured using a spray tester. It can be seen from the results in Table 2 that the top fabric T2 has a better water repellency compared to fabric T1. Analysis of the textile water resistance (Table 2) shows that the fabric T1 corresponds to level 3 (descriptive scale according to ISO 4920: 2012 – Wetting of specimen face at

spray points). In turn the fabric T2 corresponds to level 4 (descriptive scale according to ISO 4920: 2012 – Slight random wetting of the specimen face).

These investigations allow choosing for further investigations as top fabric in a package the fabric T2 that has low air permeability and better water repellency properties. The study of the air permeability of the packages (package A and package B) showed that package B has less breathability than package A (Table 2). And taking into account that the top fabric T2 has better water repellency, therefore, package B was chosen for further research.

Temperature in the space under clothing

The temperature in the space under clothing measurements was done only for package B, according to the previous results of air permeability and water resistance (Table 2). The studies were carried out in three variants by different environmental conditions (Table 3 and Fig. 7). The input data are air temperature (T_{air} , [°C]), wind speed (V_{wind} , [m/s]), and air humidity (W , [%]). The experiment was carried out for several days under different environmental conditions.

The analysis of the results (Fig. 7) showed that the temperature changing in the space under the clothes is similar for variant of investigations №1, №2, and №3 (Connection scheme №1 – without thermocontroller). As the speed of the motorcycle increases to 60 km/h, the temperature in the space under the clothes decreases by 3.5 – 5.0 °C. At the same time, starting from a speed of 40 km/h, the change in temperature in the space under the clothes was not a statistically significantly different. The use of heating element (Connection scheme №1 – without thermocontroller) allows to maintain the temperature under clothing in the range of 41.0 – 45.0 °C, thus excluding hypothermia (less than 35 °C), but leads to overheating of the motorcyclist's body. The temperature in the space under the clothes, where the heating element is switched off, is about 20 °C – these are not comfortable conditions [33, 34], either.

To exclude overheating of the body when the heating element was turned “on” and to maintain comfortable conditions in the underwear space (temperature of the underwear space from 29 °C to 32 °C), a thermocontroller was connected to the electrical circuit (Fig. 1. b). To test the effectiveness of using a heating element with the thermocontroller turned “on”, an experiment was carried out under the same conditions as when the thermostat was turned “off”. The temperature of the thermocontroller was set at 32 °C as such that corresponds to the maximum comfortable temperature of the underwear space. The results of the study with the thermostat turned “on” and the heating element turned “on” are presented in Table 3 and Fig. 7 (Line 3 – heating element “on”, thermocontroller “on”).

The analysis of the results for Connection scheme №2 – thermocontroller “on” showed that the temperature changing in the space under the clothes is similar for variants №1, №2 and №3. The character of the curves (Line 3 - heating element “on”, thermocontroller “on”) differs from the character of the curves (Line 1 and Line 2) in Fig.7. The temperature under the clothes initially rises, then it stabilizes and, due to the thermocontroller, is maintained at the level of $32 \pm 0,5$ °C. This temperature is the comfortable

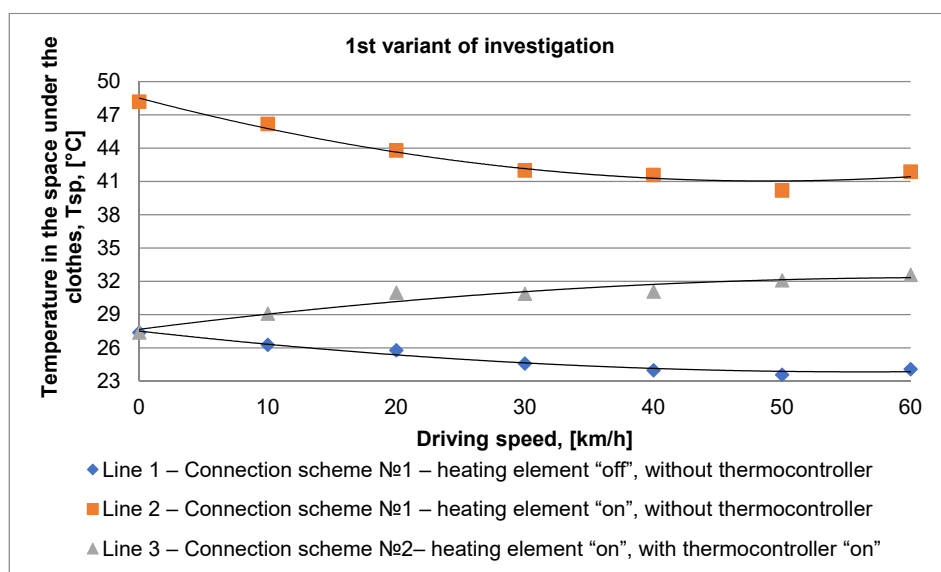
temperature of the underwear space, which does not cause hypothermia and overheating of the motorcyclist's body.

The obtained results showed that the jacket design, package composition and the use of an electric heating element with thermocontroller provide the thermophysiological comfort of the motorcyclist's body in the considered range of environmental conditions.

Table 3. Dynamic of temperature changing in the space under the clothes (package B).

Variant of investigation	Environmental conditions	Driving speed, [km/h]	The temperature in the space under the clothes, T_{sp} , [°C]		
			Connection scheme №1 Without thermocontroller		Connection scheme №2 With thermocontroller “on”
			Heating element “off”	Heating element “on”	Heating element “on”
Variant №1	$T_{air} \approx 10^{\circ}\text{C}$; $V_{wind} = 4$ m/s; $W = 94\%$	0	27.4	48.2	27.4
		10	26.3	46.2	29.1
		20	25.8	43.8	31.0
		30	24.6	42.0	30.9
		40	24.0	41.6	31.1
		50	23.6	40.2	32.1
		60*	24.1	41.9	32.5
Variant №2	$T_{air} \approx 15^{\circ}\text{C}$; $V_{wind} = 2$ m/s; $W = 80\%$	0	28.8	48.7	28.8
		10	27.1	47.8	29.6
		20	26.1	44.6	30.0
		30	25.6	42.8	29.9
		40	25.2	42.2	31.7
		50	24.8	40.9	32.0
		60*	25.2	42.0	32.0
Variant №3	$T_{air} \approx 20^{\circ}\text{C}$; $V_{wind} = 3$ m/s; $W = 53\%$	0	30.6	49.0	30.6
		10	29.0	47.9	30.9
		20	28.2	46.6	31.5
		30	27.6	44.8	32.0
		40	26.5	44.1	32.2
		50	26.0	43.2	32.5
		60*	26.3	44.8	32.5

* 60 km/h – is the speed maximum for driving in Ukraine through cities and villages



(a)

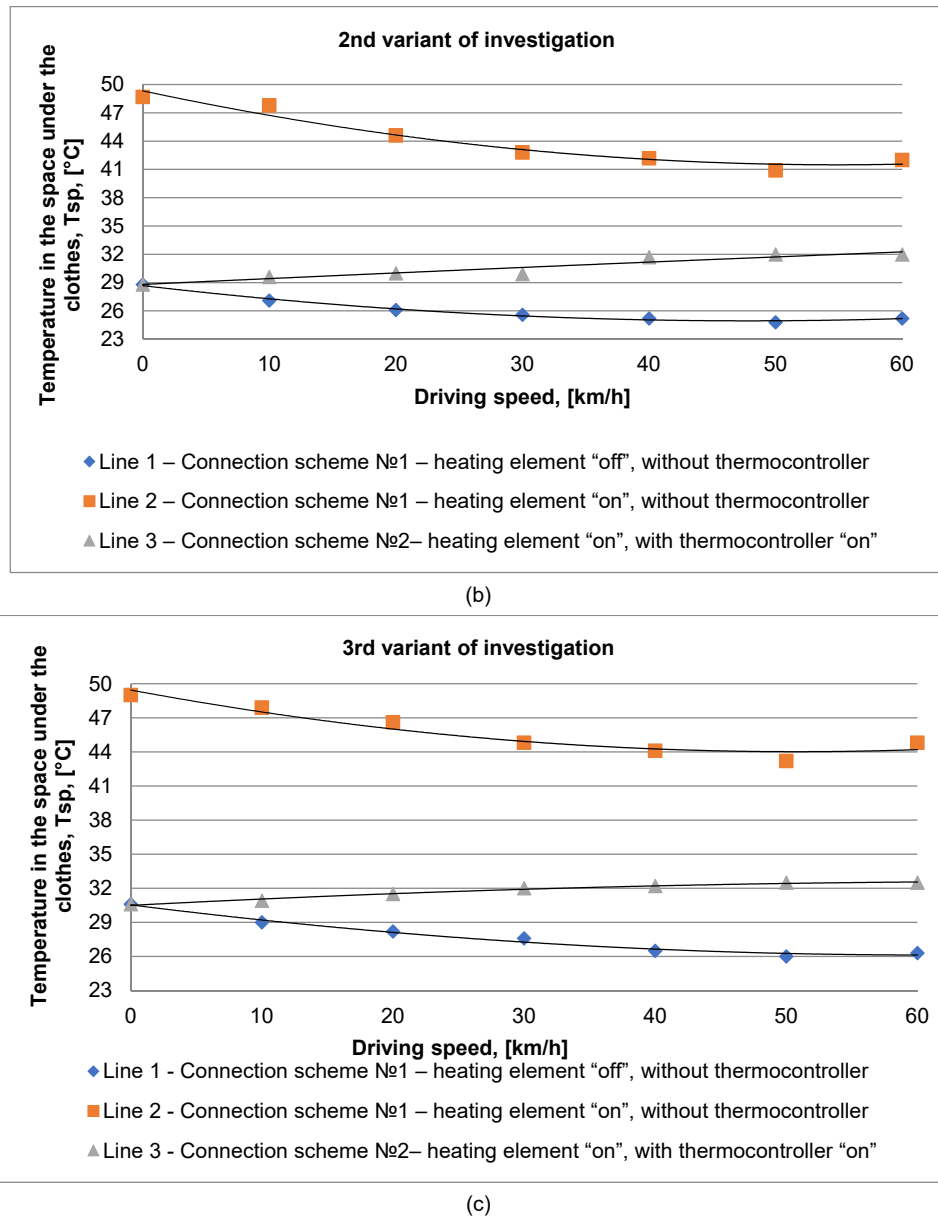


Figure 7. Temperature changing in the space under the clothes (Package B): (a) – 1st variant of investigation (environmental conditions: $T_{air} \approx 100^\circ\text{C}$; $V_{wind} = 4 \text{ m/s}$; $W = 94\%$), (b) – 2nd variant of investigation (environmental conditions: $T_{air} \approx 150^\circ\text{C}$; $V_{wind} = 2 \text{ m/s}$; $W = 80\%$), (c) – 3rd variant of investigation (environmental conditions: $T_{air} \approx 200^\circ\text{C}$; $V_{wind} = 3 \text{ m/s}$; $W = 53\%$).

CONCLUSION

Thermal comfort is one of the essential components of motorcyclist wear. A chilling effect during riding could lead to hypothermia and cause loss of concentration. Alternatively, warm clothes that are just right for cold weather could become uncomfortable once you stop. Very little research is being carried out in motorcyclists clothing design that meet requirements for thermal insulation of body during motion. Our research has confirmed the effectiveness of electric heating elements used in underwear space for increasing the thermal properties of motorcyclist clothing. It was established that the use of an electric heating element is effective only with the thermocontroller in the electrical circuit. The thermocontroller allows to maintain a comfortable

temperature in the underwear space and excludes hypothermia or overheating of the motorcyclist's body.

REFERENCES

1. RGM Report: Riding Gear Market – Growth, Trends, COVID-19 Impact, and Forecast (2021-2026). <https://www.mordorintelligence.com/industry-reports/riding-gear-market>
2. MAM Report. Motorcycle Apparel Market: Information by Product Type (Helmets, Jackets, Gloves, Shoes, Pants, Base Layers and others), End Use (On-Road Motorcycle Apparel and Off-Road Motorcycle Apparel), Distribution Channel (Store-Based and Non-Store-Based) and Region (North America, Europe, Asia-Pacific and Rest of the World) - Forecast till 2027. <https://www.marketresearchfuture.com/reports/motorcycle-apparel-market-7990>

3. MRGM Report. Motorbike Riding Gear Market Size, Share & Trends Analysis Report By Product (Protective Gear, Clothing), By Distribution Channel (Online, Offline), And Segment Forecasts, 2019–2025.
<https://www.grandviewresearch.com/industry-analysis/motorbike-riding-gear-market>
4. Council Directive 89/686/EEC of 21 December 1989 on the approximation of the laws of the Member States relating to personal protective equipment, p.18.
5. EN 13595-1:2002: Protective clothing for professional motorcycle riders. Jackets, trousers and one piece or divided suits. General requirements.
6. Personal protective gear for the motorcyclist. Cycle Safety Information. MSF – Motorcycle Safety Foundation.
<https://www.msf-usa.org/>
7. Natarajan G, and Rajan T.P.: Review on the performance characteristics and quality standards of motorcycle protective clothing. *Journal of Industrial Textiles*. 2022;51(5_suppl): 7409S-7427S.
<https://doi.org/10.1177/15280837211057578>
8. Kang Y. and Kim S.: Development of helmet mold design system using 3D anthropometric analysis, *International Journal of Clothing Science and Technology*, 32(3), 2020, pp. 446-456.
<https://doi.org/10.1108/IJCST-02-2019-0022>
9. Koo H.S. and Huang, X.: Visibility aid cycling clothing: flashing light-emitting diode (FLED) configurations, *International Journal of Clothing Science and Technology*, 27(3), 2015, pp. 460-471.
<https://doi.org/10.1108/IJCST-09-2014-0104>
10. Stapleton T. and Koo H.S.: Bicyclist biomotion visibility aids: a 3D eye-tracking analysis, *International Journal of Clothing Science and Technology*, 29 (2), 2017, pp. 262-269.
<https://doi.org/10.1108/IJCST-05-2016-0060>
11. Bulathsinghala R.L., Fernando S., Jayawardana T.S.S., et al.: An automatic air inflated tubeless safety jacket for motorbike riders, *Research Journal of Textile and Apparel*, 26(2), 2022, pp. 170-186.
<https://doi.org/10.1108/RJTA-01-2021-0002>
12. Stiles R., Benge C., Stiles P.J., et al.: Evaluation of Protective Equipment Used Among Motorbike Riders, *Kans J Med*, 11(2), 2018, pp.1-13.
13. Wardiningsih W. and Troynikov O.: Effects of hip protective clothing on thermal wear comfort of clothing ensembles, *Research Journal of Textile and Apparel*, 25 (3), 2021, pp. 226-239.
<https://doi.org/10.1108/RJTA-11-2020-0124>
14. Jamal H., Ahmad F., Azam F., et al.: Development and characterization of impact resistant fabric with better comfort for motorbike riders, *The Journal of The Textile Institute*, 2022.
<https://doi.org/10.1080/00405000.2022.2093080>
15. Shin S., Choi H.H., Kim Y.B., et al.: Evaluation of body heating protocols with graphene heated clothing in a cold environment, *International Journal of Clothing Science and Technology*, 29(6), 2017, pp. 830-844.
<https://doi.org/10.1108/IJCST-03-2017-0026>
16. Haworth N., De Rome L., Rowden P.: Motorcycle protective clothing: Stage 1. Review of Literature and development of a safety 'STAR RATING' system (RSD-0299), Report to the Centre for Accident Research & Road Safety, 2006.
17. Wang F., Gao C., and Kuklane K.: A Review of Technology of Personal Heating Garments, *International journal of occupational safety and ergonomics: JOSE* 16(3), 2010, pp. 387-404.
<https://doi.org/10.1080/10803548.2010.11076854>
18. Riabchykov M., Alexandrov O., Trishch R., et al.: Prospects for the development of smart clothing with the use of textile materials with magnetic properties, *Tekstilec*, 65(1), 2022, pp. 36–43.
<https://doi.org/10.14502/tekstilec.65.2021050>
19. Song, W., Wang, F., Zhang, C. and Lai, D.: On the improvement of thermal comfort of university students by using electrically and chemically heated clothing in a cold classroom environment, *Building and Environment*, 94, 2015, pp. 704-713.
<https://doi.org/10.1016/j.buildenv.2015.10.017>
20. Bahadir S.K. and Sahin U.K.: A wearable heating system with controllable e-textile-based thermal panel, *Wearable Technologies*. Chapter 9, 2018, pp.175-194.
<https://doi.org/10.5772/intechopen.76192>
21. Mo S., Mo M. and Ho, K.C.: Fabrication of electric heating garment with plasma-assisted metal coating (PAC) technology, *International Journal of Clothing Science and Technology*, 32(3), 2020, pp. 297-306.
<https://doi.org/10.1108/IJCST-04-2019-0050>
22. Wieżlak, W. and Zieliński, J.: Clothing heated with textile heating elements, *International Journal of Clothing Science and Technology*, 5(5), 1993, pp. 9-23.
<https://doi.org/10.1108/eb003023>
23. Liu, H., Li, J., Chen, L., et al.: Thermal-electronic behaviors investigation of knitted heating fabrics based on silver plating compound yarns, *Textile Research Journal*, 86(13), 2016, pp. 1398–1412.
<https://doi.org/10.1177/0040517515612359>
24. Havelka A., Tichy M., Soukup R. and Nagy L.: Application of hybrid heating textile structures in clothing for seniors. *Vlákna a Textil*, 4, 2018, pp. 26-30.
25. Havenith G.: The interaction of clothing and thermoregulation, *Exogenous Dermatology*, №1(5), 2002, pp. 221-230.
26. Svishchev G.N., Lyubskaya O.G., Yakutina N.V.: Investigation of indicators of thermal comfort at workplaces taking into account the hygienic characteristics of work clothes, *Proceedings of International scientific and technical conference to the 105th anniversary of A.N. Planovsky (MNTK Planovsky)*, 2016, pp. 255-258.
27. Suprun, N.: Dynamics of moisture vapour and liquid water transfer through composite textile structures, *International Journal of Clothing Science and Technology* 15(3-4), 2003, pp. 218 – 223.
28. Angelova R.A., Georgieva E., Reiners P., et al.: Selection of clothing for a cold environment by predicting thermophysiological comfort limits, *FIBRES & TEXTILES in Eastern Europe*, 1(121), 2017, pp. 95-101.
<https://doi.org/10.5604/12303666.1227888>
29. ISO 3801:1977: Textiles — Woven fabrics — Determination of mass per unit, length, and mass per unit area
30. ISO/TR 11827:2012: Textiles — Composition testing — Identification of fibers.
31. ISO 4920:2012: Textile fabrics — Determination of resistance to surface wetting (spray test).
32. ISO 9237:1995. Textiles – Determination of the permeability of fabrics to air.
33. ISO 7933: Hot environments. Analytical determination and Interpretation of thermal stress using calculation of required sweat rate.
34. ISO/CD 9920-1: Ergonomics of the thermal environment – Estimation of the thermal insulation and evaporative resistance of a clothing ensemble.

THE DEVELOPMENT AND ANALYSIS OF ECO-PRINT AND SCREEN PRINTING COMBINATION USING NATURAL DYES

TRI, YULIANA AND NOORYAN, BAHARI*

Universitas Sebelas Maret, Jl. Ir. Sutami No. 36, Kentingan, Kec. Jebres, Kota Surakarta, 57126, Indonesia

ABSTRACT

Natural dye is one of the solutions to alleviate environmental damage caused by the textile industry. Existing synthetic dyes have been proven to adversely affect the environment and human. Hence, revisiting natural dyes becomes a correct decision to alleviate existing environmental problems. Eco-print is one of the natural dyeing methods done by using plants typically found in the surroundings. This method has become the subject of various developments, both in its mordanting and making processes. Its visual aesthetics should also receive attention to avoid stagnation. Further development and innovation are necessary. The purpose of this study was to develop the visual aesthetic aspect of the eco-print method. It particularly focused on developing the design and production technique in terms of concepts, materials, and working techniques. This work also adopted a screen printing technique to enrich the motifs and colors. The method utilized in this research was art-based research with the premise of adapting artistic creativity to social research using an artistic practice approach because both are holistic and dynamic. The result showed that eco-print and screen printing methods could be combined, as the latter significantly enhance the eco-print product's visual aesthetics. However, the result of this combination exhibited poor color fastness, implying the need for further study.

KEYWORDS

Eco-print; Screen printing; Natural dye.

INTRODUCTION

The majority of industries utilize synthetic textile dyes [1], and almost 800,000 tons of dyes are used each year globally. There are more than 10,000 dyes used in the textile industry, of which 70% are synthetic [2]. Before synthetic dyes were first introduced in 1858, natural dyes were the primary component in textile dyeing. The introduction of synthetic dyes has substantially reduced the usage of natural dyes [3] because synthetic colors are brighter, cheaper, and allow mass production [4]. Despite these benefits, however, synthetic dyes are detrimental to human health, cause substantial environmental pollution [5, 6], and damage ecosystems [7]. Synthetic dyes generate industrial waste, the largest contributor to water pollution. [8]. For this reason, many countries worldwide have outlawed the use of synthetic colors such as the poisonous benzidine [9].

The use of natural dyes is one of the measures to lessen the environmental impact of industrial pollution. Natural dyeing process is a coloring technique that utilizes natural materials [10]. It is safe for the environment and provides soft, delicate hues, hence regaining popularity in recent years [11, 12].

Natural dyes can be made from many different materials, such as animals, insects, bacteria, fungi, minerals, and different parts of plants, such as roots, bark, leaves, flowers, and fruits [13]. Natural dyes could be used in various methods, one of which is the eco-print method [14]. Eco-print is a technique to transfer leaf and flower motifs to fabrics [15, 16]. Eco-print application produces environmentally friendly wastes, as the textiles and dyes used are made from natural materials [17].

Eco-print was reintroduced by India Flint in 2006 and since then has expanded rapidly worldwide, including in Indonesia. Since 2016, eco-print centers in Indonesia have expanded, notably in Jakarta, Bandung, Yogyakarta, Kudus, Surakarta, and Surabaya, with technological improvements and breakthroughs in the natural dyeing process from diverse plants and the mordanting process on fabrics as fashion materials. However, if the visual aesthetics and techniques of eco-print fail to keep up with the development, it will eventually become extinct due to stagnation. Therefore, ongoing development and innovation are necessary. This study focuses on the creation of design and production procedures, both in terms of concepts, materials as a medium of work,

* Corresponding author: Nooryan B., e-mail: nooryanbahari@staff.uns.ac.id

Received November 17, 2022; accepted April 3, 2023

and processing techniques, as well as the use of screen printing techniques to enrich the color and patterns.

METHOD

The method utilized in this research was an art-based research [18]. It adopted art creativity in social study using artistic practice approach, as both are holistic and dynamic. This research included reflection, description, problem formulation, and problem resolution, identification and explanation of intuition and creativity made during the research process. The artistic process employed a three-step experimental framework: the discovery stage, the design stage, and the embodiment stage. The eco-print method was combined with the screen printing method because these two methods had comparable printing technique. The screen printing technique could enrich the motifs of the finished works and accentuate the point of interest, preventing the work from looking flat. The work quality was evaluated using several parameters, including colorfastness to wash 40° C, sweat (acid), daylight, and ironing.

Materials

Primiissima cotton fabric used in this study possessed the following material characteristics: material (warp 56/60 dtex, weft 50/56 dtex), density (warp 42/50 threads/cm, weft 42/50 threads/cm), and 100% pure primiissima cotton. Weight 190 g/m².

The basic pre-mordant materials were alum, iron (tunjung), and chalk, (30 g/L of water each). Raw coloring materials: Terminalia bellerica, Ceriops candolleana, and mahogany (250 g/3L of water). Fixator: alum and chalk (30g/L). The screen printing materials (synthetic pigments): rubber, pigments (water-based) 0. 25 ml / 250 g of rubber, and binder (Polyurethane) 50 ml / 250 g of rubber.

The natural pigment used for eco-print was chlorophyll (C₅₅H₇₂O₅N₄Mg). The natural binders used were alum and chalk. The pigment used for the screen printing was a water-based synthetic dye usually used in printing ink. It was selected due to its easily-soluble nature, making it more environmentally friendly. The binder used was polyurethane. Equipment: scales, stainless steel pan, buckets, filters, motif-printed screen printing, and squeegee.

Procedure

Several stages were performed, including the pre-mordant stage, extraction stage, the eco-print stage, the fixation stage, and the screen printing stage.

Pre-mordant: Before the pre-mordant step, the fabric was washed using detergent and dried. It was done to remove the wax material from the fabric, allowing it to absorb color effectively. The pre-mordant stage began with dissolving alum, iron, and chalk in boiled water (the dosage information is presented in table 1).

The fabric was soaked for 30 minutes in hot mordant water, then squeezed and sun-dried.

Extraction stage: this phase began by boiling 255 grams of natural dyes (i.e., Terminalia bellerica, Ceriops candolleana, and mahogany) in 3 liters of water until a 1/4 of the water shrinks and color was extracted. After 10 minutes of soaking in the natural dye solution, the mordanted fabric was filtered to remove any remaining natural dye particles. The wet fabric was squeezed, and sun-dried.

Eco-printing stage: eco-printing is the process of creating motifs on textiles using tannin-containing leaves and flowers. The eco-printing was done using the steam method. The first step in this stage was to soak the fabric in water, and the fabric was then half-dried. The fabric was put over the plastic, and after that, leaves and flowers were then arranged over the fabric. After that, the fabric was covered with a half-dampened fabric and plastic. The material was firmly rolled and tied with rope. The fabric was placed in a steamer with hot water and steamed for three hours. After that, the cloth was left to cool. The fabric was unrolled and hung up to dry in the air. This process creates flower and leaf motifs on the fabric.

Fixation stage: The fixation phase is a color-locking phase utilizing alum and chalk as the fixator. Each fixator was dissolved in hot water to initiate this step. The eco-print fabric was then soaked for two hours after being boiled. The fabric was then squeezed and sun-dried.

Screen printing stage: This was the final stage, which was done by combining eco-print and screen printing techniques using screen printing ink.

RESULT

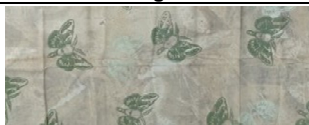

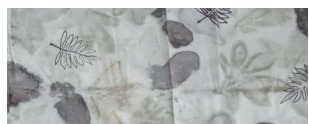
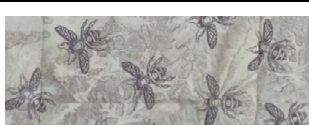
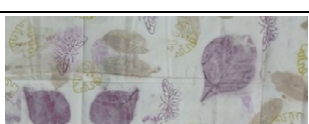
Coloring result

There were five eco-print and screen-printing combinations in this study (Fig. 1-5). Table 2 shows the comparison of dyeing results based on mordants, natural dyes, fixators and screen-printing motifs. Two combinations did not use the natural dyeing stage and only processed through the mordant, eco-print, fixation, and screen-printing stages. The other three combinations were dyed using natural dyes before the eco-print stage. Overall, the result was predominantly dark colors.

Table 1. Materials and dosage.

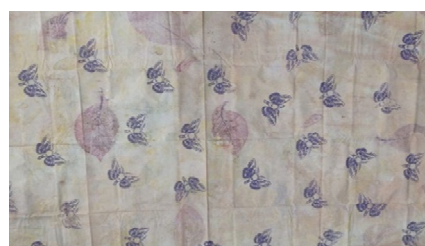
Mordant (30 g/L)	Natural Dye (85 g /L)	Fixator (30 g/L)	Screen Printing
Alum	<i>Terminalia bellerica</i>	alum	√
Chalk	<i>Ceriops candolleana</i>	alum	√
Chalk	-	alum	√
Iron	Mahogany	Chalk	√
Iron	-	Chalk	√

Table 2. Comparison of eco-print-screen printing combinations.

Pre-mordant	Natural Dye	Fixator	Coloring Result
Alum	<i>Terminalia bellerica</i>	Alum	
Chalk	<i>Ceriops candolleana</i>	Alum	
Chalk	-	Alum	
Iron	Mahogany	Halk	
Iron	-	Chalk	



(a)



(b)



(c)



(d)



(e)

Figure 1. Eco-print and screen printing combinations: (a) Alum - *Terminalia bellerica* - alum, (b) Chalk - *Ceriops candolleana* - alum, (c) Chalk - alum (no natural dye), (d) Iron – mahogany – chalk, (e) Iron - Chalk (no natural dye).

Table 3 Colorfastness test.

Score	Reading
5	Excellent
4-5	Good
4	Good
3-4	Good
3	Fairly good
2-3	Fair
2	Poor
1-2	Poor
1	Very poor

Based on the result of the eco-print, color selection and screen-printing motifs were adjusted to the eco-print motifs on the fabric. There were several forms of objects created, including butterflies, insects and leaves. The eco-print effect of each sample was intentionally made differently. The faint eco-print was used as the background to accentuate the screen-printing motifs. Meanwhile, the motif was made to accentuate the eco-print itself. The mordant-pre-mordant-fixator variations also significantly affect the eco-print result, which accounts for the highly diverse results in each sample.

Colorfastness test

Four colorfastness tests were conducted following Indonesian National Standard-abbreviated SNI (Standar Nasional Indonesia) to evaluate the product's colorfastness to 40°C wash, sweat (acid), daylight, and ironing. The test result was presented in 1-5 scale of discoloration score.

Colorfastness to 40 °C wash

Colorfastness to 40 °C wash was tested following the SNI ISO 105-C06:2010 test method. The lowest score was found in iron -chalk combination with a score of 1-2 (poor). Combinations with or without the natural dyes showed similar result. The combination with alum as fixator exhibited scores of 2-3 and 3 (fair), which was better than those using chalk as fixator. All in all, eco-print - screen-printing combination had a poor colorfastness to 40 °C wash.

Colorfastness to sweat (acid)

The colorfastness to sweat (acid) was tested following SNI ISO 105-B01:2010 test method. The result in Table 4 shows that colorfastness score was at 3-4 and 4 (good). The combination of alum - Terminalia bellerica-alum exhibited a score of 4 (good). Similarly, the combination of chalk-Cerriops candolleana-alum also exhibited a score of 4. These combinations exhibited a higher score than other

three combinations. Therefore, it could be concluded that eco-print-screen printing combination have a good colorfastness to sweat (acid).

Colorfastness to daylight

The colorfastness to daylight was tested following SNI ISO 105-B01:2010 test method. All combinations showed good colorfastness (4 and 4-5). The scores lead to a conclusion that eco-print and screen-printing combination has a good colorfastness to daylight.

Colorfastness to ironing

Colorfastness to ironing was tested following SNI ISO 105-XII: 2010 test method. The scores showed the best result among the other colorfastness tests (4-5). In other words, the eco-print – screen printing combination product's colorfastness to ironing can be categorized as good.

Based on the results of the four tests, the colorfastness to 40°C wash exhibited the lowest score (1-3), while colorfastness to sweat (acid), light (daytime), and iron heat were in the good category.

DISCUSSION

In terms of visuals, the development of eco-print by adopting screen printing to enrich patterns and colors can be considered successful. Applying the screen printing technique to the eco-print method exhibited significant impacts, as the eco-print product looks more compelling and varied. Screen printing adds a point of interest and emphasis through the presented motifs, preventing the work from looking flat. However, the quality of this combination still cannot be categorized as good for a 40°C wash. Several factors were possibly responsible for poor colorfastness to 40°C wash, including short dyeing duration, too early fixation process, and insufficient dyeing processes.

First of all, the natural dyeing duration. The process of dyeing fabrics in natural dyes was done for only 10 minutes. This short time caused the dyes not to soak properly on the fabrics. Second, the dyeing was done only once, causing only a few amounts of natural dyes to be absorbed. Repeated dyeing of fabrics in natural dyes would produce rich and strong colors. Third, the eco-print result was fixed too early. In the process, the fabric was aerated for 8 hours after the eco-print steaming process until it was fixed. The fabric airing process was too fast. Hence the eco-print and natural dyes were not fully absorbed into the fabric.

Table 4 Colorfastness test result

Process	Test Result			
	Colorfastness to 40°C wash	Colorfastness to sweat (acid)	Colorfastness to daylight	Colorfastness to Ironing
Iron - chalk (no natural dye)	1 - 2	3 - 4	4 - 5	4 - 5
Iron - mahogany- chalk	1 - 2	3 - 4	4 - 5	4 - 5
Chalk – alum (no natural dye)	3	3 - 4	4 - 5	4 - 5
Alum - Terminalia bellerica - alum	3	4	4 - 5	4 - 5
Chalk - Cerriops candolleana - alum	2 - 3	4	4	4 - 5

CONCLUSION

The combination of eco-print and screen printing done in this study was built on previous works on eco-print. This development was carried out to prevent eco-print from stagnant and as an initiative to use natural dyes to reduce the use of synthetic dyes—one of the causes of environmental pollution.

This study concluded that the screen printing technique plays a significant visual aesthetic role in eco-print. Screen-printing makes eco-print appear to have more patterns and be colorful. Moreover, screen-printing also becomes the point of interest when combined with eco-print, making the final work more compelling and not plain. However, the colorfastness of the eco-print and screen-printing combination cannot be categorized as completely good. The low score of colorfastness to wash may be accounted for by fading of natural dyes and screen-printing ink. Therefore, further research is required.

REFERENCES

1. Pangestu A.G., Santoso R.E.: Murai bird motif design with eco-print technique combination embroidery for outwear, *Melayu Arts Performance Journal*, 4(2), 2021, pp. 182-187. <https://doi.org/10.26887/mapj.v4i2.2038>
2. Simanungkalit Y.S., Syamwil R.: Eco-print technique by utilizing rose waste (*Rosa* sp.) on cotton fabric, *Fashion and Fashion Education Journal*, 9(1), 2020, pp. 90–98.
3. Periyasamy A.P.: Natural dyeing of cellulose fibers using syzygium cumini fruit extracts and a bio-mordant: A step toward sustainable dyeing, *Sustainable Materials Technology*, 33(8), 2022, pp. 1-9. <https://doi.org/10.1016/j.susmat.2022.e00472>
4. Groeneveld I., Pirok B.W.J., Molenaar S.R.A., et. al. The development of a generic analysis method for natural and synthetic dyes by ultra-high-pressure liquid chromatography with photo-diode-array detection and triethylamine as an ion-pairing agent, *Journal of Chromatography A*, 1673, 2022. <https://doi.org/10.1016/j.chroma.2022.463038>
5. Sharma J., Sharma S., Soni V.: Classification and impact of synthetic textile dyes on Aquatic Flora: A review, *Regional Studies in Marine Science*, 45, 2021. <https://doi.org/10.1016/j.rsma.2021.101802>
6. Dutta P., Mahjebin S., Sufian M.A., et al.: Impacts of natural and synthetic mordants on cotton knit fabric dyed with natural dye from onion skin in perspective of eco-friendly textile process, *Materials Today Proceedings*, 47(10), 2021, pp. 2633–2640. <https://doi.org/10.1016/j.matpr.2021.05.229>
7. Kaur N., Kaushal J.: Screening the six plant species for phytoremediation of synthetic textile dye waste water, *Materials Today Proceedings*, 2022. <https://doi.org/10.1016/j.matpr.2022.08.512>
8. Haque M.M., Haque M.A., Mosharaf M.K., et al.: Biofilm-mediated decolorization, degradation and detoxification of synthetic effluent by novel biofilm-producing bacteria isolated from textile dyeing effluent, *Environmental Pollution* 314(8), 2022 pp. 1-14. <https://doi.org/10.1016/j.envpol.2022.120237>
9. Mongkholrattanasit R., Saiwan C., Rungruangkitkrai N., et al.: Eco-dyeing of silk fabric with *garcinia dulcis* (roxb.) kurz bark as a source of natural dye by using the padding technique, *Journal of Natural Fibers*, 13(1), 2016, pp. 65–76. <https://doi.org/10.1080/15440478.2014.984056>
10. Pressinawangi R.R.N., Widiawati D.: Exploration of eco-printing techniques using iron waste and natural dyes for fashion products, *Jurnal Tingkat Sarjana Bidang Seni Rupa dan Desain*, 1, 2008, pp. 1–7.
11. Sobandi B., Triyanto, Rohidi T.R., et al.: The use of clove leaves (*syzygium aromaticum* L.) as natural dye for batik production in kasumedangan batik industry, Indonesia, *Vlakna a Textil*, 28(1), 2021, pp. 86–94.
12. Rather L.J., Shahid-ul-Islam, Shabir M., Bukhari M.N., et al.: Ecological dyeing of woolen yarn with *Adhatoda vasica* natural dye in the presence of biomordants as an alternative copartner to metal mordants, *Journal of Environmental Chemical Engineering*, 4(3), 2016, pp. 3041–3049. <https://doi.org/10.1016/j.jece.2016.06.019>
13. Mongkholrattanasit R., Klaichol C., Sasithorn N., et al.: Screen printing on silk fabric using natural indigo, *Vlakna a Textil*, 25(3), 2018, pp. 51–56.
14. Cantika M.I., Hendrawan A.: Pemanfaatan Daun Ketapang Sebagai Pewarna Alami dengan Teknik Eco Print, *e-Proceeding Art Design*, 8(6), 2021, pp. 3601–3615.
15. Annesha B., Ciptandi F.: The design of the gedog woven textile uses the eco-print technique with the inspiration of Batik Tuban, *eProceeding of Art & Design*, 7(2), 2020, pp. 3957–3976.
16. Flint, *Eco Colour: Botanical dyes for beautiful textiles*. UK: Murdoch Book, 2008, 240 p.
17. Rahmaningtyas W.D., Hendrawan A., Ramadhan M.S.: Pemanfaatan daun eceng gondok sebagai pewarna alami, *e-Proceeding of Art Design*, 8(6), 2021, pp. 3601–3615.
18. Leavy P.: *Research Design*. New York: The Guildford Press, 2017. 301 p.

MULTI-CRITERIA NUMERICAL OPTIMIZATION OF MECHANICAL PROPERTIES IN ULTRASONIC WELDING PROCESS PARAMETERS OF PVC-COATED HYBRID TEXTILES FOR WEATHER PROTECTION

HUSSEN, MUKTAR SEID^{1,2*}; KYOSEV, YORDAN²; PIETSCH, KATHRIN²; BOLL, JESSICA² AND KABISH, ABERA KECHE¹

¹ Ethiopian Institute of Textile and Fashion Technology, Bahir Dar University, Bahir Dar, Ethiopia

² Institute of Textile Machinery and High-Performance Material Technology, TU Dresden, Dresden, Germany

ABSTRACT

A series of research was carried out to determine the correlation between ultrasonic welding process parameters and weld seam mechanical properties. However, multi-objective numerical optimization of coated hybrid textiles for weather protection has not been addressed. To ensure a comprehensive evaluation of ultrasonic weld seams, the research investigates the optimal solution of the multi-objective function of ultrasonic welding process parameters and formulates a single criteria objective function. Lapped and superimposed types of seams were applied based on 3^3 factorial designs of experiments for 6 and 12 mm welding widths. Single-criteria objective functions instead of three independent problems were developed as a generalized utility function. A single-criteria optimization method was introduced through predetermined weight and normalization within the range of acceptable/unacceptable values. Numerical and graphical optimization methods were also applied to determine possible optimal solutions through generalized utility functions. The best optimal value of the generalized utility function (0.670425 and 0.944374) was attained at welding speed (2 and 2.01564 m/min), power (93.756 and 117.973 W), and pressure force (198.803 and 239.756 N) of 6 and 12 mm welding widths, respectively. The acceptable range of satisfactory values was determined for the roof and wall of awnings and camping tents through standard, in which seam performance level indicated. Nonlinear quadratic numerical models were formulated to estimate the generalized utility function, and their results were close to the regressed diagonal line against the actual points. The statistical analysis was shown a statistically significant effect of welding process parameters on the generalized utility function.

KEYWORDS

Ultrasonic welding; Welding process parameters; Tensile strength; Hydrostatic pressure resistance, Peel strength, Multi-objective optimization.

INTRODUCTION

Ultrasonic welding is one of the most popular industrial welding techniques for joining thermoplastic materials, and it becomes an important method for welding polymeric composites, especially for coated and laminated hybrid textile materials. Ultrasonic welding is a technique that uses high-frequency ultrasonic vibration applied locally to workpieces held together under pressure to generate heat during welding for various technical applications. Ultrasonic welding is also a physical process in which no chemical changes are observed during welding. The other method that has to be discussed in this paper is multi-criteria optimization. The method of multi-criteria decision-making provides a solution when

multi-objective optimization is necessary. Multi-criteria optimization issues emerge when there isn't a single criterion to evaluate the quality of a doable solution. It can be troublesome to discover a single viable solution that meets all of the criteria if several criteria are contradictory. Hence, a few compromises are required. Multi-objective optimization has recently become a useful tool for making a decision. There has been a lot of effort put into solving actual industrial challenges with multiple objectives in mind. For example, Szafranska and Korycki [1] have reported the multi-criteria optimization of mechanical properties and explored the impact of temperature, time, and pressure on laminated seam durability and stability. The authors obtained a good mathematical model of generalized utility function to forecast

* Corresponding author: Hussen M.S., e-mail: muktar1450@gmail.com; muktar.seid@bdu.edu.et

Received November 6, 2022; accepted April 3, 2023

variations in seams of mechanical properties due to lamination process parameters. Sathananthan et al. [2] have also achieved the optimal welding condition at maximum weld joint strength using multi-objective optimization of plastic welding parameters through grey relational analysis to improve the weldability of plastic material and production rate. The authors investigated the effect of joint configurations, hold time, weld time, and pressure on welding tensile strength and percent elongation of polymethyl methacrylate.

As Ramesh and Panneerselvam [3] analyzed the optimization of ultrasonic welding in high-density polyethylene 5%-polybenzimidazole composite, the optimal amount of input parameters for multi-objective optimization criteria (shear strength and shore hardness) have been revealed by combining the entropy weight approach with the combinative distance-based assessment technique. The authors attained a relative evaluation score of 2.444 at 60 ms welding time, 21 Hz amplitude, and 2.5 MPa pressure. To clarify these issues further, Meng et al. [4] have studied the multi-objective optimization of peel and shear strengths in ultrasonic metal welding using machine learning-based response surface methodology and optimized both quality indices jointly. Mongan et al. [5] have researched multi-objective optimization of ultrasonically welded dissimilar joints through machine learning and investigated the influence of weld process parameters on lap shear strength, process repeatability, and defects. Satpathy et al. [6] reported the modeling and optimization of ultrasonic welding on dissimilar sheets using a fuzzy-based genetic algorithm and found the optimal amplitude, pressure, and time to tensile shear stress, T-peel stress, and weld area and better results on fuzzy than genetic algorithm. He et al. [7] have studied multi-objective optimization using network-based multi-agent reinforcement learning. Sada [8] has noted the use of the multi-objective genetic algorithm for optimizing the process parameters and predicting weld quality and explored an optimal weld strength (546.8 N/mm²) and hardness (159.1 N/mm²) at welding current (140 A), voltage (24.9 V), gas flow rate (20 l/min), and filler rod diameter (2.4 mm). Zhang et al. [9] have stated the multi-objective optimization of the welding process of glass fiber-reinforced polypropylene composites and investigated the optimal process parameters of weld current (12.5 A), pressure (2.5 MPa), and time (540 s). Cerda-Flores et al. [10] have reviewed the applications of multi-objective optimization to industrial processes that presented a broad panorama of applications, including future perspectives and open questions.

Apart from these, the weld seams of PVC-coated hybrid textile materials were analyzed according to the selected mechanical properties and applied welding widths, including the sewn seam conventionally [11,12]. According to these, the effect

of welding process parameters (welding pressure force, power, and speed) for 6 and 12 mm welding widths and sewing parameters (stitch pattern, width, and length) have been investigated on hydrostatic pressure resistance, peel strength, and tensile strength, including thermal and chemical analysis as well as variation in the width of a heat-affected zone of the weld seam [11-13]. The value of hydrostatic pressure resistance decreased with the increase in welding pressure force and speed for both welding widths [12]. Whereas, the value of tensile and peel strength increased with the increase in welding pressure force and power for both welding widths [11, 13, 14]. However, the optimization was performed for every single objective function independently. Szafranska and Korycki [15] have researched on mechanical properties of laminated seams to analyze the seam quality by the influence of lamination process parameters (temperature, time, and pressure) on laminated seam strength properties. Hussen et al. [13] analyzed the parametric influence of ultrasonic welding on the seam quality of peel strength and examined the effective weld locations and morphology at the joining interface. Since the width of the weld seam and depth of weld penetration are the most important factors to determine the weld seam quality, Hussen et al. [11] have used the weld seam width variation to estimate weld seam tensile strength through ultrasonic welding parameters. The influences of ultrasonic welding parameters on the quality of weld seam bond strength, water permeability, and peel strength were discussed further as follows. Wu et al. [16] have investigated the weld strength of polyolefin and reported that the amplitude of vibrations is a dominant factor. Rani et al. [17] have stated the joint strength of ultrasonic welding for acrylonitrile butadiene styrene and high-density polyethylene and found that the welding time and pressure significantly affected the joint strength. Ayse and Bahar [18] investigated the water permeability of ultrasonic seaming on PU-coated fabrics and observed that the waterproofing values decreased with the increase in seaming velocity. Rajput et al. [19] have studied the peel strength of ultrasonic welding on polypropylene and investigated that the amplitude had a significant effect on the peel strength and the most influencing variable than hold time and weld time.

Although a lot of previous studies have been performed on the multi-objective optimization of ultrasonic welding for rigid materials using a plunge type of welding, the research on multi-objective optimization of PVC-coated hybrid textile materials using a continuous type of ultrasonic welding is relatively rare including bonding and heating mechanisms. The impact of ultrasonic welding process parameters on comprehensive mechanical properties with their quality aspect of the weld seam for technical applications, especially for weather protection, has not been addressed to the knowledge

of the authors. Most knowledge on ultrasonic welding of hybrid textile materials has been acquired with one objective function. This paper aims to introduce the multi-criteria seam quality optimization of two distinct welding widths for weather protection, concerning the effect of welding process parameters (pressure force, power, and speed) on mechanical properties (hydrostatic pressure resistance, tensile strength, and peel strength) of the seams with their tendencies in the relations. The single-criteria optimization is introduced rather than three independent optimization problems to obtain an objective function called the generalized utility function through a weighted average of criteria with predetermined weight values. A review of available literature has revealed that the multi-criteria optimization of PVC-coated hybrid textile welded seam for 6 and 12 mm welding widths are generally unknown. It is, therefore, that the following points can be recognized originally. (i) Instead of solving three individual optimization problems, the generalized utility function was developed and applied as a weighted average of criteria functions. (ii) Statistical significances of welding pressure force, power, and speed on generalized utility function were analyzed for both weld seams. (iii) The ranges of satisfactory and very good values were determined based on preliminary experimental results according to ISO 10966 standards [20]. (iv) The predetermined weight and acceptable values of the range were used to solve the multi-criteria weighted optimization. (v) The method is ubiquitous and simply necessitates statistical calculations. It is not necessary to conduct new seams tests if alternate satisfactory and very good ranges and/or weights of specific features are adopted.

EXPERIMENTAL PROCEDURE

A hybrid textile material (H5571-0283-ECO) was used in this study. It was provided by a HEYtex Bramsche GmbH Company in Germany as a common tent material for light structures. It had a plain weave construction with the same fabric setting (8 PPC and 8 EPC) using 100 % air-jet polyester filaments at 1100 dtex linear density in both warp and weft directions. It was coated with PVC using a plasticizer to make the material more flexible and durable. It was intended to use for awnings and camping tents. According to ISO 10966 standards [20], the material requirements were split into two

levels (A and B) for awnings and camping tents. Level A requirements were applied for the severe strain caused by weather conditions or long-term use; whereas, the requirements for level B were applied for less severe use. The physical and mechanical properties of the tested hybrid textile material listed in Table 1 were fulfilled the minimum requirements of ISO 10966 standards [20] for the roof and wall (the outer tent's fabric directly exposed to the influence of weather in practical use) of awnings and camping tents made of coated fabrics for both levels. Due to this, PVC-coated hybrid textile material was selected for this research purpose in addition to its ultrasonic welding compatibility. It is, therefore, applicable for weather protection or the roof and wall of awnings as snow, residential, and touring awnings and for camping tents as sleeping with standard and light-weight, touring, and residential tents for both levels.

A new-generation NUCLEUS ROTOSONIC DX1 continuous ultrasonic machine was used to carry out welding. It was produced by NUCLEUS GmbH Company in Germany with DG1 1000 W ultrasonic generator at a 35 kHz frequency. Ultrasonic welding was carried out with a flat anvil wheel for 6 and 12 mm welding widths considering the application area of the material. Welding pressure force, speed, and power were considered as input ultrasonic welding process parameters. The working ranges of these welding process parameters for selected PVC-coated hybrid textile material were investigated during the preliminary experiments. The welding power, speed, and pressure force of (40-100 W, 1-3 m/min, and 40-300 N) for 6 mm welding width and (60-120 W, 1-3 m/min, and 40-350 N) for 12 mm welding width were found as a working range of the material, respectively. Experimental design levels for both welding widths were set after identifying the material working range. Thus, 3³ factorial designs of experiments were developed for both welding widths. It is, therefore, 27 different combinations of welding parameters were used considering three factors and three levels for each 6 and 12 mm welding width. The welding speed, pressure force, and power of ([2, 2.5, and 3 m/min], [150, 225, and 300 N], and [40, 70, and 100 W]) for 6 mm welding width and ([2, 2.5, and 3 m/min], [200, 275, and 350 N], and [60, 90, and 120 W]) for 12 mm welding width were selected level as per the preliminary experiments, respectively.

Table 1. Physical and mechanical properties of H5571-0283-ECO tentorium 650 materials [21].

Parameters	Base Fabric	Coating Material	Total Weight	Tensile Strength (W/F)	Tear Resistance (W/F)	Coating Adhesion	Flex Resistance	Temperature Resistance	Translucency
Specifications	100% PET	100% PVC	650 g/m ²	2200/2000 N/50mm	250/250 N	100 N/50mm	at least 100,000 bends	-30 to 70 °C	17%
Standards	DIN ISO 2076	DIN ISO 2076	DIN EN ISO 2286-2	DIN EN ISO 1421-1	DIN 53363	DIN EN ISO 2411	DIN 53359 A	DIN EN 1876-1 & N-Q-PA-1057	PA 2001/41

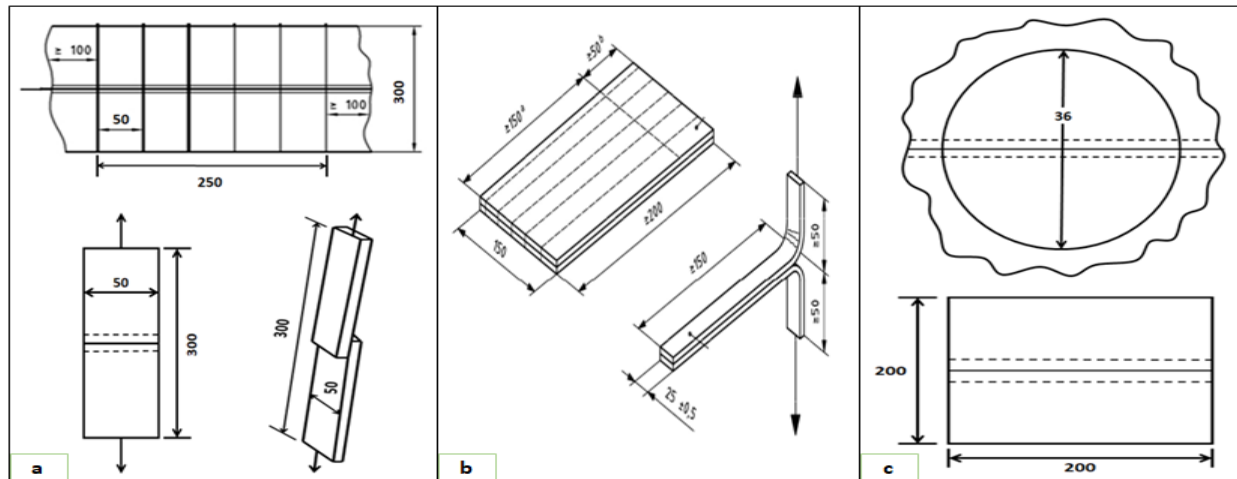


Figure 1. Method of sample preparation and testing procedure for tensile strength (a), peel strength (b), hydrostatic pressure resistance (c), and all measurements are in millimeters.

Based on the developed experimental design and/or welding parameters combinations, the ultrasonic weld samples were prepared using lapped and superimposed types of seams in the warp direction. A suitable lapped type of seam was applied for weld seam tensile strength and hydrostatic pressure resistance, while a superimposed type of seam was used for the case of peel strength during welding. Out of 27 combinations for each welding width and the response variable, only 21 and 24 welding combinations were able to produce welded seams properly for 6 and 12 mm welding widths, respectively. The response or output variables were also selected according to ISO 10966, ISO 8937, and ISO 5912 standards [20, 22–23] as well as the functional requirements of specific end-use or applications. Due to this, the ultrasonic weld seams were tested for tensile strength, peel strength, and hydrostatic pressure resistance. The tensile strength of the ultrasonically welded sample was determined using Zwick/Roell-Zmart.Pro strip tensile testing machine at 100 mm/min rate of extension and 200 mm gauge length according to DIN EN ISO 13935-1 standards [24], cf. Figure 1(a). The adhesive/peel strength of the ultrasonically welded sample was also tested on the Zwick/Roell-Zmart.Pro tensile testing machine with a constant test speed of 100 mm/min and clamping length of 50 mm according to DIN EN ISO 11339 standards [25], cf. Figure 1b. Whereas, the hydrostatic pressure test for water penetration resistance of ultrasonically welded sample was measured on the TEXTTEST INSTRUMENTS FX 3000 HYDROTESTER III testing machine with 60 + 3 cmH₂O/min rate of increasing water pressure on the face of the fabric from the bottom side of the test specimen until penetration occurs in three places using distilled water according to DIN EN ISO 811 standards [26], cf. Figure 1c. The method of sample preparation and testing procedure for tensile strength, peel strength, and hydrostatic pressure resistance are further elaborated by Figures 1a, 1b, and 1c,

respectively. Furthermore, all measurements were performed under DIN EN ISO 139 standards [27] at a temperature of 20 + 2°C and relative humidity of 65 + 4 % after conditioning for 24 hours. The geometric means of the test results were determined and presented for each combination of welding widths in each tensile strength, peel strength, and hydrostatic pressure resistance test.

RESULTS AND DISCUSSION

The physical and mechanical properties of the material have met the requirements of awnings and camping tents for long-term use in all weather conditions. Hence, it is required to investigate the joint/connection properties of the material. Not only the material but also the joint/connection properties of the material shall meet the requirements specified in ISO 5912 standards [23]. Due to this, multiple-factor experiments were conducted to determine the weld seam mechanical properties (tensile strength, hydrostatic pressure resistance, and peel strength) and their optimal value of ultrasonic welding process parameters (welding power, pressure force, and speed) using hybrid textile material. Five samples were tested for each welding combination in both welding widths for weld seam tensile strength and peel strength. Whereas, three samples were tested for each welding combination in both welding widths for hydrostatic pressure resistance. The geometric mean value of each experiment is presented in Table 2 as weld seam tensile strength (N/50 mm), hydrostatic pressure resistance (cmH₂O), and peel strength (N/welding widths). Because geometric mean better reflects a situation when a shortage in one element limits the result and cannot be compensated by other elements. The joint/connection strength should not be lower than 10 % of the tensile strength of the required strength of connected material for a given application as per ISO 5912 standards [23].

Table 2. Geometric mean (SD) results of weld seam tensile strength (N/50 mm), hydrostatic pressure resistance (cmH₂O), and peel strength (N/welding widths) for 6 and 12 mm welding widths.

For 6 mm welding width						For 12 mm welding width					
Press ure Force (N)	Power (W)	Spe ed (m/ min)	Geometric Mean (SD)			Press ure Force (N)	Pow er (W)	Spe ed (m/ min)	Geometric Mean (SD)		
			Tensile Strength of F max. (N/50 mm)	Hydrostatic Pressure Resistance (cmH ₂ O)	Peel Streng th (N/6 mm)				Tensile Strength of F max. (N/50 mm)	Hydrostatic Pressure Resistance (cmH ₂ O)	Peel Strengt h (N/12 mm)
150	40	2	656.73 (31.75)	177.33 (9.66)	15.23 (1.36)	200	60	2	1499.35 (97.83)	438.58 (10.50)	19.59 (0.80)
		2.5	-	-	-			2.5	384.51 (54.49)	373.93 (9.17)	17.08 (2.13)
		3	-	-	-			3	-	-	-
	70	2	975.22 (86.98)	201.85 (51.91)	16.95 (1.43)		90	2	1853.75 (76.32)	476.89 (12.53)	25.74 (2.11)
		2.5	952.26 (56.75)	152.50 (14.80)	14.65 (1.50)			2.5	1727.85 (74.54)	403.22 (11.68)	21.07 (1.85)
		3	972.84 (38.09)	142.41 (6.26)	13.98 (0.63)			3	735.81 (131.28)	298.21 (20.40)	18.39 (2.14)
	100	2	831.12 (66.64)	206.26 (12.13)	23.72 (0.99)		120	2	2025.48 (40.75)	554.50 (16.44)	30.58 (1.84)
		2.5	943.25 (134.46)	187.94 (6.08)	18.90 (1.39)			2.5	1894.54 (110.82)	478.93 (10.00)	28.36 (2.51)
		3	928.87 (64.28)	144.96 (4.36)	16.40 (1.27)			3	1697.93 (80.56)	379.00 (19.55)	23.56 (2.45)
225	40	2	819.22 (78.54)	166.34 (9.04)	16.16 (1.25)	275	60	2	1544.81 (72.76)	387.92 (9.54)	21.01 (2.70)
		2.5	-	-	-			2.5	483.74 (45.91)	321.54 (11.02)	18.24 (1.99)
		3	-	-	-			3	-	-	-
	70	2	992.75 (62.14)	164.89 (7.55)	18.22 (1.01)		90	2	1895.36 (97.77)	435.13 (16.26)	27.93 (1.32)
		2.5	952.50 (73.61)	163.96 (4.58)	15.67 (1.43)			2.5	1812.03 (19.17)	357.78 (15.39)	23.03 (2.15)
		3	960.99 (55.71)	142.82 (8.89)	15.37 (1.23)			3	827.76 (84.71)	254.66 (16.00)	19.71 (0.62)
	100	2	956.58 (138.34)	177.66 (13.23)	24.80 (0.82)		120	2	2072.73 (19.45)	502.80 (17.52)	32.60 (3.54)
		2.5	1095.93 (115.15)	156.76 (10.54)	19.73 (0.79)			2.5	1952.34 (31.72)	434.13 (16.26)	31.87 (2.24)
		3	1014.08 (28.67)	136.91 (6.08)	17.47 (1.51)			3	1822.83 (48.44)	330.16 (12.90)	26.37 (1.52)
300	40	2	770.46 (48.20)	151.94 (5.29)	17.00 (0.46)	350	60	2	1595.85 (114.06)	348.55 (11.24)	23.41 (1.34)
		2.5	-	-	-			2.5	568.20 (62.99)	278.20 (10.50)	21.38 (1.80)
		3	-	-	-			3	-	-	-
	70	2	1062.42 (119.32)	144.97 (3.61)	19.99 (1.43)		90	2	1919.71 (17.76)	401.06 (18.01)	28.46 (1.31)
		2.5	999.81 (36.40)	134.80 (8.89)	17.28 (1.29)			2.5	1882.19 (104.23)	317.04 (16.50)	25.93 (1.65)
		3	993.38 (51.16)	157.81 (9.54)	15.88 (1.04)			3	1025.22 (61.43)	220.88 (9.00)	21.38 (1.80)
	100	2	1245.21 (56.66)	147.29 (9.50)	25.39 (0.99)		120	2	2113.03 (94.46)	409.18 (13.87)	34.77 (1.32)
		2.5	1045.80 (91.97)	139.40 (6.50)	19.99 (1.53)			2.5	2055.81 (28.75)	341.55 (11.06)	32.67 (2.48)
		3	966.79 (51.26)	139.98 (14.91)	18.16 (1.28)			3	1894.54 (110.82)	301.11 (14.19)	29.17 (1.41)

Table 3 Determination of weight for particular criteria through the pair-wise comparison matrix and normalization

Source	Pairwise comparison matrix			Normalization			Weight
	Tensile strength	Hydrostatic pressure resistance	Peel strength	Tensile strength	Hydrostatic pressure resistance	Peel strength	
Tensile strength	1	2	4	1/1.75	2/3.33	4/8	0.56
Hydrostatic pressure resistance	1/2	1	3	0.5/1.75	1/3.33	3/8	0.32
Peel strength	1/4	1/3	1	0.25/1.75	0.33/3.33	1/8	0.12
Total sum	1.75	3.33	8	-	-	-	1

Due to this, more than 7 % (residential and snow awnings) and 62 % (touring awnings) of the welding combination of weld seam tensile strength investigated for 6 mm welding width attained the required roof standards for severe and long-term use while 62 % (residential, touring, and snow awnings) attending for the wall. Whereas for 12 mm welding width, more than 66 % (residential and snow awnings) and 70 % (touring awning) of the welding combination achieved the required roof standards of weld seam tensile strength for severe and long-term use while 70 % (residential, touring, and snow awnings) attending for the wall. On the other hand, more than 7 % (residential tent) and 62 % (touring tent) of the welding combination of weld seam tensile strength investigated for 6 mm welding width attained the required roof standards for severe and long-term use while 74 % (residential and touring tents) and 77 % (standard-weight and light-weight tents) attending for the wall. Whereas for 12 mm welding width, more than 66 % (residential tent) and 70 % (touring tent) of the welding combination achieved the required roof standards of weld seam tensile strength for severe and long-term use while 74 % (residential tent) and 77 % (touring, standard-weight, and light-weight tents) attending for wall, cf. Table 2. It was found that a higher standard weld seam was possible to produce for a 12 mm welding width than 6 mm for awnings and camping tents. This is due to the impact of welding width on welding pressure force to weld seam strength.

Formulation of generalized utility function

Developing a numerical equation for one selected objective function doesn't give a full picture of one specific application of the material, but it is important to analyze all necessary objective functions and their tendencies in the relationship at once. Thus, the goal of this paper is to evaluate welded seams for 6 and 12 mm welding widths using multi-criteria statistical optimization and generalized utility function, while all three investigated indexes (criteria of weld seam tensile strength, hydrostatic pressure resistance, and peel strength and a higher value of each property corresponds to better quality) change simultaneously. A generalized utility function is used to express a multi-objective function in a single-objective function. There are different solution strategies for converting a set of multi-objective problems into a single-

objective problem. One of the most well-known methods is scalarization [28] through the weighted sum method using linear weighting to the quality of importance of different objective functions in the problem. The generalized utility function (U) is, therefore, expressed using Equation (1) and described as the weighted geometric mean of criteria functions. Where, ' w_i ' denotes the weights assigned to each criterion and ' $y^{(i)}$ ' represents each criterion; $0 \leq w_i \leq 1$; ' $y_G^{(i)}$ ' denotes the minimum value of the criteria while ' $y_L^{(i)}$ ' is assigned to the maximum and ' n ' for the number of criteria; $i = 1, 2$, and $n = 3$.

$$U = \sum_{i=1}^n w_i * \frac{y^{(i)} - y_G^{(i)}}{y_L^{(i)} - y_G^{(i)}}, \quad \sum_{i=1}^n w_i = 1 \quad (1)$$

To convert multi-objective problems into a single-objective problem called a generalized utility function, the first step is determining the weight of particular criteria and the second is scalarization through the weighted sum method. First, the individual criteria are defined by non-negative weighting factors, which reflect the importance of each criterion based on the analytic hierarchy process, regardless of the range of satisfactory values. As per the analytic hierarchy process, the weight of particular criteria was determined according to Saaty's [29,30] scales of relative importance for multi-attributes decision-making problems. The weighting factor's sum should always equal one.

The analytic hierarchy process of this research was started by developing the pair-wise comparison matrix based on the comparison of criteria through their relative scale of importance, and then the step followed the normalization process of the pair-wise comparison matrix through the linear scale transformation (sum) method by dividing each number with their total sum. And finally, the weight of particular criteria was set by taking the average of each row matrix after normalization, cf. Table 3. On the other hand, the weights of particular criteria and ranges of satisfactory values can be adopted depending on the technical requirements and consultations with the garment manufacturer's production engineers. This observation was also supported by Szafranska and Korycki [1] research. Although the weight of each criterion was determined, it required checking their consistency through consistency ratio. Thus to determine a consistency ratio; first, it should be determined consistency index

Table 4. Determination of lambda max through weighted sum value and lambda.

Source	Tensile strength	Hydrostatic pressure resistance	Peel strength	Weighted sum value	Lambda	Lambda Max
Weight	0.56	0.32	0.12	-	-	-
Tensile strength	1*0.56	2*0.32	4*0.12	1.68	1.68/0.56	3.016
Hydrostatic pressure resistance	1/2*0.56	1*0.32	3*0.12	0.96	0.96/0.32	
Peel strength	1/4*0.56	1/3*0.32	1*0.12	0.3656	0.3656/0.12	

after finding the value of lambda max using Equation (3); where 'n' is the number of criteria.

$$\text{Consistency Ratio} = \frac{\text{Consistency Index}}{\text{Random Index}} \quad (2)$$

$$\text{Consistency Index} = \frac{\text{Lambda max.} - n}{n - 1} \quad (3)$$

The value of lambda max was determined through the following steps: first, the pair-wise comparison matrix was multiplied by their weight before normalization and found the weighted sum value. And then the value of lambda was calculated by dividing the weighted sum value by their weight. Finally, lambda max was found by taking the average value of lambda, cf. Table 4. Since the number of criteria for this research is three, the calculated consistency index is equal to 0.008 based on the evaluated result of lambda max. Using the random index (standard value) stated by Saaty [29, 30] for three criteria (0.58), the consistency ratio was calculated by taking a ratio of consistency index to random index (0.008/0.58) as mentioned in Equation (2), which is equal to 0.0138. If the consistency ratio is less than 0.1, the weight is accepted, but if it is greater than 0.1, it needs to re-evaluate the pair-wise comparison matrix. Hence, it can be concluded that the developed weight for this research is accepted. The most essential index, according to the evaluated results of the multi-criteria functions, was the maximum breaking force of tensile strength (N/50 mm) with the greatest weight of 0.56. The other indexes for hydrostatic pressure resistance (cmH₂O) and peel strength (N/welding widths) were distinguished by lower weights of 0.32 and 0.12, respectively. The sum of all three assigned weights is one, as presented in Table 3.

The second step is scalarization through the weighted sum method as mentioned above. To sum up all three criteria into one, the experimental value of each criterion has to be normalized first and determine the weighted sum values of all criteria second; and based on the regression analysis of weighted sum values, the generalized utility function can be developed at the end. The normalization of each criterion was performed with the minimum-maximum normalization method to make all criteria scale-less and to scale down the values between 0 and 1. Thus, all considered values of criteria were ranked on a scale with no dimensions. A scale was created by selecting a range of values for each criterion by limiting the worst and best values. After normalizing each value

of the criteria, the weighted sum values of all criteria were determined through a simple additive weighting method as mentioned above. The values of the generalized utility function or weighted sum values were obtained based on the experimental results considering the values with appropriate ranges and weights of specific criteria, cf. Table 2. The value of the generalized utility function is, therefore, characterized by values in the range of 0 to 1. This is because of the normalization process performed early. Numbers near 0 correlate to the feature's most unfavorable values, while numbers close to 1 correspond to the feature's most favorable values. In the other words, the higher the value, the more advantageous the tested weld seam's qualities are seen. Thereby, the specific value of the generalized utility function enabled the evaluation of the tested weld seam in terms of the whole set of adopted criteria and their relative importance. It was included in Table 5 that the values of the generalized utility function for 6 and 12 mm welding widths were tested at varying values of welding pressure force, power, and speed.

The values of the generalized utility function were determined based on the experimental results and ranged from 0.204 to 0.736 for 6 mm welding width and from 0.137 to 0.943 for 12 mm welding width. At the highest welding pressure force (300 N) and highest welding power (100 W) of 2 m/min welding speed, the maximum value of generalized utility function was achieved, but the lowest welding pressure force (150 N) and lowest welding power (40 W) yielded the minimum value of generalized utility function at 2 m/min welding speed for 6 mm welding width, cf. Table 5. In the case of 12 mm welding width, the maximum value of generalized utility function was attained at the lowest welding pressure force (200 N) and highest welding power (120 W) of 2 m/min welding speed, whereas the lowest welding power (60 W) and medium welding pressure force (275 N) of 2.5 m/min welding speed provided the minimum value of generalized utility function, cf. Table 5. According to these results, the minimum and maximum values of generalized utility function were attained at different welding process parameters compared to the minimum and maximum values of tensile strength, hydrostatic pressure resistance, and peel strength independently. This is due to the impact of welding pressure force on tensile strength, hydrostatic pressure resistance, and peel strength

Table 5. Values of generalized utility function for 6 and 12 mm welding widths at different pressure force, power, and speed.

For 6 mm welding width					For 12 mm welding width				
Pressure Force (N)	Power (W)	Speed (m/min)	Value of generalized utility function	Predicted value of generalized utility function	Pressure Force (N)	Power (W)	Speed (m/min)	Value of generalized utility function	Predicted value of generalized utility function
150	40	2	0.204	0.217	200	60	2	0.587	0.572
150	40	2.5	-	-	200	60	2.5	0.147	0.248
150	40	3	-	-	200	60	3	-	-
150	70	2	0.635	0.574	200	90	2	0.780	0.776
150	70	2.5	0.368	0.393	200	90	2.5	0.637	0.525
150	70	3	0.335	0.322	200	90	3	0.197	0.274
150	100	2	0.588	0.655	200	120	2	0.943	0.980
150	100	2.5	0.562	0.466	200	120	2.5	0.813	0.802
150	100	3	0.330	0.387	200	120	3	0.621	0.625
225	40	2	0.319	0.216	275	60	2	0.563	0.553
225	40	2.5	-	-	275	60	2.5	0.137	0.246
225	40	3	-	-	275	60	3	-	-
225	70	2	0.499	0.577	275	90	2	0.769	0.751
225	70	2.5	0.430	0.407	275	90	2.5	0.634	0.518
225	70	3	0.340	0.345	275	90	3	0.194	0.284
225	100	2	0.591	0.663	275	120	2	0.923	0.949
225	100	2.5	0.577	0.485	275	120	2.5	0.813	0.789
225	100	3	0.386	0.415	275	120	3	0.634	0.629
300	40	2	0.217	0.193	350	60	2	0.558	0.535
300	40	2.5	-	-	350	60	2.5	0.144	0.245
300	40	3	-	-	350	60	3	-	-
300	70	2	0.495	0.559	350	90	2	0.747	0.726
300	70	2.5	0.361	0.399	350	90	2.5	0.638	0.510
300	70	3	0.443	0.347	350	90	3	0.237	0.294
300	100	2	0.736	0.650	350	120	2	0.861	0.917
300	100	2.5	0.454	0.481	350	120	2.5	0.763	0.775
300	100	3	0.362	0.421	350	120	3	0.648	0.633

Table 6. Fit and model summary statistics of generalized utility function for 6 and 12 mm welding widths.

Source		For 6 mm welding width				For 12 mm welding width			
		Linear	2FI	Quadratic	Cubic	Linear	2FI	Quadratic	Cubic
Utility Function	R ²	0.8274	0.8291	0.9323	0.963	0.9271	0.955	0.9572	0.9766
	Adjusted R ²	0.8049	0.7779	0.8965	0.9039	0.9176	0.9415	0.9346	0.9391
	Predicted R ²	0.7633	0.6881	0.8239	0.6092	0.8995	0.9278	0.8984	0.8577
	Sequential p-value	0.0001	0.9758	0.0011	0.3886	0.0001	0.0197	0.8293	0.3934
	Remarks	-	-	Suggested	Aliased	-	Suggested	-	Aliased

being different collectively and independently including their difference in weights. This perception was strengthened by research [12] according to which the welding pressure force had an inverse

relationship with hydrostatic pressure resistance and had a positive relationship with tensile and peel strength up to certain limits.

Table 7. Coefficients and actual equation factors analysis of generalized utility function for 6 and 12 mm welding widths.

Source		For 6 mm welding width				For 12 mm welding width			
		Coefficient estimate	Actual equation factor	P-values	VIF	Coefficient estimate	Actual equation factor	P-values	VIF
Utility function	Intercept	0.405	1.0737	-	-	0.518	2.25882	-	-
	Pressure Force (F)	0.0026	0.000081	0.8788	1	-0.0073	-0.001028	0.6849	1
	Power (P)	0.2138	0.029472	0.0001	1	0.2713	-0.002491	0.0001	1
	Speed (V)	-0.1159	-1.33834	0.0001	1	-0.2333	-1.03822	0.0001	1
	F*P	0.0049	2.16E-06	0.8167	1	-0.0061	-2.72E-06	0.7797	1
	F*V	0.01	0.000266	0.6353	1	0.0176	0.00047	0.4236	1
	P*V	-0.0082	-0.000543	0.6982	1	0.0737	0.004913	0.0028	1
	F ²	-0.0108	-1.92E-06	0.7166	1	-	-	-	-
	P ²	-0.1381	-0.000153	0.0002	1	-	-	-	-
	V ²	0.0542	0.216939	0.0809	1	-	-	-	-

The statistical analysis was performed for the values of the generalized utility function at a five-percent significance level to formulate the final generalized utility function and to investigate the significant effect of welding process parameters using Design Expert 11. The fit and model summary statistics of the generalized utility function are explained with their suggestion for 6 and 12 mm welding widths in Table 6. Using the result of fit summary analysis, a sequential model sum of square's analysis and model summary analysis based on the values of generalized utility function for both welding widths, nonlinear (quadratic) and linear numerical models were suggested and developed with a two-factor interaction (2FI) for generalized utility function of 6 and 12 mm welding widths, respectively. It was also inferred from Table 8 that the regression equations were formulated based on the range of acceptable values of the generalized utility function and allowed us to estimate the sensitivity of tested weld seam mechanical properties for various factors. For both welding widths, the regression models were significant, indicating that the input variables were a significant predictor of the generalized utility function. Thereby, the derived models adequately characterized the welding process, as evidenced by the value of the coefficient of determination (R^2). The R^2 was quite high (above 0.9) as shown in Table 8; consequently, the fitted models can be utilized to anticipate the relationship between the generalized utility function and input variables. Adequate precision measures the ratio of signal to noise. Since the ratio is more than four as shown in Table 8 for both welding widths, the design space can be navigated using this model. The models were also fitted to the experimental data given the difference between Adjusted R^2 and Predicted R^2 was smaller than 0.2. Moreover, the regression analysis revealed that the following factors had a significant impact: the main independent variables (welding power (P) and

speed (V)) were significant predictors of generalized utility function for both welding widths except for the welding pressure force. The interaction effect between the welding power and speed (P*V) was the only significant predictor of the generalized utility function for 12 mm welding width; whereas, the interaction effect of welding power square (P^2) was the only significant predictor of the generalized utility function for 6 mm welding widths. This is supported by the low statistical significance values shown in Table 7, which states the estimated coefficient and actual equation factor analysis of a generalized utility function with a significant P-value for welding widths of 6 and 12 mm.

Substituting the numbers into the generated regression equations presented in Table 8, a set of predicted values of generalized utility function were obtained in the range from 0.041 to 0.663 for 6 mm welding width and from 0.245 to 0.98 for 12 mm welding width, cf. Table 5. These results indicated that the predicted values of the generalized utility function are being stayed within 0 to 1. The feature corresponding to the unfavorable values was specifically marked when the numbers were close to 0, whereas the feature corresponding to the most favorable values was specifically designated when the numbers were close to 1. It is, therefore, possible to anticipate the impact of welding process parameters on multi-objective functions through a single objective equation without experimental investigation on tensile strength, hydrostatic pressure resistance, and peel strength once the equation is formulated. The scale was also created by selecting a range of unsatisfactory, satisfactory, and very good values on the values of the generalized utility function based on standards [20, 22, 23]. It was developed for the roof and walls of awnings and camping tents for long and short-term uses. It indicated the performance level of weld seam for mentioned specific application. The range of values identified as

satisfactory and very good scale within the effective application of weld seam required for awnings and camping tents as per the standards [20, 22, 23] based on the experimental test results of PVC-coated hybrid textiles for 6 and 12 mm welding widths, cf. Table 2. Furthermore, a set of values in the range of 0.322 to 0.499 and 0.217 to 0.443 for 6 mm welding width and 0.294 to 0.648 and 0.274 to 0.572 for 12 mm welding width were found as satisfactory values for the roof and wall of awnings to long and short-term use, respectively; whereas, the values of 0.559 to 0.736 and 0.454 to 0.736 for 6 mm welding width and 0.726 to 0.98 and 0.625 to 0.98 for 12 mm welding width were also investigated as very good values. On the other hand, the range of values from 0.322 to 0.577 and 0.217 to 0.443 for 6 mm welding width and 0.294 to 0.648 and 0.284 to 0.572 for 12 mm welding width were found as satisfactory values for the roof of camping tents to long and short-term use, respectively; whereas, the values of 0.65 to 0.736 and 0.454 to 0.736 for 6 mm welding width and 0.726 to 0.98 and 0.625 to 0.98 for 12 mm welding width were also investigated as very good values. Similarly, a set of values in the range of 0.193 to 0.499 and 0.193 to 0.443 for 6 mm welding width and 0.274 to 0.572 and 0.245 to 0.553 for 12 mm welding width were found as satisfactory values for the wall of camping tents to long and short-term use, respectively; whereas, the values of 0.559 to 0.736 and 0.454 to 0.736 for 6 mm welding width and 0.625 to 0.98 and 0.572 to 0.98 for 12 mm welding width were also investigated as very good values. Thus, these satisfactory and very good values were considered to be acceptable values for the roof and wall of awnings and camping tents requirement [20] based on the actual and predicted value of generalized utility functions. The rest unmentioned values were considered to be unacceptable including unsatisfactory and rejected values.

In the vicinity of this range, the generalized utility function is the most vulnerable to change in the value of a particular attribute. The broad range of acceptable and unacceptable values in the generalized utility function precludes the use of any variety of the tested variables. Users and producers want the seam to be maximum as durable and stable as possible. The following variants of variable factors ensured the generalized utility function within the range of satisfactory values for roof and wall of awnings and camping tents to long-term use as well as within the range of very good values. The following are the 6 mm welding width variants: welding pressure force (150, 225, and 300 N), power (70 and 100 W), and speed (2, 2.5, and 3 m/min) for satisfactory values and welding pressure force (150, 225, and 300 N), power (70 and 100 W), and speed (2 and 2.5 m/min) for very good values. The values are listed for welding widths of 12 mm as follows: welding pressure force (200, 275, and 350 N), power

(60, 90, and 120 W), and speed (2, 2.5, and 3 m/min) for satisfactory values and welding pressure force (200, 275, and 350 N), power (90 and 120 W), and speed (2 and 2.5 m/min) for very good values. As a result of these findings, more variants of variable factors are possible to apply for 12 mm welding width than 6 mm welding width practically. Fewer variants of variable factors were found for the roof of camping tents compared to awnings for 6 mm welding width within the range of very good values. But in the case of 12 mm welding width, the variants of variable factors were the same for both awnings and camping tents. It was found that the welding speed and power were limited for both welding widths within the range of very good values and only welding power was limited for the 6 mm welding width within the range of satisfactory values for awnings and camping tents. This is due to the higher requirement set for very good values than satisfactory. It very likely causes the number of variants of variable factors in the range of satisfactory and very good values to reduce since the influence of welding pressure force on the value of generalized utility function was statistically negligible for both welding widths. A higher standard requirement was set for the roof compared to the wall of awnings and camping tents. The generalized utility function was used to assess both welding widths, taking into consideration all selected features and their importance. The selected variants of variable factors ensured the generalized utility function was at least within the acceptable range of satisfactory values. The results will be valid for other flexible and lightweight coated/laminated textile material for the roof and wall of awnings and camping tents if the material and welding conditions fulfilled the following aspects: a lower melting temperature difference ($<22^{\circ}\text{C}$) and a high amount of thermoplastic content ($>65\%$) with a closer thickness in addition to performing ultrasonic welding in the working range of welding parameters as part of a high-quality welding process based on a closer welding width and an identical anvil engraving. The values of combination factors resulted in a higher predicted value of generalized utility function of 0.663 and 0.98 for 6 and 12 mm welding widths, respectively.

The surface plots of generalized utility functions were constructed using the equations, to demonstrate the design points above and below the projected value for 6 and 12 mm welding widths at welding speeds of 2, 2.5, and 3 m/min in Figures 2 and 3, respectively. The surface plot also depicted the influence of welding process parameters on the generalized utility function. As the welding power increased from the lowest to the highest value for both welding widths, the generalized utility function of the weld seam drastically increased for all welding pressure forces at 2, 2.5, and 3 m/min welding speeds.

Table 8. Equation of generalized utility function for 6 and 12 mm welding widths based on actual equation factors.

Anvil wheel	General utility function (U)	R ²	Model P-value	Adequate Precision
For 6 mm welding width	$U = 1.0737 + 0.000081*F + 0.029472*P - 1.33834*V + 0.00000216207*F*P + 0.000266*F*V - 0.000543*P*V - 0.00000191775*F^2 - 0.000153*P^2 + 0.216939*V^2$	0.9323	0.0001	15.5604
For 12 mm welding width	$U = 2.25882 - 0.001028*F - 0.002491*P - 1.03822*V - 0.00000272112*F*P + 0.00047*F*V + 0.004913*P*V$	0.955	0.0001	27.7504

The effect of welding power is high for the highest welding speed than the lowest for all welding pressure forces. The effect of welding power is higher for the lowest welding pressure force than the highest at 2 and 2.5 m/min welding speeds while the opposite is true for a welding speed of 3 m/min. These results showed that the welding power positively affected the generalized utility function of the weld seam. The generalized utility function of the weld seam drastically decreased for all welding pressure forces with the rising welding speed from 2 to 3 m/min for both welding widths. The effect of welding speed is high for the lowest welding power than the highest for all welding pressure forces. These results showed that the welding speed had a higher negative effect on the generalized utility function of the weld seam. When the welding pressure force increased from the lowest to the highest value for both welding widths, the generalized utility function of the weld seam slightly decreased for all welding power at a welding speed of 2 m/min. The weld seam generalized utility function similarly decreased for the welding power of 90 and 120 W at 2.5 m/min welding speed with the rising welding pressure force from 200 to 350 N for 12 mm welding width while showing insignificant change for welding power of 60 W. But in the case of 6 mm welding width at 2.5 m/min welding speed, the weld seam generalized utility function for the welding power of 70 and 100 W slightly increased with the rising welding pressure force from 150 to 225 N while decreasing from 225 to 300 N. Whereas, the weld seam generalized utility function slightly increased for 70 and 100 W welding power of 6 mm welding width and 90 and 120 W welding power of 12 mm welding width at 3 m/min welding speed when the welding pressure force increased from the lowest to the highest value. The effect of welding pressure force increased with increasing welding power while decreased with increasing welding speed. Generally, the surface plot of the generalized utility function is quite different for 6 and 12 mm welding widths. It was observed that the influence of welding process parameters is different for each welding width, which is proved by the surface plots of 6 mm welding width, cf. Figures 2a, 2b, and 2c and 12 mm welding width, cf. Figures 3a, 3b, and 3c. The impacts of welding power and speed on the generalized utility function were higher for 6 mm welding width than 12 mm, and both welding widths were particularly sensitive to the welding speed than power according to the

developed regression equations. Because the amount of energy transferred into the welding area is determined by the amount of vibration, and the number of cycles of mechanical vibration reached up to the material interface is affected by the welding speed. The surface plot analysis also allowed us to anticipate the maximum value of the generalized utility function for both welding widths. Based on the developed range of acceptable values, the maximum value of the generalized utility function was determined in a more extensive range of welding process parameters for 12 mm welding width while obtaining from a narrow range of values for 6 mm welding width. This observation is also explained and supported by the contour plot of the generalized utility function for 6 and 12 mm welding widths at 2, 2.5, and 3 m/min welding speeds shown in Figures 4 and 5, respectively. Furthermore, the actual verse predicted value of the generalized utility function is shown in Figure 6a for 6 mm welding width and Figure 6b for 12 mm welding width counting zero as a no-weld condition. According to these figures, the actual and predicted points were very close to the regressed diagonal line, especially for 12 mm welding width than that of 6 mm to the generalized utility function.

Statistical optimization

Graphical and numerical optimization methods were used to obtain the optimal value of ultrasonic welding process parameters for the generalized utility function. A generalized utility function is a converted single-objective function from a multi-objective function. It was developed by the regression analysis on the values of the generalized utility function, and these values were determined through a predetermined weight and normalization process. It is, therefore, used to express the multi-objective mechanical properties into a single form, and the statistical optimization was carried out through the generalized utility function. Because a single statistical optimization technique for one selected mechanical property or response variable doesn't show the correct optimal value of ultrasonic weld seam for the selected awnings or/and camping tents application. This is due to mainly the standard requirements set to express the selected application. Tensile strength, hydrostatic pressure resistance, and peel strength were the main important mechanical properties required for awnings and camping tents as per standards [20, 22, 23].

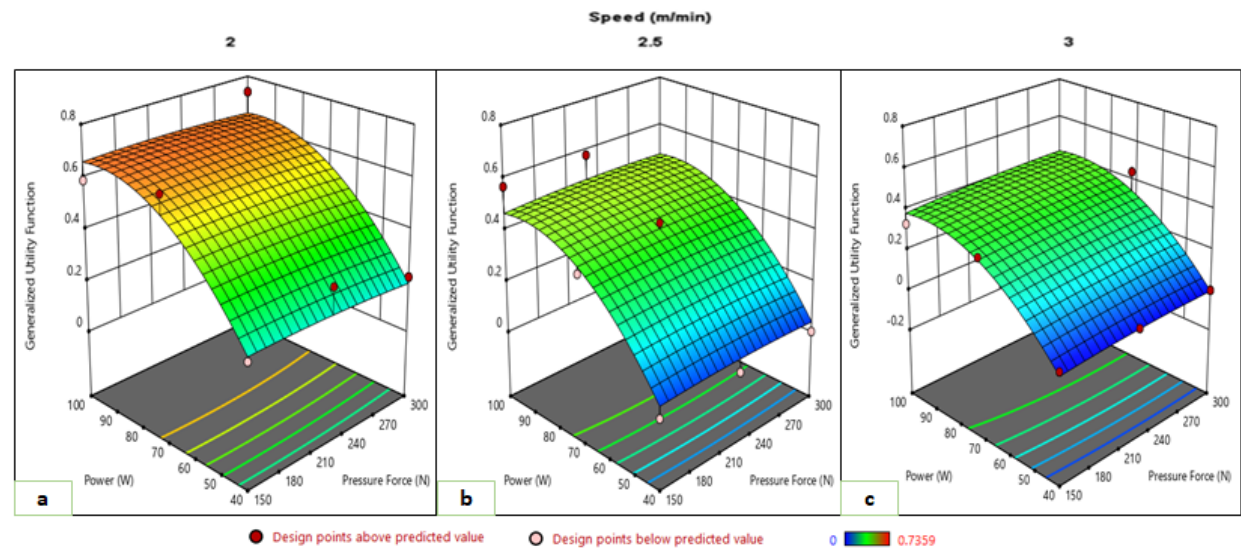


Figure 2. Surface plot of generalized utility function for 6 mm welding width at 2 (a), 2.5 (b), and 3 (c) m/min welding speeds.

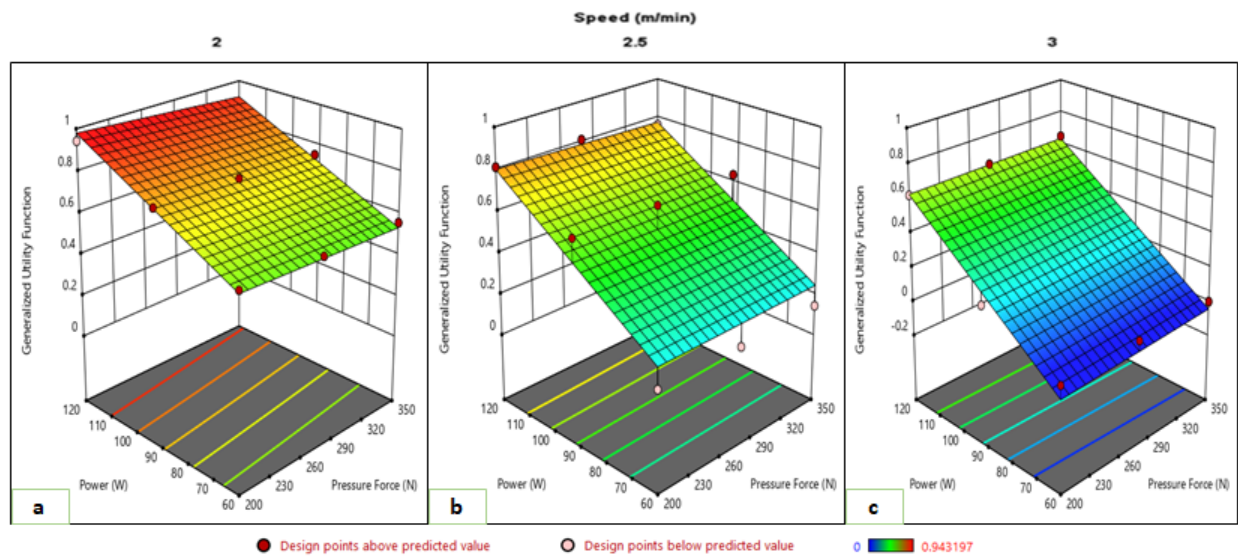


Figure 3. Surface plot of generalized utility function for 12 mm welding width at 2 (a), 2.5 (b), and 3 (c) m/min welding speeds.

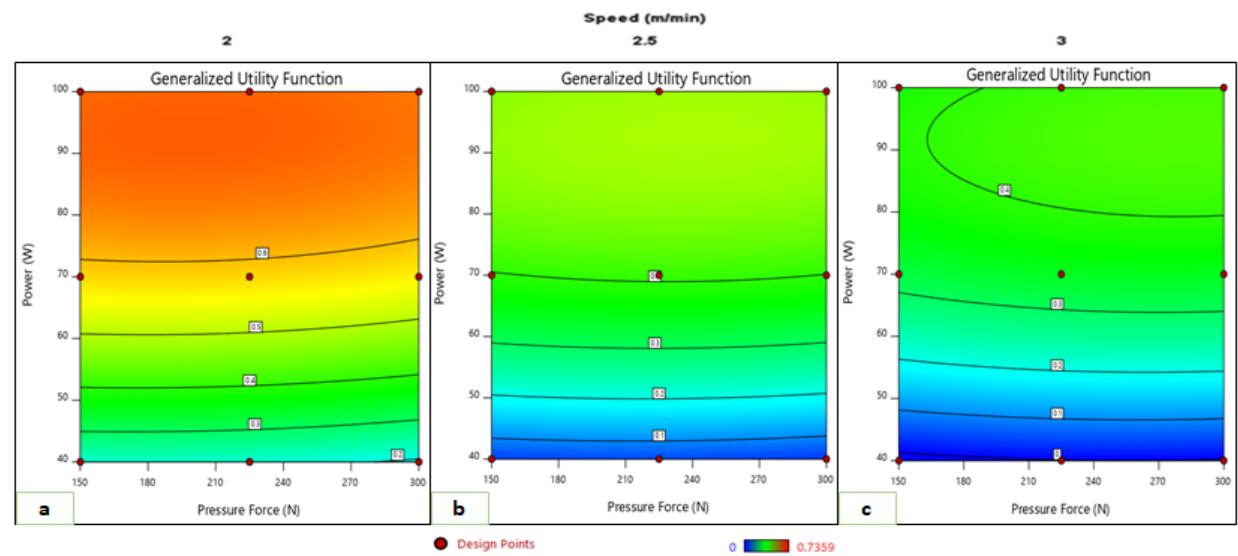


Figure 4. Contour plot of generalized utility function for 6 mm welding width at 2 (a), 2.5 (b), and 3 (c) m/min welding speeds.

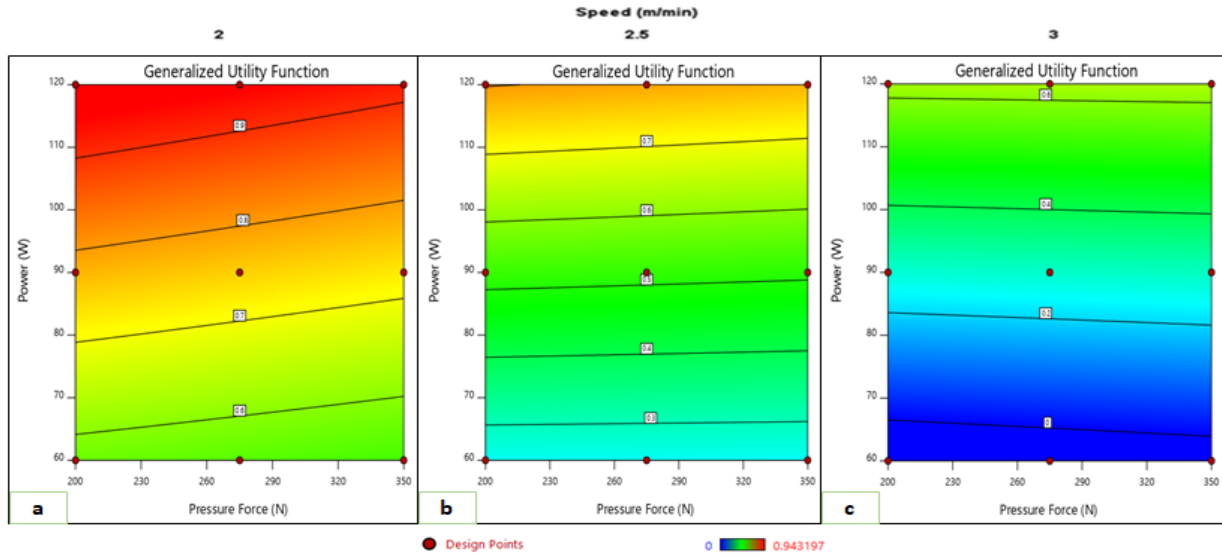


Figure 5. Contour plot of generalized utility function for 12 mm welding width at 2 (a), 2.5 (b), and 3 (c) m/min welding speeds.

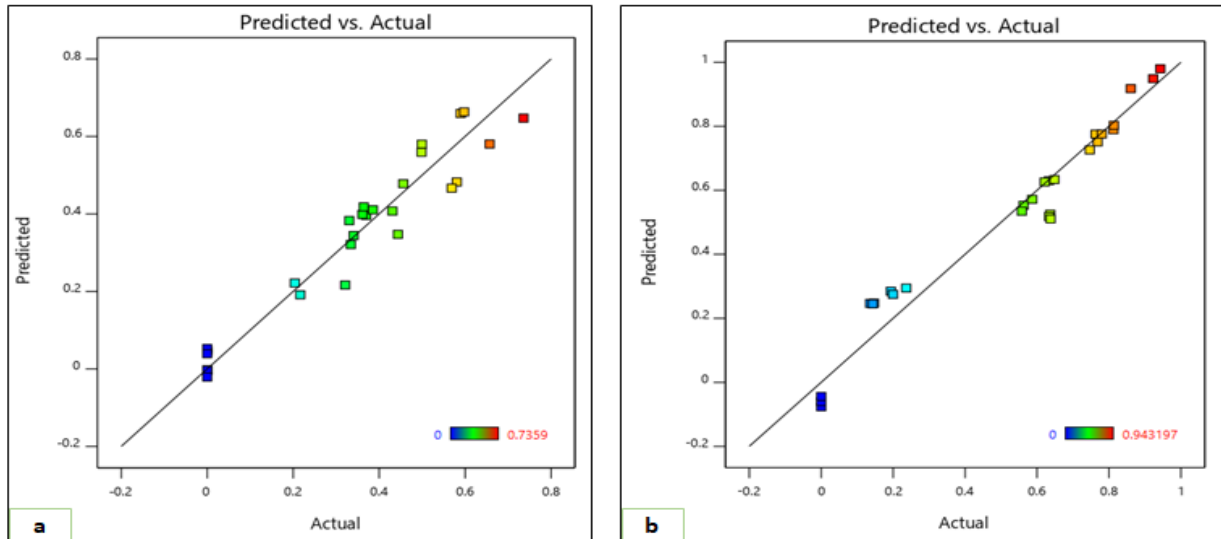


Figure 6. Actual vs predicted values for generalized utility function of 6 mm (a) and 12 mm (b) welding widths.

Additionally, Hussien et al. [11-13] stated that the welding pressure force had an inverse relationship with hydrostatic pressure resistance while having a direct relationship with tensile and peel strength up to certain limits. It is, therefore, important to find out the optimal value for all response variables simultaneously instead of finding them independently. Multi-objective optimization is an optimization technique for more than one desired goal and can be applied directly or indirectly. A direct approach commonly used all response variables at a time directly, while an indirect approach used the values of a single converted representative response variable called the generalized utility function. Both approaches consequently simplify the problem, but expressing a set of the response variable in a single objective function can make the result easy to understand for one selected application. Once the range was set and categorized into unacceptable

(unsatisfactory and rejected) and acceptable (satisfactory and very good) values for the roof and wall of awnings and camping tents, it can be simple to understand and decide the weld seam performance in the application without analyzing them independently. On the other hand, it can be applied to a wide range of problems in which difficult to figure out the best solution directly and used the evaluation of standard functions and operations with several design constraints. These are the advantages of the proposed indirect approach. Thus, the optimal value of ultrasonic welding process parameters has been evaluated in graphical and numerical optimization methods where the generalized utility functions are maximized. These two different optimization methods were considered in this research for the seek of comparison purposes. The optimal weld seams are, therefore, produced for the highest values of all criteria.

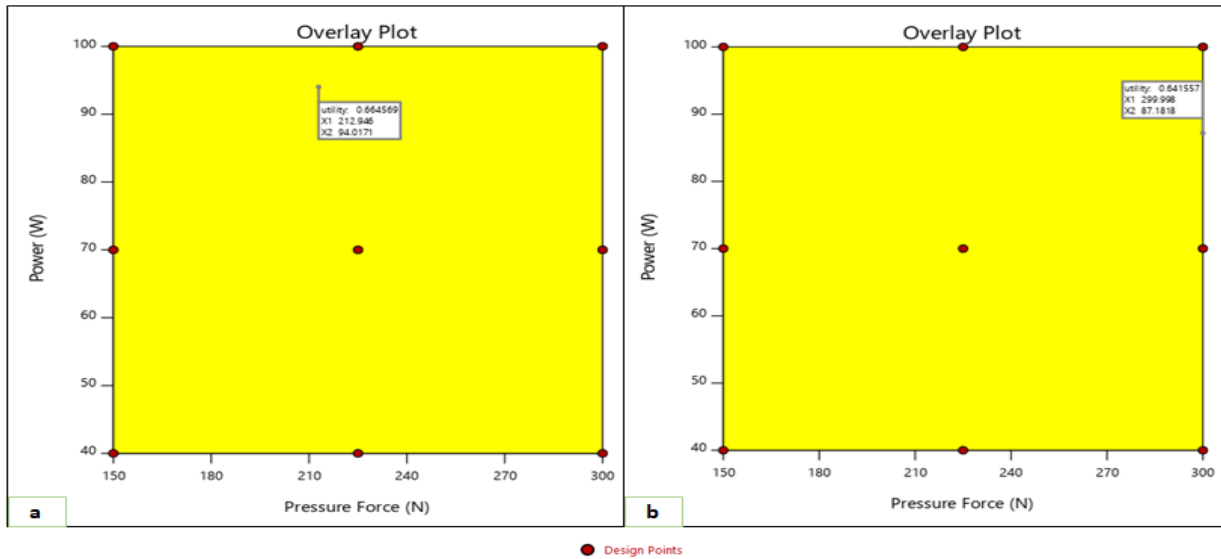


Figure 7. The best (a) and the least (b) optimal overlay plot of generalized utility function at 2 m/min welding speed for 6 mm welding width.

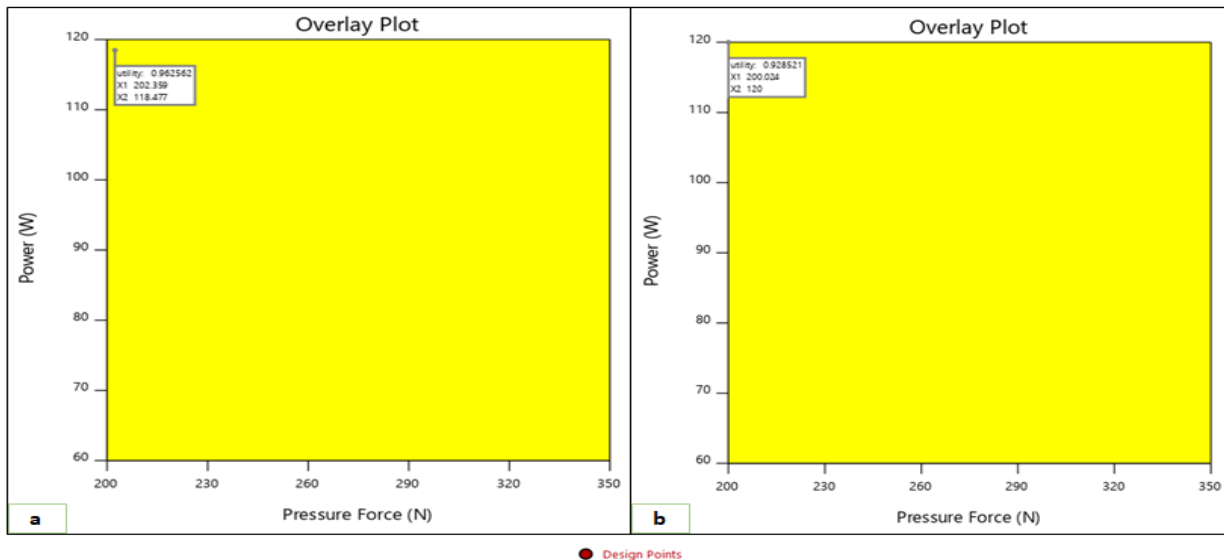


Figure 8. The best (a) and the least (b) optimal overlay plot of generalized utility function at 2.017 (a) and 2.145 (b) m/min welding speed for 12 mm welding width.

Graphical optimization: The minimum and maximum values of the generalized utility function were required to feed as input for further graphical optimization process using Design Expert 11. The values of 0.20357 and 0.7359 were set for the minimum and maximum value of the generalized utility function of 6 mm welding width, respectively; to find the optimal value of ultrasonic welding process parameters in the given range. Whereas for 12 mm welding width, the values of 0.13656 and 0.94318 were set for minimum and maximum values of the generalized utility function, respectively. As per the overlay plot of the generalized utility function, 84 different solutions were investigated for 6 mm welding width while 100 solutions were explored for 12 mm welding width. The solution was presented according to their order starting from the best to the least. The best (1st) optimal solution of the generalized utility

function (0.665 at 0.903 desirability) was obtained at a welding speed of 2 m/min, power of 94.017 W, and pressure force of 212.946 N for 6 mm welding width; whereas, the least (88th) optimal solution of the generalized utility function (0.642 at 0.872 desirability) was investigated at a welding speed of 2 m/min, power of 87.182 W, and pressure force of 299.998 N. Similarly for 12 mm welding width, the best (1st) optimal solution of the generalized utility function (0.963 at 1 desirability) was obtained at a welding speed of 2.017 m/min, power of 118.477 W, and pressure force of 202.359 N. Whereas, the least (100th) optimal solution of the generalized utility function (0.929 at 0.984 desirability) were investigated at a welding speed of 2.145 m/min, power of 120 W, and pressure force of 200.024 N. Figures 7a and 7b demonstrate the best (1st) and the least (88th) optimal overlay plot of generalized utility

function obtained using 6 mm plain anvil wheel at 2 m/min welding speed. For 12 mm welding width, Figures 8(a) and 8(b) exhibit the best (1st) and the least (100th) optimal overlay plot of the generalized utility function at 2.017 and 2.145 m/min welding speed, respectively.

Numerical optimization: Ultrasonic welding process parameters (welding pressure force, power, and speed) and generalized utility functions were set as a constraint during a multi-objective numerical optimization. This multi-criteria numerical optimization was performed after setting the goal, limit, weight, and importance of all listed constraints on Design Expert 11. The available options for selecting the goal of each constraint included maximize, minimize, in range, equal to, and targets. The upper and lower limits were taken from the actual value of the generalized utility function of the hybrid textile material for 6 and 12 mm welding widths. Each constraint's importance can be adjusted from one to five. Thus, the importance of welding pressure force, power, and speed were assigned as three out of five considering their goal within the range. For a welding width of 6 mm, the lower to upper limits of welding pressure force, power, and speed was established at 150 to 300 N, 40 to 100 W, and 2 to 3 m/min, respectively; while for a welding width of 12 mm, the lower to upper limits were set at 200 to 350 N, 60 to 120 W, and 2 to 3 m/min. Since the sum of all response variable weights was designed to be one as explained above, the weight considered for the generalized utility function was also equal to one. The goal of the weld seam generalized utility function was to maximize the result while staying within the lower to higher limit (0.20357 to 0.7359) for a 6 mm welding width and (0.13656 to 0.94318) for a 12 mm welding

width, taking their importance into consideration as five of five.

The optimal value of the generalized utility function (0.665 and 0.963) was obtained at welding speed (2 and 2.017 m/min), power (94.017 and 118.477 W), and pressure force (212.946 and 202.359 N) of 6 and 12 mm welding widths, respectively. According to the numerical optimization results, generated numbers of possible iterated solutions were 88 and 100 for 6 and 12 mm welding widths, respectively; these iterated solutions were ordered based on the importance, desirability, and target setup of the generalized utility function. This observation is supported by Figures 9 and 10 that the first (1st) and the least (88th) optimal solution contour graphs for desirability and generalized utility function are produced for 6 mm welding width at the optimal welding speed of 2 m/min; and also supported by the Figures 11 and 12 that the first (1st) and the least (100th) optimal solution contour graphs are formed for 12 mm welding width at the optimal welding speeds of 2.017 and 2.145 m/min, respectively. Welding power is proportional to cost, while welding speed is relevant to production efficiency. Thus, the best numerically obtained optimal solutions indicated a lower product output rate and energy efficiency in terms of power savings. Furthermore, it was observed the same optimal values through both optimization methods used in this research. According to these findings, the best optimal setting parameters of the ultrasonic welding process should be suggested using either numerical or graphical optimization methods. The best optimal values of the generalized utility function for both welding widths were found in the range of very good values for the roof and wall of awnings and camping tents in which a very good weld seam performance was produced.

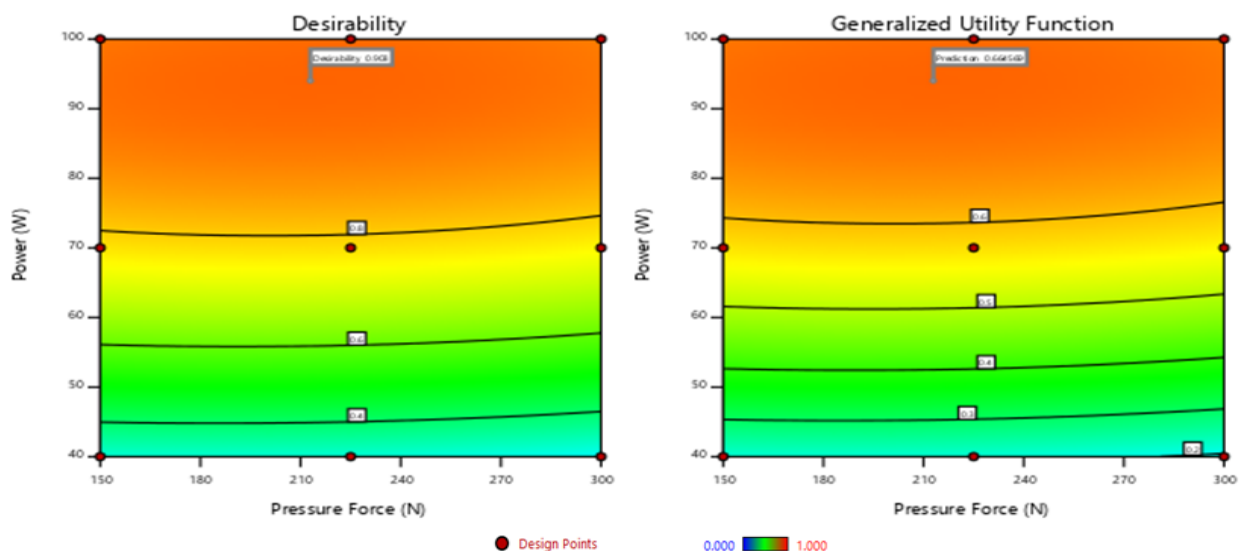


Figure 9. The first optimal solution contour plot of desirability and generalized utility function for 6 mm welding width at 2 m/min welding speed.

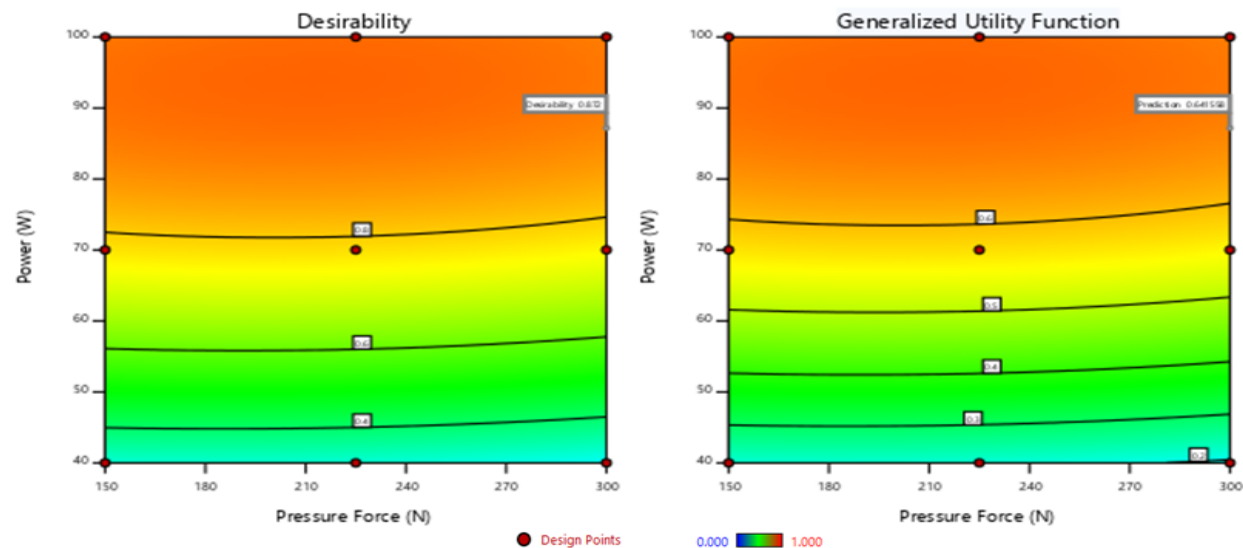


Figure 10. The least optimal solution contour plot of desirability and generalized utility function for 6 mm welding width at 2 m/min welding speed.

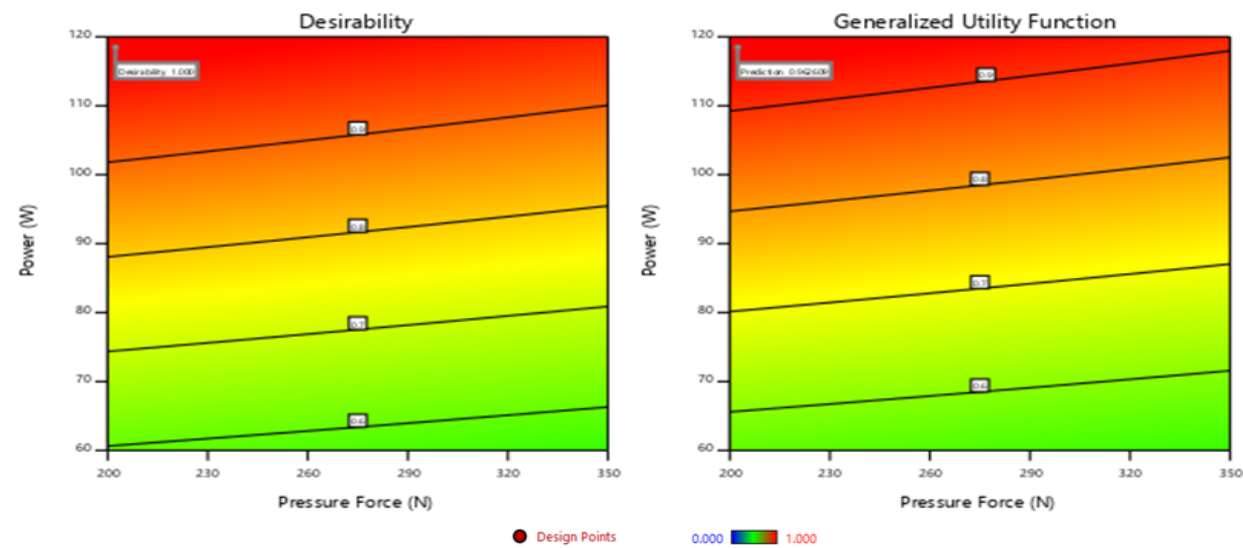


Figure 11. The first optimal solution contour plot of desirability and generalized utility function for 12 mm welding width at 2.017 m/min welding speed.

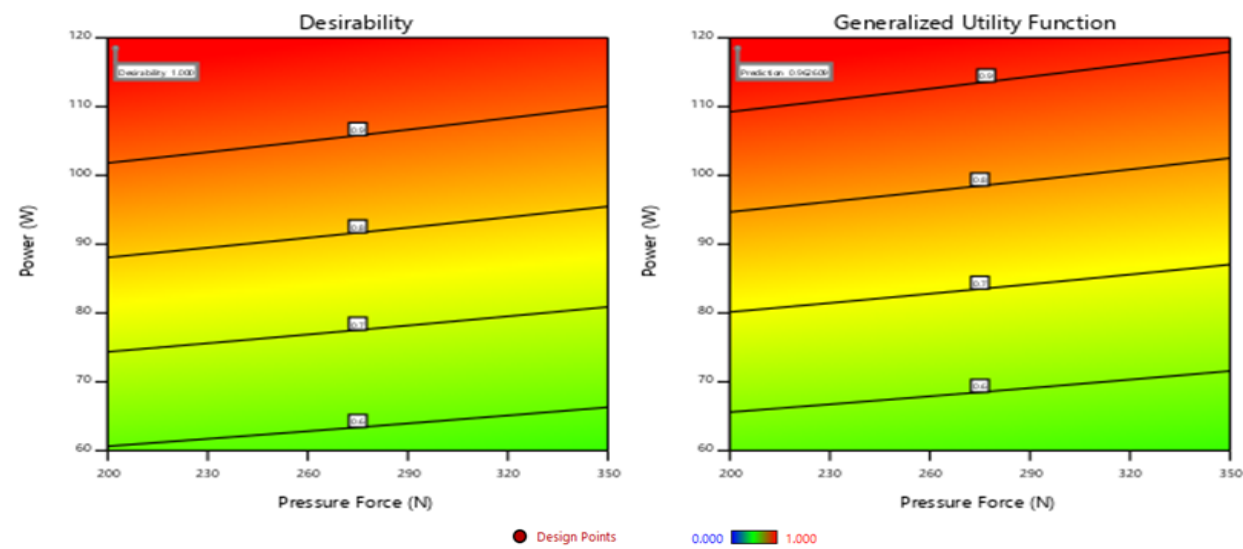


Figure 12. The first optimal solution contour plot of desirability and generalized utility function for 12 mm welding width at 2.017 m/min welding speed.

CONCLUSION

According to the statistical analysis, a significant effect of welding power and speed on generalized utility function was shown for both welding widths except welding pressure force. Tensile strength is the most important index with the greatest weight value of 0.56 than that of hydrostatic pressure resistance (0.32) and peel strength (0.12). It was investigated that the effect of welding power and speed on the generalized utility function was higher for 6 mm welding width than 12 mm. The generalized utility function was particularly sensitive to the welding speed than power for both welding widths. The lowest and highest values of generalized utility function were attained at different welding process parameters compared to the values of tensile strength, hydrostatic pressure resistance, and peel strength independently. It was observed that more variants of variable factors were possible to apply for 12 mm welding width than 6 mm. The number of variants of variable factors was smaller for the roof of camping tents compared to awnings for 6 mm welding width within the range of very good values. It was investigated that the variants of variable factors were higher within the range of satisfactory values compared to very good values for both welding widths. According to the multi-criteria statistical optimization, the optimal value of weld seam generalized utility function (0.665 and 0.963) was obtained at welding pressure force (212.946 and 202.359 N), power (94.017 and 118.477 W), and speed (2 and 2.017 m/min) of 6 and 12 mm welding widths, respectively. The optimal values were found within the range of very good values for both welding widths, and the same results were attained through numerical and graphical optimization methods. It can be concluded that the effect of ultrasonic welding process parameters on multi-objective functions can be predicted through a single equation without the experimental investigation of mechanical properties for PVC-coated textile materials. Furthermore, the research findings are important to adapt in the industrial production of the roof and wall of awnings and camping tents for infrequent and short-term use, moderate weather conditions, and extreme and long-term use.

Acknowledgement: *The authors would like to thank ITM, DAAD, MOSHE, and EITEX for their valuable support of this research, and appreciate the Nucleus GmbH for allowing us to work on their machine, and also present special thanks to Mr. Tilo Pilling for his valuable assistance during testing.*

Funding: *This research was funded by DAAD through EECBP Home Grown Ph.D. Scholarship Program 2019. The APC was funded by the publication fund of the TU Dresden and Saxon State and University Library Dresden (SLUB).*

REFERENCES

1. Szafranska H. and Korycki R.: Multicriteria optimization of the Mechanical Properties in Laminated Seams. *Materials* 2021; 14: 1-10.
<https://doi.org/10.3390/ma14112989>
2. Sarhananrhan R., Madhu M., Suresh K.S.: Multi-Objective Optimization of Plastic Welding Parameters In USPW of PMMA CM-205 Using Grey Relational Analysis, *International Research Journal of Engineering and Technology*, 4(6), 2017, pp. 1324-31.
3. Ramesh M. and Panneerselvam K.: Welding analysis and optimization of ultra-sonic welding in HDPE-5%PBI composite by CODAS decision-making approach, *Physica Scripta*, 97, 2022, pp: 1-17.
<https://doi.org/10.1088/1402-4896/ac8120>
4. Meng Y, Rajagopal M, Kuntumalla G, et al.: Multi-objective optimization of peel and shear strengths in ultrasonic metal welding using machine learning-based response surface methodology, *Mathematical Biosciences and Engineering*, 17, 2020, pp. 7411-27.
<https://doi.org/10.3934/mbe.2020379>
5. Mongan PG, Modi V, McLaughlin JW, et al.: Multi-objective optimization of ultrasonically welded dissimilar joints through machine learning, *Journal of Intelligent Manufacturing*, 33, 2022, pp. 1125–1138.
<https://doi.org/10.1007/s10845-022-01911-6>
6. Satpathy M.P., Moharana B.R., Dewangan S. and Sahoo S.K.: Modeling and optimization of ultrasonic metal welding on dissimilar sheets using a fuzzy-based genetic algorithm approach, *Engineering Science and Technology*, 18, 2015, pp.634-47.
<https://doi.org/10.1016/j.jestech.2015.04.007>
7. He Z., Tran K.P., Thomassey S., Zeng X., Xu J. and Yi C. Multi-objective optimization of the textile manufacturing process using deep-Q-network based multi-agent reinforcement learning, *Journal of Manufacturing Systems*, 62, 2022, pp. 939-49.
<https://doi.org/10.1016/j.jmsy.2021.03.017>
8. Sada S.O.: The use of a multi-objective genetic algorithm (MOGA) in optimizing and predicting weld quality, *Cogent Engineering*, 7, 2020.
<https://doi.org/10.1080/23311916.2020.1741310>
9. Zhang G., Lin T., Luo L., et al.: Multi-objective optimization of resistance welding process of GF/PP composites. *Polymers*, 13, 2021, pp. 2560.
<https://doi.org/10.3390/polym13152560>
10. Cerda-Flores S.C., Rojas-Punzo A.A. and Nápoles-Rivera F. Applications of multi-objective optimization to industrial processes: A literature review, *Processes*, 10, 2022, pp. 133.
<https://doi.org/10.3390/pr10010133>
11. Hussien M.S., Kyosev Y.K., Pietsch K., et al.: Effect of ultrasonic welding process parameters on seam strength of PVC-coated hybrid textiles for weather protection. *Journal of Industrial Textiles*, 51, 2022, pp. 1–44.
<https://doi.org/10.1177/15280837211057579>
12. Hussien M.S., Kyosev Y.K., Pietsch K., et al.: Effect of ultrasonic welding process parameters on hydrostatic pressure resistance of hybrid textiles for weather protection, *Textile Research Journal*, 92, 2022, pp. 1-16.
<https://doi.org/10.1177/0040517520988124>
13. Hussien M.S., Kyosev Y.K., Pietsch K., et al.: Effect of ultrasonic welding process parameters on peel strength of membranes for tents, *Journal of Engineered Fibers and Fabrics*, 17, 2022, pp. 1-19.
<https://doi.org/10.1177/15589250221101463>
14. Hussien M.S., Kyosev Y.K., Pietsch K., et al.: Investigation of actual phenomena and auxiliary ultrasonic welding parameters on seam strength of PVC-coated hybrid textiles, *AUTEX Research Journal*, 2022, pp. 1-21.
<https://doi.org/10.2478/aut-2022-0011>
15. Szafranska H. and Korycki R.: Analysis of mechanical properties of laminated seams, *Journal of Natural Fibers*, 17, 2018, pp. 398–411.
<https://doi.org/10.1080/15440478.2018.1498424>

16. Wu C-Y, Benatar A and Mokhtarzadeh A. Comparison of Ultrasonic Welding and Vibration Welding of Thermoplastic Polyolefin. *Weld World* 2012; 56: 69–75. <https://doi.org/10.1007/BF03321148>
17. Rani R.M., Suresh K.S., Prakasan K. and Rudramoorthy R. A.: Statistical study of parameters in ultrasonic welding of plastics, *Experimental Techniques*, 31, 2007, pp. 53-8. <https://doi.org/10.1111/j.1747-1567.2007.00182.x>
18. Macit A.S. and Tiber B. Investigation of water permeability of ultrasonic seaming on PU coated fabrics, *International Periodical of Recent Technologies in Applied Engineering*, 1 2019, pp. 25-9. <https://doi.org/10.35333/porta.2019.22>
19. Rajput C., Kumari S., Prajapati V., Dinbandhu and Abhishek K.: Experimental investigation on peel strength during ultrasonic welding of polypropylene H110MA, *Materials Today: Proceedings*, 26, 2020, pp. 1302-5. <https://doi.org/10.1016/j.matpr.2020.02.259>
20. EN-ISO-10966:2005. Sports and recreational equipment—Fabrics for awnings and camping tents—Specification. 2005, p. 7.
21. HEYtex. *Texineering—Tarps & Tents HEYtent*. In: Gruppe H, (ed.). *tentorium 650 (H5571-ECO)*. Germany: Heytex Gruppe, 2019.
22. EN-ISO-8937:2000. Caravan awnings—Functional requirements and test methods. 2000, p. 11.
23. EN-ISO-5912:2020. Camping tents—Requirements and test methods. 2020, p. 24.
24. EN-ISO-13935-1:2014. Textiles—Seam tensile properties of fabrics and made-up textile articles—Part 1: Determination of maximum force to seam rupture using the strip method. 2014, p. 7.
25. EN-ISO-11339:2010. Adhesives—T-peel test for flexible-to-flexible bonded assemblies. 2010, p. 6.
26. EN-ISO-811:2018. Textiles—Determination of resistance to water penetration—Hydrostatic pressure test. 2018, p. 5.
27. EN-ISO-139:2005. Textiles—Standard atmospheres for conditioning and testing. 2005, p. 6.
28. Gunantara N.: A review of multi-objective optimization: Methods and its applications, *Cogent Engineering*, 5, 2018, pp. 1-17. <https://doi.org/10.1080/23311916.2018.1502242>
29. Saaty R.W.: The analytic hierarchy process—what it is and how it is used. *Mathematical Modelling*. 1987; 9: 161-76. [https://doi.org/10.1016/0270-0255\(87\)90473-8](https://doi.org/10.1016/0270-0255(87)90473-8)
30. Rozkowska E.: Rank ordering criteria weighting methods—A comparative overview, *OPTIMUM STUDIA EKONOMICZNE*, 5, 2013, pp. 14-33. <https://doi.org/10.15290/ose.2013.05.65.0>

ANTIMICROBIAL ACTIVITY OF COTTON FIBRES TREATED WITH PARTICLES EXTRACTED FROM CITRUS PLANTS: A REVIEW

ALI, REHMAT¹; KARAMAT, UM E HABIBA²; NAZIR, HAFIZA SABA²; BAIG, MIRZA MUHAMMED MOHSIN³; KHAN, BILAL ALAM⁴; ULLAH, ASAD⁵; USMAN, OSAMA⁶; WASEEM, TANYA⁷; TAHIR, MUHAMMAD FARRUKH^{8*}

¹ Department of Medicine, University of Health Sciences Lahore, Khayaban-e-Jamia Punjab, Lahore, Pakistan

² Amna Inayat Medical College, Lahore-Islamabad Motorway, Lahore, Sheikhupura, Pakistan

³ Department of Physics, University of Barcelona, Gran Via de les Corts Catalanes, Barcelona, Spain

⁴ Department of Applied Science and Technology, Politecnico di Torino, Corso Duca degli Abruzzi, 24, Torino, Italy

⁵ Department of Mechanical Engineering, Balochistan University of Information Technology, Airport Road, Quetta, Pakistan

⁶ Department of Physics, University of Lahore, 1-Km Defence Road, Lohore, Pakistan

⁷ Shifa College of Pharmaceutical Sciences, Shifa Tameer-e-Millat University Islamabad, Islamabad, Pakistan

⁸ Department of Biochemistry, University of Jhang, 89RG+G4, Jhang, Pakistan

ABSTRACT

Nanotechnology is an emerging technology in textile sector for the fabrication of functional textiles with different properties such as antibacterial, hydrophobicity, UV-protection, flame retardancy, anti-static and self-cleaning. In current COVID-19 crises, the development of antimicrobial textiles through the deposition of nanoparticles has emerged as a research subject of particular interest. Recently, the green-synthesis of nanoparticles from plant extracts has become an effective alternative to conventional physical and chemical synthesis methods due to being environmentally benign and nontoxic. In this review article, the significance of nanotechnology in antibacterial finishing of textiles, mechanism of antibacterial activity of nanoparticles, significance of green synthesis methods for nanoparticles have been discussed. The green-synthesis of different nanoparticles from the citrus plant extracts and their application on textiles for imparting antibacterial activity is reviewed in particular. The chemical composition of citrus plant extracts and their role as bio-reductants in the synthesis of nanoparticles is also highlighted. Moreover, different qualitative and quantitative standard testing protocols employed for the antimicrobial characterization of plant extracts and textiles have been discussed. The major challenges and limitations associated with the plant-based biosynthesis of nanoparticles have also been highlighted

KEYWORDS

Nanotechnology; Nanoparticles; Green synthesis; Citrus plants; Antimicrobial Textiles.

INTRODUCTION

The biosynthesis of nanoparticles remains executable through the usage of numerous natural resources involving microorganisms, fruits, plant tissues, plant extracts, and plants [1]. However, distinctive attention is being associated with the use of plant extracts. The popularity of the aforementioned pathway is primarily rooted in the features such as, simplicity of the process, facile synthesis and economic feasibility [2]. Further, the plant extracts are found to be of dual utility by paying the desirable character of acting as stabilizing agent as well as reducing agent. Moreover, the plant extracts with the addition of metallic nanoparticles are enumerated to reveal excellent antimicrobial

attributes and thus have earned prime candidature in the fabrication of bioactive textiles [3]. The use of plant-oriented antimicrobial agents such as, Aloe vera, Eucalyptus, Turmeric, Neem, and Basil has already been delineated in stream of applications encapsulating health surveillance, e-textile and sport gears [4]. The demand for hygienic materials, such as biocidal coatings in textiles (sportswear, undergarments, and bedding linen), is escalating with the advancement of living standards. The antibacterial finishing treatments has become an essential aspect of medical, therapeutic, and healthcare practises due to various potentially infectious microorganisms in hospital environments that might cause cross-infection disorders [5]. Antimicrobial finishing is one of the most significant

* Corresponding author: Tahir M.F., e-mail: drfarrukh@uoj.edu.pk

Received November 5, 2022; accepted April 24, 2023

functional finishes applied to hospital textiles, as well as everyday garments. The negative consequences of microbial proliferation involve unpleasant smell, loss of tensile characteristics, staining, and discoloration of textile materials. Antimicrobial finishes are applied to textiles to prevent the growth of microorganisms. Numerous antimicrobial agents are applied, including quaternary ammonium compounds, triclosan, metal salts based on cobalt, copper, zinc and silver nanoparticles to prevent the deterioration of textile materials [6]. These synthetic chemicals are all hazardous and have a negative impact on the environment [7]. Due to this problem, synthetic antimicrobial agents are being replaced by natural antimicrobial agents that have strong antibacterial action. Neem, Aloe vera, Eucalyptus, Basil and Turmeric are a few examples of natural antibacterial agents that have been used for the finishing of textiles. Citrus fruit peel exhibits an effective anti-microbial agent, making it suitable for use in the development of healthcare textiles [8].

The antimicrobial activity of copper and silver nanoparticles coated textiles has been widely reported. However, the antimicrobial activity of Cu-coated textiles from citrus plants source has not been reported. In the current study, the green-synthesis of different nanoparticles from the citrus plant extracts and their application on textiles for imparting antibacterial activity is reviewed in particular. The chemical composition of citrus plant extracts and their role as bio-reductants in the synthesis of nanoparticles is also highlighted. The various qualitative and quantitative standard testing protocols utilized for the antimicrobial characterization of textiles have also discussed in this review. The developed Cu-coated textiles could be effectively applied in the field of hospital textiles for the preparation of antibacterial scrub suits, surgical gowns, panel covers, protective clothing, bedding textiles, coveralls, wound dressings, table covers, curtains, and chair covers etc.

What are antimicrobials or antimicrobial agents (antimicrobial finishes)

The antimicrobial agents are usually projected as substances capable of killing or suppressing the microbial growth and thus provide protection against microbe-based adversities such as odor, discoloration, and degradation [9]. However, the performance of antimicrobial agents remains susceptible of multifaceted complexities such as, chemical structure, surrounding environment, in-plant handling and multiplicity of surface.

Natural antimicrobial agents

The natural antimicrobial agents are plants-fetched or animal-derived substances popular for their bioactivity and ecological capabilities. A stream of applications associated with natural pathogens can be witnessed in textile-based functionalities,

pharmaceutical manufacturing, and biomedical industries. One may notice the applicability of marine species, Aloe vera, neem, turmeric, tulsi, pomegranate, prickly chaff flower, clove, and other natural herbs in the role of antibacterial agent in textile finishing [9].

Necessity of antimicrobial agents

Microbes are almost always present on the human body, with a mean density of 100–1000 microbes/cm², even with clean skin. Numerous organisms, including bacteria, yeast, and fungi, can invade the wearer at this level. Numerous unfavorable side effects of these microbial disorders include offensive odors and stains brought on by material discoloration. As a result, the person as well as the textile are both negatively impacted by the microbial activity on textiles. Textiles serve as an ideal medium for the adhesion, transfer, and proliferation of infection-causing microbial species due to their characteristics and proximity to the human body [10] [11]. Natural fibers are more susceptible to microbial invasion than synthetic fibers because of their permeability and hydrophilicity. The structure of natural fibers traps nutrients, moisture, and oxygen, providing the ideal supplemented culture for quick microbial growth. Direct contact with the human body also offers warmth, nutrients, and humidity, which fasters the growth of microorganisms. The infections are bacterial and fungal. Moreover, the algae can develop on them if they are kept damp for a long time. Fungi also produce an unpleasant odor and a slimy, sticky feeling, in addition to discoloring, damaging the fibers, and staining textiles. The chemistry and structure of the textile fibers may also promote the growth of microbes. The low molecular weight contaminated compounds in textile finishing may not facilitate microbial multiplication, but they may provide enough nourishment for damp microbe growth. This weakens the fabrics strength and gives out an unpleasant odor. It also stains the fabric. It is crucial to limit microbial growth on textiles throughout use and preservation because of all these reasons [12].

Interaction of microbes with textile fibres

Natural and manmade fibers respond to microbial growth quite differently. Both may function as suitable substrates, however the underlying mechanisms vary significantly depending on the situation. Natural fibers are good targets for microbial breakdown because they retain water well and can easily have their polymer bonds hydrolyzed by microbial enzymes. Most protein and cellulose fibers are attacked by microbes. According to research, the fabrics most vulnerable to microbial attack are jute, cotton, flax, silk, and wool [13].

Microorganisms develop more slowly on synthetic fibers than on natural fibers because the polymeric framework of synthetic fibers does not hold as much

water. On the other hand, these fibers increase the retention of state perspiration in the intercellular spaces, where bacteria grow faster. For instance, synthetic fiber socks have reportedly been found to be more likely than natural fiber socks to cause a foot infection. According to study, the proportion of polyester in a fabric affects how well bacteria attach to it. When synthetic fibers undergo finishing chemicals like polysiloxane and polyethylene emulsions, they are more vulnerable to microbial degradation [14]. These chemicals enable bacteria to break down the polymer into "chewable bites," initiating the hydrolysis cycle, by exploiting the acidic as well as basic metabolic by-products. In this way, even the hardest polyurethanes could well be decomposed. Polypropylene, polyester, and nylon synthetic fibers have all shown signs of microbial deterioration when exposed to conductive conditions [15].

However, the textiles might act as active agents in the proliferation of microbes as well as substrates for bacterial development, which is of more concern. Viruses can persist for up to 16 hours on materials including terry towels, washable wool suits, cotton shirts, polyester/cotton shirts, nylon jersey, and cotton/polyester shirts. Synthetic fibers are more suitable to viral survival and spread than cotton [16]. The virus could well be physically removed from the fabric during washing. However, it was found in the laundry wastewater indicating that it has not been completely inactivated. All of these bacterial growth requirements can be satisfied by textiles, which can have a number of negative side effects. The existence of microbes and their growth can cause odor, health problems, and eventually fabric deterioration [17]. Microbes can damage the additives used in textiles, causing staining and the loss of functional properties including tensile strength and elasticity. One of the most notable adverse effects is the formation of malodor. When microorganisms multiply, they break down nutrients found in the environment, such as sweat and soil, to produce chemicals that give off odors. For instance, it is hypothesized that bacteria produce 3-methyl-2-hexenoic acid and is responsible for the distinctive body odor [18]. In addition to other factors, bacteria turn human perspiration into odorous substances like aldehydes, amines, and carboxylic acids that have an unpleasant odor [19].

Significance of nanotechnology in textile finishing

Nanotechnology has evolved to be a major area with several applications for engineering science at the nano-scale to produce goods with distinctive features [20]. The science and engineering involved in developing, producing, and analysing nanostructures having outstanding functional qualities in comparison to their bulk counterparts can be summed up as nanotechnology. Additionally, nanotechnology is

becoming increasingly important in interdisciplinary fields of science, including biology, chemistry, physics, and materials science [21]. As a result, synthesized nanomaterials are very useful in a variety of industries, such as energy electronics, biomedicine and pharmaceuticals, environmental remediation, and functional textiles. Among these applications, nanotechnology plays major role in the development of functional smart textiles with insect repellent, self-cleaning, flame-resistant, UV protection, hydrophobic, anti-static, and antimicrobial resistance properties [17]. The development of novel nanostructures and nanoparticles with promising bioactivity to be used in a variety of biomedical applications is mostly due to the acceleration of developments in the field of nanotechnology. Numerous studies have been conducted recently on the potential applications of nanoparticles in biomedicine, particularly as antimicrobial agents, and they have been recognized as a potential substitute for conventional antimicrobials to combat the multi drug resistance of microorganisms [22]. The overuse and exploitation of synthetic antibiotics, as well as the absence of new approaches for the production of antimicrobial compounds to address the issues, have all contributed to the rise in bacterial resistance to antibiotics, which has been a significant cause of concern. The development of innovative nanostructures for use in pharmaceutical and biomedical applications has benefited tremendously by bioactive features of nanoparticles, such as their antifungal, antibacterial, antiviral, antioxidant, and anti-inflammatory actions [23]. Nanoparticles' high surface-to-volume ratio improves their ability to interact with microorganisms and raises the level of their antibacterial activity. As shown in Fig. 4, different nanoparticle types, their chemistry, particle size, structure, and charge density all affect the antibacterial activity of nanosized particles such as nanocomposites, metal, carbon-based nanoparticles, and metal oxides [24]. Copper, platinum, gold, silver and other nanoscale metal particles are frequently used to exhibit antibacterial action, particularly to prevent bacterial development. Additionally, in recent years, these nanoparticles have been integrated into textile to prevent the growth and transmission of infectious bacterial strains through fabrics. Due to the increased demand for functional textiles in recent years, primary attention of researchers has thus shifted to developing these materials using nanoparticles [25].

Nanotechnology has added a new dimension to the finishing procedures used on textile materials. The fact that traditional or conventional finishing techniques frequently have short-term effects on textile materials (such as fabrics or clothing) is one of the key distinctions between them and nanotechnology finishing processes. These functional finishes lost some of their effectiveness after washing or wearing [26]. Fabric treated with

nanotechnology, on the other hand, develops more durability. The increased durability of a certain functional effect is due to the larger surface area of nanoparticles relative to the same volume of material produced with larger particles [27].

Mechanism of antibacterial activity of nanoparticles

The mode of antibacterial action for nanoparticles is currently unclear, and research is actively being done to determine the mechanism of antibacterial action. Recently, the proposed mechanism of antibacterial activity of nanoparticle include (i) bacterial cell wall and membrane destruction, (ii) invasion into bacteria, and (iii) oxidative stress [28]. Additionally, it has been noted that the presence of amino groups, carboxyl groups, and phosphate groups, gives negative charge on the surface of bacterial cell membrane. As a result, positively charged nanoparticles typically bind to the cell membranes by electrostatic interaction [29]. Eventually, the nanoparticles can directly enter the bacterial membrane and assimilate there, enabling them to interact with substances including protein, lipids, and DNA. According to Yun'an Qing et al. [29], the interactions of nanoparticles with cellular interactions cause cell damage and ultimately cell death. Additionally, in order to cause oxidative stress in the bacterial cells, nanoparticles release reactive oxygen species (ROS) including singlet oxygen (O_2), superoxide radicals (O^-), hydrogen peroxide (H_2O_2), and hydroxyl radicals (OH^-). The ions generated by the disintegration of nanoparticles cause ROS, which prevents bacterial growth or harms the organelles or cells of the bacteria. Additionally, the major factors that affect the nanoparticles' action mechanism towards bacteria are their size, topology, shape, morphologies, and surface charge [30]. Yan et al. [31]

investigated the interaction of Ag nanoparticles interacted with *Pseudomonas aeruginosa* and performed detailed analysis to explain the antibacterial mechanism. The outcomes showed that the key mechanisms for their efficient antibacterial mechanism are the contact of the nanoparticle with the cellular membranes and the formation of ROS [31]. Similar to this, Concha Guerrero et al. [32] revealed the interaction of nanoparticles with bacteria by TEM analysis while examining the mechanism of antibacterial action for copper oxide nanoparticles with different 11 bacterial strains. The findings showed that the copper oxide nanoparticles have potent antibacterial action through membranes and bleb disintegration, hole and cavity production, and bacterial cellular disintegration and rupture [32]. It was proposed that the ionic interaction between nanoparticles and bacteria, as well as the formation of redox reactions and ROS in bacteria, are the causes of the damaging effects of nanoparticles [32]. Additionally, Azam et al. [33] demonstrated that copper oxide nanoparticles with sizes between 20 and 28 nm have size-dependent antibacterial efficacy against both gram-positive and gram-negative bacteria. According to the findings, the smaller-sized copper oxide nanoparticles had strong antibacterial action with very low minimum bactericidal concentration (MBC) and minimum inhibitory concentration (MIC) values. This study revealed that the mechanism of antimicrobial activities is also influenced by the size of nanoparticles other than the production of ROS and oxidative stress [33]. It should be emphasised that the nanoparticles deposited in textile fabrics will follow the same mechanism of antimicrobial activities as described above, and Figure 1 provides a review of the possible antibacterial processes that are hypothesised to be shown by nanoparticles.

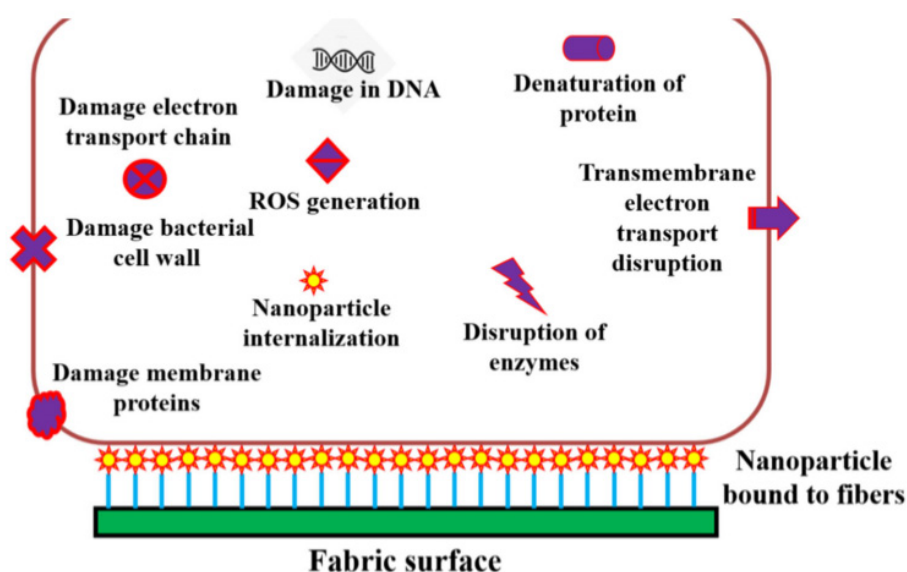


Figure 1. Possible antibacterial processes shown by nanoparticles. [34]

Different synthesis approaches for nanoparticles and their limitation

The uniqueness of nanoparticles to be employed in intended applications is typically determined by synthesis methods. The synthesis techniques determine the surface charge, size, morphology, and topology of nanoparticles, which in turn affects their characteristics. The following are the three main synthesis methods for the production of nanoparticles:

1. Physical methods,
2. Chemical methods,
3. Biological methods.

Each of these methods for synthesising nanoparticles has a number of benefits and drawbacks that can affect how well they exhibit biological characteristics, particularly when it comes to using them to inhibit pathogenic bacterial species [35]. Furthermore, the synthesis method-mediated antibacterial activities play a significant role in defining the effectiveness of antibacterial action while depositing the nanoparticles on the surface of fabrics. Physical synthesis methods which include laser ablation [36], physical vapour deposition [37], and ball milling [38] are effective in order to produce monodispersed nanoparticles with the necessary morphology and size. Although these technologies produce nanoparticles with antibacterial property employing them for textile applications presents difficulties due to the high cost and difficult production method. The most widely used techniques for synthesizing nanoparticles include sol-gel, hydrothermal synthesis, and precipitation techniques. This approach produces stable nanoparticles with the appropriate form and size along with the potential to change their surface charge, which is useful in biological applications, particularly for their antibacterial property. However, the dispersion of nanoparticles and their cytotoxicity against human cells as a result of using toxic chemicals during synthesis are the challenging aspects which cannot be modified via chemical approach [39]. It also affects their efficiency in using them as an antibacterial agent for the pilot-scale production of bactericidal textiles. Green or biosynthetic methods have recently become increasingly important to synthesize nanoparticles that are safe for humans and the environment. Algae, plants, and bacteria, fungi, as well as their extracts, have been frequently used to synthesize biocompatible nanoparticles that were effective in medicinal applications [40, 41]. As a result, the green synthesis has become the most effective method in recent years for depositing nanoparticles on the surface of textiles as antibacterial finishes to suppress the growth of pathogenic microorganisms [34].

Significance of green synthesis methods for nanoparticles

Due to the significance of ecologically sustainable production process, green synthesis of nanoparticle has attracted a lot of attention. The fabrication of nanoparticles using plant extracts is a suitable substitute for chemical reduction methods. The use of plant extracts as stabilizing or reducing agents for the synthesis of nanoparticles extracts has been found as alternative [42]. As a result, many researchers have adopted the green synthesis of NPs, which is seen as a viable alternative to chemical processing and used for a variety of applications. According to earlier research, phytochemicals stabilise metal nanomaterial for a longer period of time by reducing metal ions to metal nanoparticles. It facilitates this by capping the synthesised nanoparticles [43]. Additionally, green nanoparticles are said to have superior catalytic activity when compared to nanoparticles produced chemically.

Citrus plants from the *Rutaceae* family are among the many plants that have a lot of potential for use as bio-reductants in the environmentally friendly synthesis of nanoparticles. One of the most important and widely grown fruit crops is citrus tree [44]. Citrus plant extracts include numerous active phytochemicals that can be employed as a reducing and stabilising agent, making them ideal for use as a reducing agent in the synthesis of nanoparticles including zinc oxide and silver nanoparticle [45]. In addition, coumarins, cellulose, pectin, carotenoids, hemicellulose, lignin, essential volatile oils, phenolic components, etc. are found in the peel and juice of the majority of citrus fruits [46]. Citrus plant extracts have the potential to treat textiles for the improvement of functional properties of textiles which includes UV protection, antibacterial activity, and mosquito repellent properties [47]. Citrus plants are therefore thought to be effective bio-reductants for the formation of nanoparticles and active compounds for the antimicrobial finishing of textiles.

Chemical composition of citrus plant extracts

Citrus peels are an excellent source of pectin as well as essential oils and contain a number of bioactive substances, particularly flavonoids [48]. Citrus peels have a variety of biological actions that have been attributed to their complex composition, including antioxidant properties, anti-inflammatory effects, and other biological advantages for human health, including the capacity to fend off cancer and cardiovascular disorders [49]. Citrus peels are not waste rather; they are a unique natural resource as they exhibit such important biological functions. Table 1 summarizes some of the important chemical components present in the extract of citrus fruits and plants.

Table 1: The names and amount of major functional groups present in Citrus plants extract.

Sr. #	Chemical Component	Plant Name				Ref.
		Orange	Lemon	Grapefruit	Mandarin	
1	Hesperidin	1.22–42.56	20.62	0.13–0.59	0.01–5.46	[50]
2	Narirutin	0.02–20.21			0.587	[51]
3	Naringin	0.002–0.03	0.81–5.37	0.09–1.60		[52]
4	Eriocitrin		0.01–0.21			[53]
5	Nobiletin	0.14–0.24	0.13–0.42	0.01–0.05	1.24–1.77	[54]
6	Tangeretin	0.02–27.5	0.07–0.21		0.20–0.49	[54]
7	3,5,6,7,8,3',4'-hepatamethoxyflavones	0.55–17.37				[50]
8	Sinensetin	0.16–36.92			0.09–0.17	[50]
9	5-demethylnobiletin		0.02–0.36			[53]
10	5-demethyltangeretin	0.35–0.12				[53]
11	5-OH-3,6,7,8,3',4'-hexamethoxyflavone			0.02–0.21		[53]
12	Sudachitin	0.16–1.21			0.15	[53]
13	Vicenin-2	0.17				[52]
14	Hesperetin	0.002–0.007				[54]
15	Limonin	0.03–0.14	0.26–0.32	0.02–0.20	0.05–0.20	[54]
16	Nomilin	0.01–0.12				[54]
17	Obacunon		0.03–0.12			[54]
18	Limonexic acid			0.02–0.62		[54]
19	Synephrine	11.71–13.84				[55]
20	N-methyl tyramine					[55]
21	Limonene	60.44–97.3	63.67–76.99	88.6–91.5	66.91–91.51	[56]
22	β -Pinene	1.45–1.82	9.31–14.74	0.8–1.2	0.73–1.90	[57]
23	α -Pinene	0.21–3.53	0.99–1.59	0.40–0.70	0.54–2.43	[57]
24	Valencene	0.14–0.40			0.03–0.74	[56]
25	Linalool	0.04–4.11		0.12–1.10	0.10–3.23	[57]
26	β -Elemene	0.02–0.06	0.01–0.24			[57]
27	α -Copaene	0.04–0.24		0.03–0.13	0.03–0.10	[56]
28	γ -Terpinene	0.02–0.32	5.51–10.38		0.13–14.22	[56]
29	α -Humulene	0.02–0.04		0.03–0.10		[56]
30	β -Myrcene	0.03–0.05	0.38–0.96	0.03–2.16	2.54–24.77	[56]
31	Sabinene	0.10–0.29		0.16–0.63	0.30–0.60	[56]
32	β -Sinensal	0.04–0.14	0.05–2.21			[56]
33	α -Sinensal	0.02–0.04	0.20–0.60	0.34–2.13		[56]

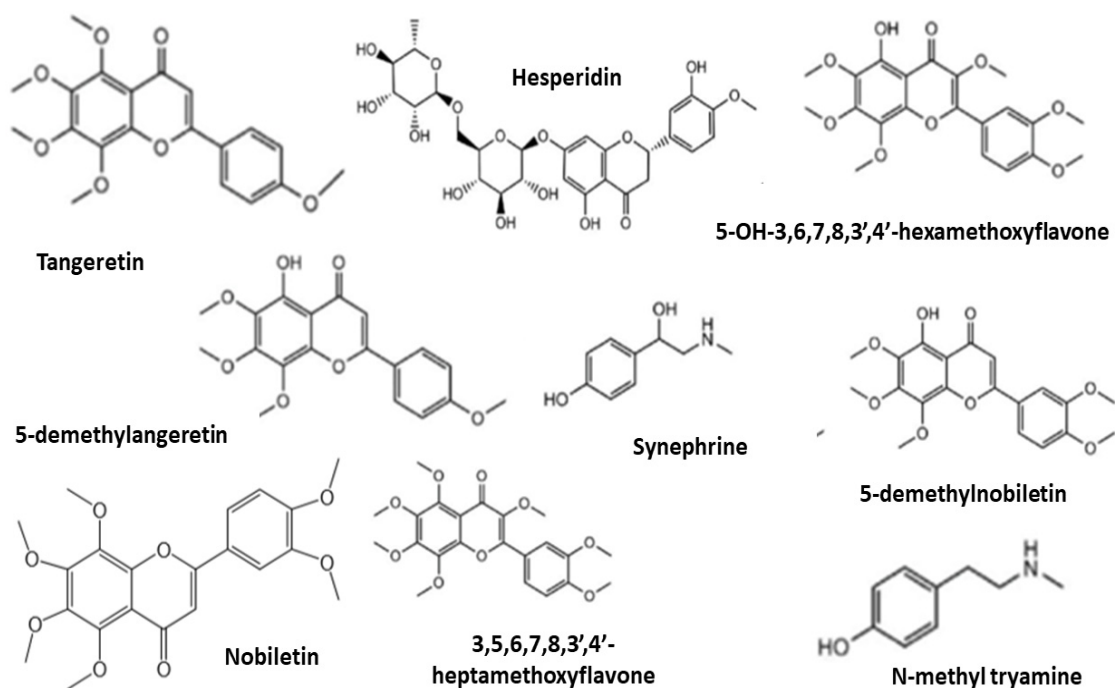
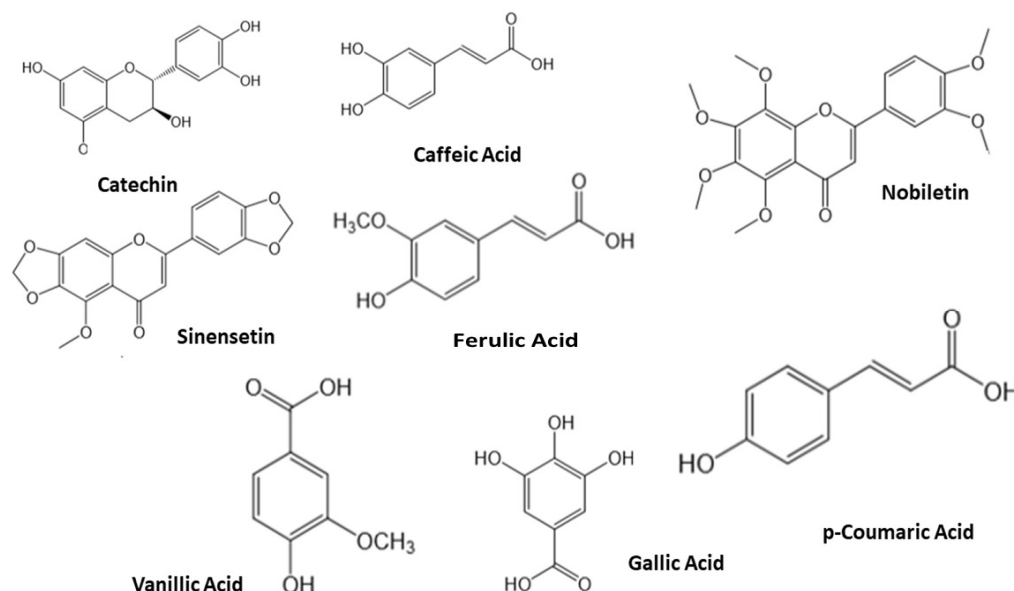
**Figure 2.** Molecular structure of flavonoids and alkaloids present in citrus plant extract [54].

Table 2. The type and name of phenolic compounds detected by DART-MS analysis in Citrus plants extract.

Sr #.	Compound	Type	m/z
1.	Nobiletin	Flavonoids	403
2.	Catechin	Flavonoids	290
3.	Sinensetin	Flavonoids	373
4.	Ferulic acid	Hydroxycinnamic acid	194
5.	Vanillic acid	Hydroxycinnamic acid	168
6.	Gallic acid	Hydroxycinnamic acid	172
7.	Caffeic acid	Hydroxycinnamic acid	180
8.	Coumaric acid	Hydroxycinnamic acid	164

**Figure 3.** Molecular structure of phenolic components detected in citrus plant extracts [59].

Loizzo et al. [58] used HPLC to investigate extracts in order to determine and measure the most prevalent flavonoids in the polar extracts considering that flavonoids are primarily responsible for citrus's health benefits. Citrus is a major source of many kinds of flavonoids, including flavonols, flavones, flavanones, and polymethoxylated flavones, according to a review of the literature available on citrus species. They chose to assess the quantitative and qualitative features of ten flavonoids, including rutin, naringenin, naringin, quercetin, hesperidin, tangeretin, hesperetin, diosmin, apigenin, and nobiletin. It was also noted that environmental and genetic factors play a significant role in the contents and dispersion of flavonoids in several Citrus species [58]. Figure 2 shows the molecular structure of alkaloids and flavonoids present in the citrus fruits and plant extract.

Rehan et al. [59] effectively used DART-MS for the identification of phenolic components in the aqueous extract of orange peel (OP) (Figure 3). The determination of OP components was made by examining the extracted-ion analysis results of the ion flow at m/z levels comparable to [M - H]⁻ and [M + H]⁺ ions of the examined compounds. Orange peel extracts were subjected to a DART-MS analysis, which revealed the presence of eight phenolic chemicals, including three flavonoids and five phenolic acids (Table 2) [59].

In addition to being one of the richest sources of vitamin C, citrus plant extracts also include significant levels of essential oils, carotenoids, flavonoids, and several minerals. Due to the presence of these compounds, citrus fruit peel exhibits an effective antimicrobial activity which makes it ideal for use in the production of medical fabrics [60].

Methods for extraction of essential oils from citrus plants

Citrus essential oils have been employed as flavoring agents and for aromatherapy in a variety of goods, including meals, drinks, cosmetics, and medications. They are also employed for their anticancer, antioxidant, and bactericidal effects. Monoterpene hydrocarbons, which have a high amount of unsaturation and are typically unstable due to several causes, including light, heat, oxidation, and hydration, dominate citrus essential oils. Few studies have been carried out so far regarding the application of novel isolation techniques for citrus fruit essential oils. According to ISO specifications, essential oils are products obtained from unprocessed plant sources that can only be physically extracted. The physical procedures include dry distillation of organic substances, expression (often referred as "cold pressing" for citrus peel oils), and distillation (water, steam, and steam/water) [61]. The essential oils are

physically isolated from the aqueous phase after distillation or expression. The citrus peels are often cold pressed in order to isolate volatile components to be utilized as essential oils. The citrus fruits peel and cuticles contain oil glands or sacs at various depths that contain citrus essential oil. Cold pressing physically removes peels and cuticle oils, and as cold pressing produces an aqueous emulsion, this emulsion is subsequently centrifuged to isolate the essential oil [61].

In certain countries, distillation is also utilized to economically collect essential oils from citrus by-products. Citrus peels subjected to steam or hot water during distillation liberate their essential oils via evaporation process. By distilling two immiscible liquids, particularly essential oils and water, the extraction of the essential oils is assisted on the assumption that, at boiling temperature, the total vapor pressure of the liquid matches the ambient pressure. As a result, the components of essential oils having boiling points typically ranging from 200 to 300 °C, evaporate at a temperature similar to that of water. The essential oil-filled steam passes and reaches a small tube that is being cooled from the outside. Steam as well as the essential oil droplets are recovered and separated after condensation in a container known as a "Florentine flask,". Essential oil floats on top being less dense than water, while water sinks to the bottom and could be readily separated [62].

There are some drawbacks to using traditional methods to extract citrus essential oils. The high temperatures and extended extraction times during hydro-distillation and steam distillation can change the chemical composition of the oil components and frequently lead to the loss of the most volatile compounds. Citrus essential oils are vigorously stirred with water during cold pressing, and the concentration of terpene alcohols and citral gradually decreases. Additionally, air is whipped into the liquid during agitation, which promotes resinification, hydrolysis, and oxidation. Due to these drawbacks, the use of novel essential oil and aroma extraction methods has been taken into consideration [63]. These methods include ultrasound extraction [64], a controlled pressure drop process [65], supercritical fluid extraction [66], subcritical water extraction [67], and microwave extraction [68]. These methods typically increase the quantity of essential oils, preserve their quality, and consume less energy.

A novel patented process called fast microwave-accelerated distillation, also referred to as microwave "dry" distillation or "MAD," isolates essential oils from natural materials by fusing microwave radiation with traditional distillation [69]. In this technique, fresh vegetable materials are added to a microwave reactor. The in-situ liquid (mostly water) within the plant material expands as a result of heat produced, causing the glands and oleiferous vesicles to rupture.

Thus, the essential oils that were trapped in the in-situ water of the plant matter via azeotropic distillation is released through this method. After passing via a condenser outside of the microwave cavity, the vapors are then condensed. In a bottomed flask, the distillate is continually collected. Cohobation restores the moisture of the plant material, refluxes surplus water and recycles it to the extraction vessel. The essential oil is immediately extracted and dried without performing an additional solvent extraction step. Essential oils have been extracted using MAD from a variety of source materials. The modified microwave-assisted extraction (MAE) approach, which employs organic substances, and the modified hydro-distillation (HD) technique, which needs a lot of water, are not comparable to the MAD method. Essential oils from aromatic spices and herbs such as thyme, basil, mint, star anise, ajowan, and cumin have been extracted using MAD [69].

Citrus plants as bio-reductants in synthesis of nanoparticles

Nanotechnology is becoming a significant research area due to its various potential applications in all domains of science, technology, healthcare, pharmacology, and other related fields. It includes materials as well as their applications with a single dimension between 1 and 100 nm. Nanoparticles (NPs) are often synthesized using a variety of processes, including milling, laser ablation, sputtering, chemical reduction, etc. These traditional methods, including the chemical reduction method, which uses a variety of harmful chemicals to synthesize nanoparticles, later pose several health problems due to their toxicity and raise severe environmental concerns, while other methods are expensive and require a considerable amount of energy. However, for biomedical application where purity is a priority, the biogenic synthesis process to synthesize nanoparticles is ecologically responsible and free of chemical pollutants. The extracts of natural plants, proteins or enzymes, are employed as reducing or stabilizing agents in the biological process of nanoparticles synthesis. Considering this, Ain Samat et al. employed *Citrus aurantifolia* extract in the biosynthesis of zinc oxide (ZnO) nanoparticles. They used zinc acetate as the precursor of Zn at various concentrations, and they reported that the synthesized ZnO nanoparticles were between 50 and 200 nm in size using FESEM [5].

Manal et al. [70] attempted to synthesize Ag-nanoparticles using biological waste material from citrus lime peels, and to characterize the produced green Ag-nanoparticles for their antibacterial properties and cytotoxic effects. According to a UV-visible spectrophotometer analysis of the synthesized Ag-nanoparticles, spherical and irregularly agglomerated Ag-nanoparticles development was reported. According to DLS measurements, the

synthesized Ag NPs had an average size of 59.74 nm. The majority of the examined human pathogenic bacteria exhibited significant activity against the produced Ag-nanoparticles in varied degrees in antimicrobial experiments. At last, two types of cell cultures human breast cancer cell line (MCF-7) and colon carcinoma cell line (HCT-116) were used to assess the cytotoxic effect of the greenly produced Ag-nanoparticles. The findings showed that cell viability and concentration are directly related [70]. Amanulla et al. [71] used extract of orange peel to synthesize TiO₂ nanoparticles. An agar well diffusion was used to measure their antibacterial action against *S. aureus*, *E. coli*, and *P. aeruginosa*. *P. aeruginosa* exhibited more activity when exposed to the nanoparticles [71].

In another study, orange peel waste can be used to produce silver nanoparticles in a natural, sustainable, and environmentally beneficial way. Orange peel-extracted Ag nanoparticles have strong photocatalytic properties against dyes and can also be widely used to treat dye effluent and treat wastewater [60].

Employing a biosynthetic process that uses plant extracts can greatly increase anti-microbial efficacy of zinc oxide nanoparticles. The presence of components (phytochemicals) that are intrinsically resistant to microorganisms may be the primary reason for the enhanced anti-microbial action of ZnO nanoparticles using plant extracts. This suggests that biologically synthesized zinc oxide nanoparticles could be an efficient substitute of conventional agents because of their benefits associated, such as their affordability and eco-friendliness. According to the literature, *Citrus aurantifolia*, *Citrus limon*, and *Limonia acidissima* are the three citrus species that were most frequently used in the green synthesis of ZnO nanoparticles [72]. N. Ain Samat and R. Md Nor [73] used *Citrus aurantifolia* fruits to prepare the extract. The fruit-skin was removed from these fruits after they were peeled, and the pulp was chopped and homogenized with deionized water. Following filtration, the filtrate was employed in further experiments. They used the zinc acetate (Zn (OAc)₂·2H₂O) as zinc precursor. Various amounts of zinc acetate were added in the *Citrus aurantifolia* extract. The mixture was then agitated at 90°C for three hours. This produced a white precipitate, which was then washed and dried at 100°C for 6 hours. The ZnO nanoparticles were successfully synthesized from this method [72]. In contrast to other citrus fruit (lime, grapefruit, lemon, tangelo, and orange) peel extracts, orange peel extract produced Ag nanoparticles (7.36–8.06 nm) in 15 minutes when employed in the microwave-assisted production of Ag-nanoparticles. These extracts revealed improved inhibitory activity against *E. coli*, *P. aeruginosa*, *S. aureus*, and *B. subtilis* [74].

In another study, plant powders most commonly are obtained from, *Citrus sinensis*, *Centella asiatica*,

Solanum tricornatum, and *Syzygium cumini* were used to synthesize silver nanoparticles from AgNO₃ solution as silver precursor. Agar well diffusion approach was used to test the antibacterial action of green-synthesized silver nanoparticles. The Ag-NPs synthesized from *C. sinensis* and *C. asiatica* exhibited highest antibacterial action (16 mm) towards *Pseudomonas aeruginosa*. It was observed that the Ag-nanoparticles produced by this technique have effective antibacterial activity towards harmful microorganisms [75]. Naikoo et al. [76] reported the synthesis of Au nanoparticles using citrus fruits with lemons and reticulate. Lemons were first smashed to extract the juice, which was then placed over polyamide mesh with fine pores. The extract was centrifuged at 10,000 rpm for ten minutes. In order to facilitate vigorous homogeneous mixing, 1 mM of a 50 mL composition of hydrogen tetrachloroaurate trihydrate was eventually heated to a boil. The extracted juice was diluted with the host solution using a range of 1–6 mL. There was a noticeable transition in colour from colorless to dark violet to ruby red. The granular solution was vigorously agitated again after 20 minutes, and it was then cooled to room temperature. After that, it was moved to another container where it was stored. Peak of the surface plasmon resonance was seen in the 530–550 nm range. In-depth TEM analysis was done to elucidate the structural characteristics of Au nanoparticles [76].

Sudhir et al. reported a non-toxic, low-cost, and environmentally friendly technique for the production of copper nanoparticles by employing citron juice (*Citrus medica*). The biologically active copper nanoparticles were identified using a UV-Vis spectrophotometer, which exhibited a typical resonance (SPR) for Cu-nanoparticles at about 631 nm. The FCC composition of nanoparticles with a mean size of 20 nm was determined using X-ray diffraction. The antibacterial activity of copper nanoparticles was assessed by using the Kirby-Bauer disc diffusion method on specific chosen bacterial species and plant pathogenic fungi. *E. coli* strains were found to be the first pathogen that the produced Cu-nanoparticles significantly inhibited, following *K. pneumoniae*, *P. aeruginosa*, *Cutibacterium acnes*, and *Salmonella typhi*. *Fusarium graminearum*, *Fusarium culmorum*, and *Fusarium oxysporum*, were shown to be the most vulnerable plant pathogenic fungus [77].

In another study, researchers used *Citrus sinensis* peel extract as a reducing and capping agent in a novel, efficient green chemistry process to produce silver nanoparticles [53]. The particles were 10 and 35 nm in size at 60 and 25 °C., respectively according to TEM measurements. Generally spherical particles with a diameter range from 15 to 50 nm were produced during the development of stable Ag nanoparticles at various concentrations of AgNO₃. The reductive potency of orange peel (*Citrus sinensis*), a typical waste of the food processing

industry, has been documented to be used to generate biodegradable polymer templated "green" silver nanoparticles in an attempt to make nanoscale research more environmentally sustainable. TEM analysis revealed spherical particles of 3–12 nm in size. The fact that the majority of the particles had a diameter of 6 nm was particularly noteworthy. The synthesized Ag nanoparticles revealed excellent antibacterial activity [78]. Ali et al. [79] reported the use of green synthesized (GS) ZnO nanoparticles to make nanostructured ZnO thin films by employing a spray pyrolysis technique. Investigations were conducted into how the deposition rate affected the optical, electrical, and structural characteristics of the ZnO thin films. In order to prepare the ZnO nanoparticles, a Zn (Ac)₂·2H₂O solution was dissolved in an aqueous *Citrus reticulata* peel extract. FE-SEM was used to describe the morphological properties of the GS samples, and XRD analysis was used to determine the crystal structures [79].

Citrus plant extracts as antimicrobial finishing for cotton fabric

The textile dyeing and finishing sector has established the significance of green finishing compositions. K. A. Hammer et al. [80] investigated the antibacterial activities of 52 plant oils and extracts against different Gram positive, Gram negative bacteria, and yeast such as *Acinetobacter baumannii*, *Aeromonas veronii* by using agar and broth dilution procedures. At concentrations under 2.0% (v/v), it was revealed that bay, lemon grass, and oregano prevented the growth of microorganisms [80]. Thangamani, K., and Periasamy, R. [81] conducted a research study on the herbal finishing of natural fabrics, such as soya bean, cotton, and bamboo fabrics to assess their antimicrobial property. They selected *Plectranthus amboinicus*, *Terminalia chebula*, *Ocimum tenuiflorum* (tulsi), *Aloe barbadensis*, *Cymbopogon flexuosus* and *Asteraceae* as natural antimicrobials. These herbal sources antibacterial methanol extracts were applied directly to fabrics using the pad-dry-cure procedure. They observed that textiles made up of cotton and bamboo treated with asteraceae exhibited no antibacterial action. However, soya bean fabric had good microbial activity. Lemon grass oil applied to cotton fabric was found to have the strongest antibacterial effects on both Gram-negative and Gram-positive bacteria [81]. FeCl₂·4H₂O and FeCl₃·6H₂O were added in 100 ml distilled water in a 250 ml conical flask for the bio-synthesis of magnetite nanoparticles. The mixture was then heated at 80 °C with gentle stirring using a magnetic stirrer. The aqueous solution of lemongrass leaves extract was added to the above mixture after 10 minutes, and it was heated for 5 minutes while being constantly stirred. For homogenous magnetite precipitations, 20 ml of 0.1N NaOH aqueous solution were added to the stirring solution at a rate of 3 ml/min after 5 minutes.

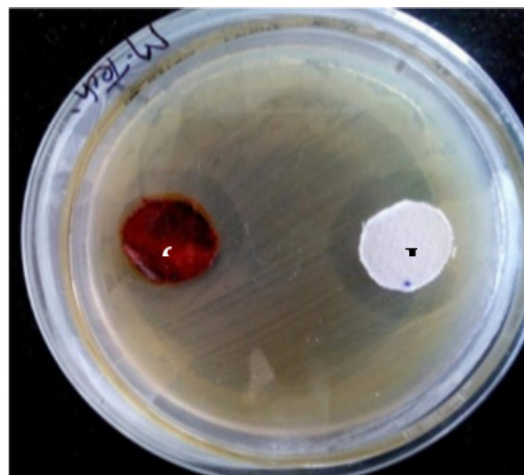


Figure 4. Antibacterial action of fabric treated with synthesized NPs and control fabric (ampicillin) against *E. coli*.

The solution was then cooled down to the room temperature. The aqueous solution was diluted using sterile distilled water and centrifuged at a speed of 15,000 rpm for 15 minutes after being decanted. After centrifugation, the magnetite particles were separated and dried for 48 hours at 80°C in a hot air oven. The obtained dried form was mashed with a pestle and mortar. The ultrasonication process and dipping were used to coat the particles onto the textiles. Magnetite nanoparticles were successfully coated onto cotton textile samples using the ultrasonication process. The antibacterial action of the produced magnetite nanoparticles towards *B. subtilis* and *E. coli* was evaluated using the agar well diffusion method and the disc-diffusion method. In the disc diffusion method for *E. coli*, the first disc was the sterilized untreated fabric with as control sample for ampicillin while the second disc was treated cotton sample, which was also sterilized. There was a significant inhibition of microbial growth from it in the disc diffusion method (Figure 4) [82].

Biological synthesis of nanoparticles has always been significant because there are no hazardous synthetic substances involved in the process. This study also reported the use of citrus plant extract in the synthesis of nanoparticles. *Citrus sinensis* fruit fresh peel juice was used to make Ag nanoparticles. Field emission scanning electron microscopy (FESEM), X-ray diffraction, and UV-visible spectroscopy were used to analyze the synthesized nanoparticles. The produced Ag nanoparticles were immobilized on the cotton fabric after being characterized. The antifungal and antibacterial properties of synthesized Ag nanoparticles were also evaluated. Ag nanoparticles exhibited significant growth reduction against methicillin-resistant *S.aureus*, *Candida albicans*, and *Candida tropicalis* in antimicrobial investigations [83]. Vankar and Shukla [84] used *Citrus limon* leaf aqueous extract to produce silver nanoparticles. The synthesized Ag nanoparticles were then tested for antifungal action on silk and cotton fabrics. Agar diffusion was used to measure the antifungal activity

Table 3. The values of zone of inhibitions (ZOI) of citrus lemon peel extract against *S. aureus* and *E. coli*.

Sr #.	Zone of Inhibition (mm)		
	Sample	<i>S. aureus</i>	<i>E. coli</i>
1.	Orange lemon	20-24	17-21
2.	Green lemon	24-30	22-26
3.	Black lemon	18-26	18-25

towards *Fusarium oxysporum* and *Alternaria brassicicola*. The antifungal activity of the cotton and silk materials was strong and long-lasting [84].

This research work was aimed to investigate, identify, and assess the bioactive substances that can be obtained from orange peels (OP) using an ultrasonic extraction technique as a potential eco-friendly additive for multifunctional cellulosic textiles and fibres. The novel approach employed two methods. An environment friendly in-situ synthesis of Ag, ZnO, and ZnO/Ag nanoparticles was successfully established for the fabrication of multifunctional viscose fibres using phenolic chemicals derived from OP. The treated viscose fibres provide exceptional antioxidant, antibacterial, UV protection, photo catalytic and self-cleaning activities [59].

Similarly, another research work was conducted to investigate, assess, and compare the antibacterial properties of cotton coated with essential oils isolated from black, green, and orange (a combination of orange and green) lemon peel (*Citrus limon*). The of orange and green) lemon peel (*Citrus limon*). The citrus limon peel is highly nutritious, including essential oils and flavonoids, which have antibacterial properties. The finishing agent i.e., lemon peel extract, was obtained by steam distillation methods after being treated with methanol. By measuring the zone of inhibition, the antibacterial activity was assessed against the gram-negative *E. coli* bacteria and the gram-positive *S. aureus* bacteria. In comparison to orange and black lemon, cotton treated with green lemon peel extract exhibited strong antibacterial activity against *S. aureus* (26-30mm) and *E. coli* (20-25mm) test microbes. In comparison to orange lemon peel, black lemon peel extract had stronger antibacterial activity against *S. aureus* (18-26mm) and *E. coli* (18-25mm) test microbes. Furthermore, the durability of the biological finishing agent on cotton fabric was assessed both before and after washing, and the results were the same. The results from this study indicated that the antibacterial action of cotton fabric treated with the biological finishing agent was same before and after laundering. This study showed that citrus lemons had more robust, long-lasting antibacterial capability, with extract of green lemon peels having the most effective effect [8].

Orange peels (OP) are one of the fruit wastes produced mostly by the juicing companies that contribute to environmental issues because of their high production volume and physicochemical features, which include water and soil contamination. Orange peel has antibacterial capabilities as it is

flavonoid-rich. According to a study, orange peel and papaya skin supplemented with silver nanoparticles enhance the anti-microbial properties of the treated textiles [60]. Citrus waste extracts from orange and lemon peels were tested to evaluate the washing durability of biological antibacterial coatings. The antibacterial activity of the fabric samples against various bacterial strains was evaluated quantitatively by AATCC testing method 100-2004 following various washing conditions. The findings revealed that the cotton treated with biological finishes exhibits resistance to microbes [85]. The antimicrobial properties for textile material (56% cotton/44% polyester) was evaluated using the essential oils isolated from rosemary (*Rosmarinus officinalis*) and orange (*Citrus sinensis*) at concentrations of 1%, 3%, and 5% for each oil. The antimicrobial action was evaluated against each strain. The obtained results supported the use of textiles functionalized with orange and rosemary essential oils as effective active antimicrobial inhibitors, with a maximum reduction of 92.48% for orange extracts and 56.99% for rosemary extract [86]. With the objective of encouraging bio-based substances in textile dyeing and finishing, Shahid et al. [87] presented the use of chitosan combined with the extract of *Citrus sinensis* peel biomolecules as a method to increase the natural dyeing efficiency of cotton fabric at optimal conditions. Chitosan polymer was first soaked in acetic acid and then, using the pad-dry process, coated on cotton. Cotton samples that had been coated with chitosan were then dyed using a *Citrus sinensis* peel extract to enable the employment of chitosan biological mordant to enhance colorimetric results. This work offers great potential for use in natural dyeing technique by revealing essential information about the synergistic effects between two natural chemicals in imparting semi-durable antibacterial and antioxidant action against *S. aureus* and *E. coli* bacteria [87]. Cotton fabric was dyed with the citrus extract under various conditions, such as dye concentration, temperature, pH, and, duration and evaluated for fastness and antimicrobial effectiveness in order to investigate the possible future use of *Citrus grandis* in biological applications for strengthening human skin health. The optimised dyeing of the cotton fabric was achieved at a pH of 3, a dyeing temperature of 60°C, a dyeing time of 60 min, and a dye concentration of 80% owf. Cotton dyed with the maximum concentration of antimicrobial agent exhibited outstanding bacterial growth reduction rates against *S. aureus* for up to five launderings, indicating the need to increase washing durability [88]. In another investigation, two techniques were used to apply lemongrass oil to fabric: exhaust method and oil microcapsules applied through padding. Complex coacervation techniques were used to develop the lemongrass oil microcapsules, which were then applied to cloth using the pad dry cure method. The AATCC-100 was used

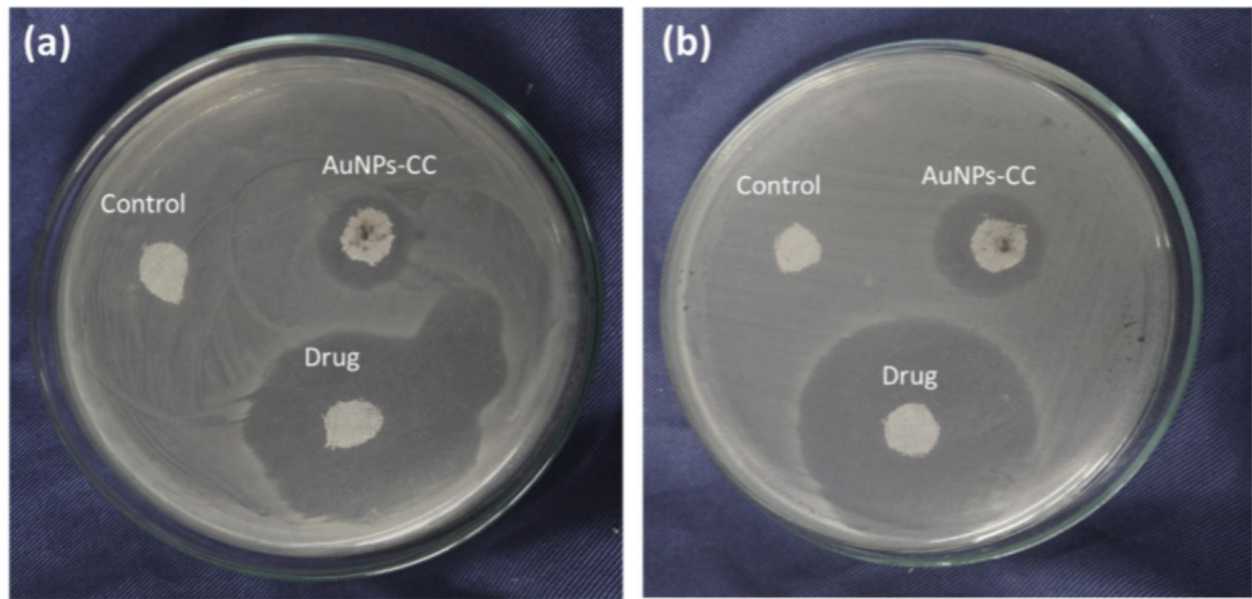


Figure 5. Antibacterial action of cotton fabric treated with synthesized nanoparticles, negative control (CC) positive control (drug) towards *E. coli* (a) and *S. aureus* (b) [90].

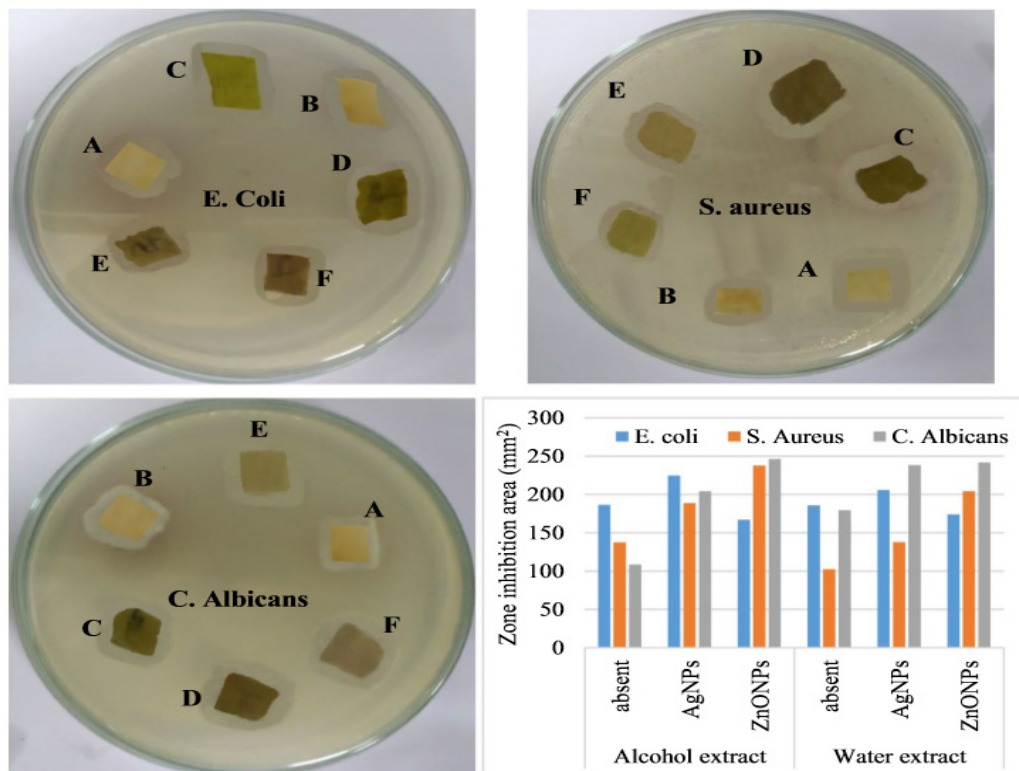


Figure 6. Antibacterial activity of cotton fabric treated with alcoholic and water extract of citrus plants [47].

to evaluate the antibacterial properties of untreated and treated cotton fabrics. The fabric treated with lemongrass oil microcapsules demonstrated an 80% bacterial growth inhibition [89].

In another study, a facile and environmentally sustainable method for producing biologically active gold nanoparticles on cotton fabric (AuNPs-CC) was established. It was established that the -OH groups in the cellulose polymers, which are abundant in cotton, ultimately reduced the Au ions into gold

nanoparticles. A citrus limon juice extract was used to expedite the kinetic process of AuNP production. Energy-dispersive spectroscopy (EDS), field emission scanning electron microscopy (FESEM), and other spectroscopic techniques were used to evaluate the developed samples. The FESEM results clearly showed the 22 nm size Au nanoparticles adhered to the cotton fabric. The development of bioactive Au nanoparticles over the CC surface was verified by the XPS and XRD. The bactericidal

abilities of the various strains of the pristine-CC and AuNPs-CC were investigated. The Citrus limon assisted synthesized AuNP-CC revealed excellent antibacterial properties against bacterial pathogens [90].

Citrus Sinensis peel (orange peel) extract was utilized in an environmentally friendly process to endow cotton fabric with multifunctional qualities. The extract has been made using both water and ethanol as solvents. Both extractions have been employed as stabilizing and reducing agents in the synthesis of zinc oxide and silver nanoparticles. Different methods, including Fourier transform infrared (FTIR), total phenolic contents, antioxidant properties, particle size analyzer, transmission electronic microscopy (TEM), and X-ray diffraction, have been used to characterize the prepared extracts and synthesized nanoparticles. Silver nanoparticles, chitosan-loaded zinc oxide nanoparticles, and orange-peel extraction were applied on cotton fabric. Scanning electron microscopy, UPF rating, antibacterial activity, mosquito repellent effects, and self-cleaning features were evaluated to examine the treated cotton samples [47].

Evaluation methods of antibacterial fabrics

Multiple testing methods have been devised to assess the potency of antibacterial textile materials. These testing standards can be divided into two main categories: quantitative analysis methods and qualitative analysis methods. The procedures to carry out these tests are briefly discussed below.

Qualitative testing protocol

Some of the methods for qualitative antimicrobial tests usually referred to as agar diffusion or disc diffusion tests include SN 195920-1992 (Swiss Norm), JIS L1902-2002 (Japanese Industrial Standards), and AATCC 147-2004 (American Association of Textile Chemists and Colorists) [91]. These assessments are only qualitative, but they are simple to do and work best when screening lots of samples for antimicrobial effect. To conduct this experiment, microbial cells are loaded onto nutrient medium plates. The untreated and treated fabric samples are then placed on the injected agar plates. The plates loaded with samples are checked for bacterial growth from around test samples (zone of inhibition) and underneath the fabrics after being incubated at 37°C for 18 to 24 hours. The lack of bacterial activity right beneath the textile swatch indicates antimicrobial efficacy. If the antimicrobial agent is strongly covalently attached to the textiles, it is unable to penetrate into the agar media, which results in the absence of a zone of inhibition. If the antibacterial chemical diffuses in the agar media, a zone of inhibition (ZOI) is developed. Its diameter gives an approximate estimate of the potential for antibacterial activities. The diameter of the ZOI is

determined using equations. Although each approach employs a different calculation method, all of the abovementioned techniques follow the same methodology. The AATCC-147 method is advised because it offers information that is generally accurate in terms of the diameter of the inhibition zone.

Another qualitative test method exists and is recognised as an international standard by the European Union (EN ISO 20645) [92]. This method of testing evaluates the impact of antibacterial treatments on plain woven, knit, and other textile cloths. The hygiene surfaces of hydrophilic and permeable materials, or antibacterial additives applied to the fibre, are subject to this standard testing. The smallest antibacterial treatment diffusion is needed for this agar test technique. Other materials should also adhere to the ISO 20645 standard for it to be effective. Testing textile items treated by antibacterial methods which react with agar is not appropriate for such a testing method [93].

Quantitative testing protocol

The primary quantitative assessment methods used for the evaluations of antibacterial are AATCC 100-2004, JIS L1902-2002, SN 195924-1992, and ISO-20743 [91,94,95]. These procedures are substantially more time-consuming than qualitative antibacterial screening, but they offer precise quantitative evaluation of the antibacterial materials. According to the appropriate norms, approximately 1ml of inoculum is completely absorbed onto test fabric swatches of different sizes. This step ensures that the analysed samples and the microorganisms have direct contact. According to standard protocol, the bacterial suspension-loaded textile sample is incubated for the required amount of time. The precise quantity of injected and recovered bacteria is counted by employing the serial dilution procedure followed by plating of dilutions on agar media plates. By comparing the quantity of injected and recovered bacteria at 0 h and after a given incubation period, antibacterial activity is assessed in terms of percentage reduction and log reduction. In order to ensure that the obtained reduction in microbial population is substantially due to the antibacterial finishing, suitable control samples, such as fabric samples that have undergone the identical processing steps without the antibacterial finishing, must be tested in each experiment. The choice of an appropriate calculation equation could be crucial. Quantitative evaluation can be done using any method, but the ISO-20743 method is believed to be the most useful for evaluating the microbe resistance of textiles. This is because no other method can accurately simulate hospital textiles as hospital textiles practically prohibit the complete absorption of an inoculum dose (typically 1 ml) onto the fabric. In this method, textile swatches are placed on infected culture plate for a certain amount of time (60

seconds), after which they are removed for further analysis.

Minimum inhibitory concentration assays

Broth tube dilution tests [96] and Liofilchem strip test procedures are used to determine the minimum inhibitory concentration (MIC) of antimicrobials [97]. The MIC value represents the lowest concentration at which the test microorganisms cannot grow. In order to assess MIC in fresh growth media, microorganism sub-cultures are subjected to various doses of the antimicrobial agent. The MIC value of that active agent is defined as the concentration of antimicrobial at which no growth is seen. The Liofilchem strip test are not economically sound due to the high cost of the strips required for this test. As a result, broth dilution tests are preferable because they do not require any additional materials like strip test methods do.

Challenges associated with green synthesis of nanoparticles

Research on nanoparticles and promising applications has advanced significantly in recent years. The green synthesis of metallic nanoparticles using a variety of biological sources, including plants, bacteria, fungi, and yeast, has been documented in numerous investigations. However, there are still a number of issues that prevent its widespread manufacture and ensuing uses. The following is a summary of some of the challenging issues encountered during the synthesis:

- Extensive optimization studies on raw materials (plant extract) and processing parameters (temperature, rotational speed, pH, etc.) are required to regulate the size and form of the nanoparticles.
- Investigations are also needed to focus on optimizing different physicochemical properties of nanoparticles for certain applications.
- It is important to thoroughly examine the effect of each metabolite found in plant extracts and cellular elements of microorganisms on the synthesis of nanoparticles.
- Prioritization must be given to expanding the synthesis of nanoparticles for industrial applications by employing green synthesis techniques.
- Optimization of different reaction parameters for the improvement of nanoparticles stability and yield with reduced synthesis time is required.

Biosynthesized nanoparticles have limited their applications in textiles due to their instability and the weak bond that forms between the textile material and nanoparticles.

Another major issue that must be investigated is the extraction and purification of nanoparticles from the reaction medium.

By overcoming these challenges, it might be possible to produce nanoparticles on a large scale more inexpensively and efficiently using green synthesis techniques than with traditional techniques.

Problems associated with green synthesised nanoparticles

Long-term stability is constrained by current techniques of nanoparticle functionalization [94]. As nanoparticles are removed from fibre material, the nanoparticle dopants are vulnerable to leaching. This would be especially important for textiles and garments that go through multiple cycles of washing and drying as well as mechanical stress. Depending upon the product, metal nanoparticle emission from textiles might reach 80% within the first wash. Additionally, copper as well as other nanoparticles like silver that are used in textiles have shown to be harmful in ecological systems. The biological treatment procedures utilised in both municipal and commercial water treatment facilities can be interfered with by these antimicrobial nanoparticles [98].

CONCLUSION

Metallic nanoparticles have found potential application in both the engineering and biological applications. In recent years, huge increase in their demand has been observed, and this development is not expected to halt. This review was aimed at summarising the significance of nanotechnology and nanoparticles (NPs) in the development of bioactive textiles, biosynthesis of NPs facilitated by the use of plant extracts while focusing on the utilization of citrus fruits and plant extracts. The chemical composition of citrus plants and fruits extract as well as the methods for the extraction of these biologically active components from citrus plants have been mentioned. This review also included the application of bio-synthesized biogenic nanoparticles on the cotton fabric for antibacterial properties, account of limitations, and challenges faced during the green synthesis of nanoparticles. The possible mechanisms exhibited by the nanoparticles to show antibacterial effect is also explained. This paper also summarizes different qualitative and quantitative standard testing protocols employed for the antimicrobial characterization of plant extracts and treated textiles. Moreover, the major challenges and limitations faced during the plant-based biosynthesis of nanoparticles have also been highlighted.

REFERENCES

- Singh P., Kim Y.J., Zhang D., et al.: Biological synthesis of nanoparticles from plants and microorganisms, *Trends Biotechnol*, 34(7), 2016, pp. 588–599.
<https://doi.org/10.1016/j.tibtech.2016.02.006>
- Kulkarni N. and Muddapur U.: Biosynthesis of metal nanoparticles: A review, *J Nanotechnol*, 2014, 2014.
<https://doi.org/10.1155/2014/510246>
- Ali A., Baheti V., Militky J., et al.: Copper coated multifunctional cotton fabrics, *Journal of Industrial Textiles*, 48(2), 2017, pp. 448–464.
<https://doi.org/10.1177/1528083717732076>
- Narayanan B.K. and Sakthivel N.: Green synthesis of biogenic metal nanoparticles by terrestrial and aquatic phototrophic and heterotrophic eukaryotes and biocompatible agents, *Adv Colloid Interface Sci*, 169(2), 2011, pp. 59–79.
<https://doi.org/10.1016/j.cis.2011.08.004>
- Afraz N., Uddin F., Syed U., et al.: Antimicrobial finishes for Textiles, *Current Trends in Fashion Technology & Textile Engineering*, 4(5), 2019, pp. 87–94.
<https://doi.org/10.19080/CTFTE.2019.04.555646>
- Periolatto M., Ferrero F., Vineis C., et al.: Novel antimicrobial agents and processes for textile applications, *Antibacterial agents*, 17, 2017.
- Ali A., Baheti V., Militky J., and Khan Z.: Utility of silver-coated fabrics as electrodes in electrotherapy applications, *J Appl Polym Sci*, 135(23), 2018.
<https://doi.org/10.1002/app.46357>
- Wolela A. D.: Antibacterial Finishing of Cotton Textiles with Extract of Citrus Fruit Peels, *Fashion Technology & Textile Engineering*, 6(1), 2020, pp. 1–7.
<https://doi.org/10.19080/CTFTE.2020.06.555676>
- Murthy L. I. and Halperin W. E.: Medical screening and biological monitoring: A guide to the literature for physicians, *J Occup Environ Med*, 1995, pp. 170–184.
- Ali A., Baheti V., Militky J., et al.: Copper coated multifunctional cotton fabrics, *Journal of Industrial Textiles*, 48(2), 2018, pp. 448–464.
<https://doi.org/10.1177/1528083717732076>
- Gan X., Wu Y., Liu L., et al.: Electroless plating of Cu–Ni–P alloy on PET fabrics and effect of plating parameters on the properties of conductive fabrics, *J Alloys Compd*, 455(1–2), 2008, pp. 308–313.
- Coleridge P. T. and Templeton I. M.: Fermi-surface radii in copper, silver, and gold, *Phys Rev B*, 25(12), 1982, p. 7818.
<https://doi.org/10.1016/j.tibtech.2016.02.006>
- Margariti C.: The Effects of micro-organisms in simulated soil burial on cellulosic and proteinaceous textiles and the morphology of the fibres, *Studies in Conservation*, 66(5), 2021, pp. 282–297.
- Landage S. M. and Wasif A. I.: Nanosilver—an effective antimicrobial agent for finishing of textiles, *International Journal of Engineering Sciences & Emerging Technologies*, 4(1), 2012, pp. 66–78.
- Kelly M., Macdougall K., Olabisi O., and McGuire N.: In vivo response to polypropylene following implantation in animal models: a review of biocompatibility, *Int Urogynecol J*, 28(2), 2017, pp. 171–180.
- Ali A. et al.: Electrical conductivity and physiological comfort of silver coated cotton fabrics, *Journal of the Textile Institute*, 109, no. January, 2018, pp. 620–628.
<https://doi.org/10.1080/00405000.2017.1362148>
- Andra S., Jeevanandam J., and Muthalagu M.: Emerging nanomaterials for antibacterial textile fabrication, *Naunyn-Schmiedeberg's Arch Pharmacol*, 394(7), 2021, pp. 1355–1382.
- Oh K. W., Park H. J., and Kim S. H.: Stretchable conductive fabric for electrotherapy, *J Appl Polym Sci*, 88(5), 2003, pp. 1225–1229.
- Rytlewski P., Jagodziński B., and Moraczewski K.: Laser-assisted electroless metallization of polymer materials: a critical review, *Reviews of Adhesion and Adhesives*, 4(3), 2016, pp. 334–366.
- Khandve P.: Nanotechnology for building material, *International Journal of Basic and Applied Research*, 4, 2014, pp. 146–151.
- Porter A. L. and Youtie J.: How interdisciplinary is nanotechnology?, *Journal of Nanoparticle Research*, 11(5), 2009, pp. 1023–1041.
<https://doi.org/10.1007/s11051-009-9607-0>
- Onyancha W., Ali M.I., Sharma G., and Moin S.: Synergistic potential of herbal plants and conventional antibiotics against multidrug-resistant bacteria, *Medicinal Plants-International Journal of Phytomedicines and Related Industries*, 13(1), 2021, pp. 13–21.
<https://doi.org/10.5958/0975-6892.2021.00003.4>
- Rai M., Ingle A.P., Pandit R., et al.: Curcumin and curcumin-loaded nanoparticles: antipathogenic and antiparasitic activities, *Expert Rev Anti Infect Ther*, 18(4), 2020, pp. 367–379.
<https://doi.org/10.1080/14787210.2020.1730815>
- Dizaj S.M., Mennati A., Jafari S., et al.: Antimicrobial activity of carbon-based nanoparticles, *Adv Pharm Bull*, 5(1), 2015, p. 19–23.
<https://doi.org/10.5681/apb.2015.003>
- Joshi M. and Bhattacharyya A.: Nanotechnology—a new route to high-performance functional textiles, *Textile Progress*, 43(3), 2011, pp. 155–233.
<https://doi.org/10.1080/00405167.2011.570027>
- Ali A. et al.: Multifunctional electrically conductive copper electroplated fabrics sensitizes by In-situ deposition of copper and silver nanoparticles, *Nanomaterials*, 11(11), Nov. 2021, p. 3097.
<https://doi.org/10.3390/nano11113097>
- Amanullah M. and Al-Tahini A. M.: Nano-technology-its significance in smart fluid development for oil and gas field application, in *SPE Saudi Arabia Section Technical Symposium*, 2009.
- Kotcherlakota R. et al.: Biosynthesized gold nanoparticles: In vivo study of near-infrared fluorescence (NIR)-based bio-imaging and cell labeling applications, *ACS Biomater Sci Eng*, 5(10), 2019 pp. 5439–5452.
<https://doi.org/10.1021/acsbiomaterials.9b00721>
- Cheng L. et al.: Potential antibacterial mechanism of silver nanoparticles and the optimization of orthopedic implants by advanced modification technologies, *Int J Nanomedicine*, vol. 13, 2018, p. 3311.
<https://doi.org/10.2147/IJN.S165125>
- Parham S., Wicaksono D. H. B., Bagherbaigi S., et al.: Antimicrobial treatment of different metal oxide nanoparticles: A critical review, *Journal of the Chinese Chemical Society*, 63(4), 2016, pp. 385–393.
<https://doi.org/10.1002/jccs.201500446>
- Yan X. et al.: Antibacterial mechanism of silver nanoparticles in *Pseudomonas aeruginosa*: proteomics approach, *Metallomics*, 10(4), 2018, pp. 557–564.
<https://doi.org/10.1039/c7mt00328e>
- Concha-Guerrero S. I. et al.: Effect of CuO nanoparticles over isolated bacterial strains from agricultural soil, *J Nanomater*, vol. 2014, 2014.
<https://doi.org/10.1155/2014/148743>
- Azam A., Ahmed A. S., Oves M., et al.: Size-dependent antimicrobial properties of CuO nanoparticles against Gram-positive and-negative bacterial strains, *Int J Nanomedicine*, 7, 2012, p. 3527.
<https://doi.org/10.2147/IJN.S29020>
- Andra S., Balu S., Jeevanandam J., and Muthalagu M.: Emerging nanomaterials for antibacterial textile fabrication, *Naunyn-Schmiedeberg's Archives of Pharmacology*, 2021, pp. 1355–1382.
<https://doi.org/10.1007/s00210-021-02064-8>
- Lee H. J., Lee G., Jang N. R., et al.: Biological synthesis of copper nanoparticles using plant extract, *Nanotechnology*, 1(1), 2011, pp. 371–374.
- Zhang J., Chaker M., and Ma D.: Pulsed laser ablation based synthesis of colloidal metal nanoparticles for catalytic applications, *J Colloid Interface Sci*, vol. 489, 2017, pp. 138–149.
<https://doi.org/10.1016/j.jcis.2016.07.050>

37. Lan C. et al.: Wafer-scale synthesis of monolayer WS₂ for high-performance flexible photodetectors by enhanced chemical vapor deposition, *Nano Res*, 11(6), 2018, pp. 3371–3384.
<https://doi.org/10.1007/s12274-017-1941-4>
38. Li Y. et al.: Solvent-free synthesis of magnetic biochar and activated carbon through ball-mill extrusion with Fe₃O₄ nanoparticles for enhancing adsorption of methylene blue, *Science of The Total Environment*, vol. 722, 2020, p. 137972.
<https://doi.org/10.1016/j.scitotenv.2020.137972>
39. Gomathi A. C., Rajarathinam S. R. X., Sadiq A. M., and Rajeshkumar S.: Anticancer activity of silver nanoparticles synthesized using aqueous fruit shell extract of *Tamarindus indica* on MCF-7 human breast cancer cell line, *J Drug Deliv Sci Technol*, vol. 55, 2020, p. 101376.
<https://doi.org/10.1016/j.jddst.2019.101376>
40. Salem S.S. and Fouda A.: Green synthesis of metallic nanoparticles and their prospective biotechnological applications: an overview, *Biol Trace Elem Res*, 199(1), 2021, pp. 344–370.
<https://doi.org/10.1007/s12011-020-02138-3>
41. Ahmed S. and Ikram S.: Biosynthesis of gold nanoparticles: a green approach, *J Photochem Photobiol B*, vol. 161, 2016, pp. 141–153.
<https://doi.org/10.1016/j.jphotobiol.2016.04.034>
42. Mohamad N.A.N., Arham N.A., J. Jai, et al.: Plant extract as reducing agent in synthesis of metallic nanoparticles: a review, *Adv Mat Res*, vol. 832, 2014, pp. 350–355.
<https://doi.org/10.4028/www.scientific.net/AMR.832.350>
43. Das R.K., et al., Biological synthesis of metallic nanoparticles: plants, animals and microbial aspects, *Nanotechnology for Environmental Engineering*, 2(1), 2017, pp. 1–21.
<https://doi.org/10.1007/s41204-017-0029-4>
44. Liu Y., Heying E., and Tanumihardjo S. A.: History, global distribution, and nutritional importance of citrus fruits, *Compr Rev Food Sci Food Saf*, vol. 11, no. 6, 2012, pp. 530–545.
<https://doi.org/10.1111/j.1541-4337.2012.00201.x>
45. Park Y., Hong Y. N., Weyers A., et al.: Polysaccharides and phytochemicals: a natural reservoir for the green synthesis of gold and silver nanoparticles, *IET Nanobiotechnol*, 5(3), 2011, pp. 69–78.
<https://doi.org/10.1049/iet-nbt.2010.0033>
46. Chavan P., Singh A. K., and Kaur G.: Recent progress in the utilization of industrial waste and by-products of citrus fruits: A review, *J Food Process Eng*, 41(8), 2018, p. e12895.
<https://doi.org/10.1111/jfpe.12895>
47. Zayed M., Ghazal H., Othman H.A., and Hassabo A. G.: Synthesis of different nanometals using citrus sinensis peel (orange peel) waste extraction for valuable functionalization of cotton fabric, *Chemical Papers*, 76(2), 2022, pp. 639–660.
<https://doi.org/10.1007/s11696-021-01881-8>
48. Meneguzzo F., Ciriminna R., Zabini F., Pagliaro M.: Review of evidence available on hesperidin-rich products as potential tools against COVID-19 and hydrodynamic cavitation-based extraction as a method of increasing their production, *Processes*, 8(5), 2020 p. 549.
<https://doi.org/10.3390/pr8050549>
49. Yi L., Ma S., and Ren D.: Phytochemistry and bioactivity of Citrus flavonoids: a focus on antioxidant, anti-inflammatory, anticancer and cardiovascular protection activities, *Phytochemistry Reviews*, 16(3), 2017, pp. 479–511.
<https://doi.org/10.1007/s11101-017-9497-1>
50. Guo C. et al.: Chemical composition, antioxidant, antibacterial, and tyrosinase inhibition activity of extracts from Newhall navel orange (*Citrus sinensis* Osbeck cv. Newhall) peel, *J Sci Food Agric*, 100(6), 2020, pp. 2664–2674.
<https://doi.org/10.1002/jsfa.10297>
51. Guo J., Tao H., Cao Y., et al.: Prevention of obesity and type 2 diabetes with aged citrus <https://doi.org/10.1016/j.jep.2018.03.031> peel (Chenpi) extract, *J Agric Food Chem*, 64(10), 2016. pp. 2053–2061.
<https://doi.org/10.1021/acs.jafc.5b06157>
52. Buyukkurt O. K., Guclu G., Kelebek H., and Selli S.: Characterization of phenolic compounds in sweet lime (*Citrus limetta*) peel and freshly squeezed juices by LC-DAD-ESI-MS/MS and their antioxidant activity, *Journal of Food Measurement and Characterization*, 13(4), 2019, pp. 3242–3249.
<https://doi.org/10.1007/s11694-019-00246-w>
53. Yu X. et al.: Citri Reticulatae Pericarpium (Chenpi): Botany, ethnopharmacology, phytochemistry, and pharmacology of a frequently used traditional Chinese medicine," *J Ethnopharmacol*, 220, 2018, pp. 265–282.
<https://doi.org/10.1016/j.jep.2018.03.031>
54. Liu N. et al.: A review of chemical constituents and health-promoting effects of citrus peels, *Food Chem*, 365, 2021, pp. 130585.
<https://doi.org/10.1016/j.foodchem.2021.130585>
55. Guo Q., Liu K., Deng W., et al.: Chemical composition and antimicrobial activity of Gannan navel orange (*Citrus sinensis* Osbeck cv. Newhall) peel essential oils, *Food Sci Nutr*, 6(6), 2018, pp. 1431–1437.
<https://doi.org/10.1002/fsn3.688>
56. Hosni K. et al.: Composition of peel essential oils from four selected Tunisian Citrus species: Evidence for the genotypic influence, *Food Chem*, 123(4), pp. 1098–1104.
<https://doi.org/10.1016/j.foodchem.2010.05.0682010>
57. Farahmandfar R., Tirgarian B., Dehghan B., and Nemati A.: Comparison of different drying methods on bitter orange (*Citrus aurantium* L.) peel waste: Changes in physical (density and color) and essential oil (yield, composition, antioxidant and antibacterial) properties of powders, *Journal of Food Measurement and Characterization*, 14(2), 2020, pp. 862–875.
<https://doi.org/10.1007/s11694-019-00334-x>
58. Loizzo M. R., et al.: Evaluation of Citrus aurantifolia peel and leaves extracts for their chemical composition, antioxidant and anti-cholinesterase activities, *J Sci Food Agric*, 92(15), 2012, pp. 2960–2967.
<https://doi.org/10.1002/jsfa.5708>
59. Rehan M., Abdel-Wahed N.A.M., Farouk A., and El-Zawahry N.M.: Extraction of valuable compounds from orange peel waste for advanced functionalization of cellulosic surfaces, *ACS Sustain Chem Eng*, 6(5), 2018, pp. 5911–5928.
<https://doi.org/10.1021/acssuschemeng.7b04302>
60. Babu K.M.: Antimicrobial finishes for textiles, *Asian Textile Journal*, 12(4), 2003, pp. 64–68.
<https://doi.org/10.19080/ctfte.2019.04.555646>
61. De Normalisation A.F.: Huiles Essentielles, Monographie Relative aux Huiles Essentielles, Tome 2, vols 1 and 2," AFNOR: Paris, 2000.
62. Guenther E. and Althausen D.: The essential oils, vol. 1. Van Nostrand New York, 1948.
63. De Castro M.D.L., Jiménez-Carmona M.M., and Fernandez-Perez V.: Towards more rational techniques for the isolation of valuable essential oils from plants, *TrAC Trends in Analytical Chemistry*, 18(11), 1999, pp. 708–716.
[https://doi.org/10.1016/S0165-9936\(99\)00177-6](https://doi.org/10.1016/S0165-9936(99)00177-6)
64. Vinatoru M.: An overview of the ultrasonically assisted extraction of bioactive principles from herbs, *Ultrason Sonochem*, 8(3), 2001, pp. 303–313.
[https://doi.org/10.1016/S1350-4177\(01\)00071-2](https://doi.org/10.1016/S1350-4177(01)00071-2)
65. Rezzoug S. A., Louka N., and Allaf K.: Effect of the main processing parameters of the instantaneous controlled pressure drop process on oil isolation from rosemary leaves. Kinetics aspects, *Journal of Essential Oil Research*, 12(3), 2000, pp. 336–344.
<https://doi.org/10.1080/10412905.2000.9699531>
66. Reverchon E. and De Marco I.: Supercritical fluid extraction and fractionation of natural matter, *J Supercrit Fluids*, 38(2), 2006, pp. 146–166.
<https://doi.org/10.1016/j.supflu.2006.03.020>
67. Jimenez-Carmona M.M., Uberta J.L., and De Castro M.D. L.: Comparison of continuous subcritical water extraction

- and hydrodistillation of marjoram essential oil, *J Chromatogr A*, 855(2), 1999, pp. 625–632.
[https://doi.org/10.1016/S0021-9673\(99\)00703-7](https://doi.org/10.1016/S0021-9673(99)00703-7)
68. Kokolakis A. K. and Goufopoulos S. K.: Microwave-assisted techniques (MATs); a quick way to extract a fragrance: A review, *Nat Prod Commun*, 8(10), 2013, p. 1934578X1300801040.
<https://doi.org/10.1177/1934578X1300801040>
 69. Lucchesi M. E., Smadja J., Bradshaw S., Louw W., and Chemat F.: Solvent free microwave extraction of *Elletaria cardamomum* L.: A multivariate study of a new technique for the extraction of essential oil, *J Food Eng*, 79(3), 2007, pp. 1079–1086.
<https://doi.org/10.1016/j.jfoodeng.2006.03.029>
 70. Alkhulaifi M.M. et al.: Green synthesis of silver nanoparticles using Citrus limon peels and evaluation of their antibacterial and cytotoxic properties, *Saudi J Biol Sci*, 27(12), 2020, pp. 3434–3441.
<https://doi.org/10.1016/j.sjbs.2020.09.031>
 71. Ngoepe N. M., Mathipa M. M., and Hintsho-Mbita N. C.: Biosynthesis of titanium dioxide nanoparticles for the photodegradation of dyes and removal of bacteria, *Optik (Stuttg)*, 224, (June), 2020, p. 165728.
<https://doi.org/10.1016/j.ijleo.2020.165728>
 72. Basnet P., Inakhunbi Chanu T., Samanta D., and Chatterjee S.: A review on bio-synthesized zinc oxide nanoparticles using plant extracts as reductants and stabilizing agents, *J Photochem Photobiol B*, 183, 2018, pp. 201–221.
<https://doi.org/10.1016/j.jphotobiol.2018.04.036>
 73. Samat N. A. and Nor R. M.: "Sol-gel synthesis of zinc oxide nanoparticles using Citrus aurantifolia extracts," *Ceram Int*, vol. 39, 2013, pp. S545–S548.
<https://doi.org/10.1016/j.ceramint.2012.10.132>
 74. Firdhouse M. J. and Lalitha P.: Biosynthesis of silver nanoparticles and its applications, *J Nanotechnol*, 2015, (September) 2014, 2015.
<https://doi.org/10.1155/2015/829526>
 75. Logeswari P., Silambarasan S., and Abraham J.: Ecofriendly synthesis of silver nanoparticles from commercially available plant powders and their antibacterial properties, *Scientia Iranica*, 20(3), 2013, pp. 1049–1054.
<https://doi.org/10.1016/j.scient.2013.05.016>
 76. Naikoo G. A. et al.: Bioinspired and green synthesis of nanoparticles from plant extracts with antiviral and antimicrobial properties: A critical review, *Journal of Saudi Chemical Society*, 25(9), 2021, p. 101304.
<https://doi.org/10.1016/j.jscs.2021.101304>
 77. Shende S., Ingle A. P., Gade A., and Rai M.: Green synthesis of copper nanoparticles by Citrus medica Linn. (Idilimbu) juice and its antimicrobial activity, *World J Microbiol Biotechnol*, 31(6), 2015, pp. 865–873.
<https://doi.org/10.1007/s11274-015-1840-3>
 78. Veeraputhiran V.: Bio-Catalytic Synthesis of Silver Nanoparticles, *Int. J. Chem Tech Res.*, 5(5), 2013, pp. 2555 – 2562.
 79. Durmuş A., Çolak H., and Karaköse E.: Production and examination of ZnO thin film for first time using green synthesized method from aqueous Citrus reticulata peel extract, *J Alloys Compd*, 809, 2019, pp. 1–9.
<https://doi.org/10.1016/j.jallcom.2019.151813>
 80. Hammer K. A., Carson C. F., and Riley T. V.: Antimicrobial activity of essential oils and other plant extracts, *J Appl Microbiol*, 86, (6), 1999, pp. 985–990.
<https://doi.org/10.1046/j.1365-2672.1999.00780.x>
 81. Thangamani K. and Periasamy R.: Study on antimicrobial activity of cotton, bamboo, and soybean fabrics with herbal finishing, *Int Res J Pharm*, 8(5), 2017, pp. 115–119.
<https://doi.org/10.7897/2230-8407.08584>
 82. Hiremath L., Narendra Kumar S., and Sukanya P.: "Development of antimicrobial smart textiles fabricated with magnetite nano particles obtained through green synthesis," *Mater Today Proc*, 5(10), 2018, pp. 21030–21039.
<https://doi.org/10.1016/j.matpr.2018.06.496>
 83. Anwar Y. and Alghamdi K. M.: Imparting antibacterial, antifungal and catalytic properties to cotton cloth surface via green route, *Polym Test*, 81, 2020, p.106258.
<https://doi.org/10.1016/j.polymertesting.2019.106258>
 84. Anwar Y. and Alghamdi K. M.: Imparting antibacterial, antifungal and catalytic properties to cotton cloth surface via green route, *Polym Test*, 81, 2020, p.106258.
<https://doi.org/10.1016/j.polymertesting.2019.106258>
 85. Verma Assistant Professor M., Yadav S., Verma M, and Rose N. M.: Assessment of total phenolic content and antimicrobial activity of plants leaves extract, 819, *Journal of Pharmacognosy and Phytochemistry*, 10(1), 2021, pp. 819–823.
 86. Ahmed S., Annu, Chaudhry S. A., and Ikram S.: A review on biogenic synthesis of ZnO nanoparticles using plant extracts and microbes: A prospect towards green chemistry, *J Photochem Photobiol B*, 166, 2017, pp. 272–284.
<https://doi.org/10.1016/j.jphotobiol.2016.12.011>
 87. Shahid-ul-Islam and Butola B. S.: A synergistic combination of shrimp shell derived chitosan polysaccharide with Citrus sinensis peel extract for the development of colourful and bioactive cellulosic textile, *Int J Biol Macromol*, 158, 2020, pp. 94–103.
<https://doi.org/10.1016/j.ijbiomac.2020.04.209>
 88. Yi E. and Yoo E. S.: A novel bioactive fabric dyed with unripe Citrus grandis Osbeck extract part 1: Dyeing properties and antimicrobial activity on cotton knit fabrics, *Textile Research Journal*, 80(20), 2010, pp. 2117–2123.
<https://doi.org/10.1177/0040517510373633>
 89. Sachidhanandham A., Textiles from orange peel waste, *Science and Technology Development Journal*, 23(2), 2020.
<https://doi.org/10.32508/stdj.v23i2.1730>
 90. Anwar Y., Ullah I., Ul-Islam M, et al.: Adopting a green method for the synthesis of gold nanoparticles on cotton cloth for antimicrobial and environmental applications, *Arabian Journal of Chemistry*, 14(9), 2021, p. 103327.
<https://doi.org/10.1016/j.arabjc.2021.103327>
 91. Pinho E., Magalhães L., Henriques M., and Oliveira R.: Antimicrobial activity assessment of textiles: standard methods comparison, *Ann Microbiol*, 61(3), 2011, pp. 493–498.
<https://doi.org/10.1007/s13213-010-0163-8>
 92. ISO 20645: Textile Fabrics - Determination of antimicrobial activity - Agar diffusion plate test from International Organization for Standardization, 2004.
 93. Pinho E., Magalhães L., Henriques M., and Oliveira R.: Antimicrobial activity assessment of textiles: standard methods comparison, *Ann Microbiol*, 61(3), Sep. 2011, pp. 493–498.
<https://doi.org/10.1007/s13213-010-0163-8>
 94. Rodriguez C. et al.: Antibacterial effects of photocatalytic textiles for footwear application, *Catal Today*, 23, 2014, pp. 41–46.
<https://doi.org/10.1016/j.cattod.2013.12.023>
 95. Zhao X., Min J., and He J.: Effect of microwave curing on antimicrobial activity of chitosan biguanidine hydrochloride treated wool fabrics, *Journal of the Textile Institute*, 102(9), 2011, pp. 801–807.
<https://doi.org/10.1080/00405000.2010.522047>
 96. Stalons D. R. and Thornsberry C.: Broth-dilution method for determining the antibiotic susceptibility of anaerobic bacteria, *Antimicrob Agents Chemother*, 7(1), 1975, pp. 15–21.
<https://doi.org/10.1128/AAC.7.1.15>
 97. Jönsson A., Jacobsson S., Foerster S., et al.: Performance characteristics of newer MIC gradient strip tests compared with the test for antimicrobial susceptibility testing of *Neisseria gonorrhoeae*, *Apmis*, 126, (10), 2018, pp. 822–827.
<https://doi.org/10.1111/apm.12887>
 98. Keller A. A. et al.: Comparative environmental fate and toxicity of copper nanomaterials," *NanoImpact*, 7, Jul. 2017, pp. 28–40.
<https://doi.org/10.1016/j.impact.2017.05.003>

AIMS AND SCOPES

“Vlákna a Textil” is a peer-reviewed scientific journal serving the fields of fibers, textile structures and fiber-based products including research, production, processing, and applications.

The birth of this journal is connected with three institutions, Research Institute for Man-Made Fibers, Svit (VÚCHV), Research Institute of Chemistry of Textiles (VÚTCH) in Žilina and Department of Fibers and Textiles at the Faculty of Chemical Technology, Slovak Technical University in Bratislava, having a joint intention to provide, utilize and deposit results obtained through the research, development and production activities dealing with the aforementioned scopes. „Vlákna a Textil“ journal has been launched as a consequence of a joining of existing magazines „Chemické vlákna“ (VÚCHV) and „Textil a chémia“ (VÚTCH). Their tradition should provide a good framework for the new journal with the main aim to create a closer link between the basic element of the product - fibre and its fabric - textile.

Since its founding in 1994, the journal introduces new concepts, innovative technologies and better understanding of textile materials (physics and chemistry of fiber forming polymers), processes (technological, chemical and finishing), garment technology and its evaluation (analysis, testing and quality control) including non-traditional applications, such as technical textiles, composites, smart textiles or garment, and nano applications among others. The journal publishes original research papers and reviews. Original papers should present a significant advance in the understanding or application of materials and/or textile structures made of them.

CONTENT

3	NAVARA, TOMÁŠ RESISTANCE OF ADDITIONAL ROOFING UNDERLAYS OF PITCHED ROOFS AGAINST ARTIFICIAL AND NATURAL AGEING
14	HOSSAIN, MOHAMMAD MOBARAK; ALIMUZZAMAN, SHAH AND AHMED, DEWAN MURSHED TEAR AND TENSILE STRENGTH OF 100% COTTON WOVEN FABRICS' BASIC STRUCTURES: REGRESSION MODELLING
26	THAO, PHAN THANH; MY, PHAM THI LE AND PHAN, DUY-NAM STATE PROBLEM OF BALANCING SEWING LINE OF INDUSTRIAL KNITTED PRODUCTS
34	KŘÍŽ, VITĚZSLAV; KŘÍŽOVÁ, HANA; KOČICH, MARTIN AND DALÍKOVÁ, JOHANA A 2D CELLULAR AUTOMATON MODEL OF LIQUID ABSORPTION INTO PAPER FIBERS WITH HYDROPHOBIC TREATMENT
43	ARABULI, ARSENI; ARABULI, SVITLANA; KYZYMCHUK, OLENA AND MELNYK, LUDMYLA ELECTRIC HEATING CLOTHING FOR MOTORCYCLISTS
51	TRI, YULIANA AND NOORYAN, BAHARI THE DEVELOPMENT AND ANALYSIS OF ECO-PRINT AND SCREEN PRINTING COMBINATION USING NATURAL DYES
56	HUSSEN, MUKTAR SED; KYOSEV, YORDAN; PIETSOCH, KATHRIN; BOLL, JESSICA AND KABISH, ABERA KECHI MULTI-CRITERIA NUMERICAL OPTIMIZATION OF MECHANICAL PROPERTIES IN ULTRASONIC WELDING PROCESS PARAMETERS OF PVC-COATED HYBRID TEXTILES FOR WEATHER PROTECTION
74	ALI, REHMAT; KARAMAT, UM E HABIBA; NAZIR, HAFZA SABA; BAGI, MIRZA MUHAMMED MOHSIN; KHAN, BILAL ALAM; ULLAH, ASAD; USMAN, OSAMA; WASEEM, TANYA; TAHIR, AND MUHAMMAD FARUKH ANTIMICROBIAL ACTIVITY OF COTTON FIBRES TREATED WITH PARTICLES EXTRACTED FROM CITRUS PLANTS: A REVIEW

